Exploring growth variability and extremes in *Arctica islandica* bivalve species in the context of large-scale climatic phenomena

Dissertation submitted by

Diana-Elena Caldarescu

in fulfillment of the requirements for the degree of

Doctor of Natural Sciences (Dr. rer. nat.)

to Faculty 2: Biology and Chemistry
at the University of Bremen

Bremen, 2024

1^{st} Reviewer

Prof. Dr. Thomas Brey
Alfred Wegener Institute,
Helmholtz Centre for Polar and Marine Research
Faculty 2 at the University of Bremen
Bremen, Deutschland

2^{nd} Reviewer

Prof. Dr. Gerrit Lohmann
Alfred Wegener Institute,
Helmholtz Centre for Polar and Marine Research
Faculty 1 at the University of Bremen
Bremen, Deutschland

Submission: 27^{th} of June, 2024
Defense: 16^{th} of September, 2024

Dedicated to my father

Scientific environment

This research was conducted at the Paleoclimate Dynamics section of the Alfred Wegener Institute (AWI) – Helmholtz Centre for Polar and Marine Research in Bremerhaven, Germany. There, I was additionally enrolled with the Helmholtz Graduate School for Polar and Marine Research (POLMAR).

This work was supported by the AWI strategy fund „PALEX“, an interdisciplinary project aimed at deriving new insights on climate extremes during the pre-industrial (1850 CE) using high-resolution terrestrial and marine proxies.
The focus of my research lies within the marine realm, where I investigate the variability and extremes in growth proxy records of bivalve shells and their association with large-scale climatic signals.

Abstract

Hidden within the carbonate shells of *Arctica islandica* (*A. islandica*) bivalve species lies a wealth of information about past environmental conditions. Starting with the 1980s, this clam species surged not only in commercial popularity, but it quickly became one of the most important biorecorders in the field of sclerochronology – which focuses on growth patterns in the hard tissues of accreting organisms – owing to individual lifespans exceeding centuries in the northern North Atlantic basin. Growth increments are typically annually deposited and can be precisely dated, thereby facilitating cross-dating of multiple specimens to construct century-long master chronologies, and hence, long-term environmental records. However, compared to the isotopic composition of the growth bands, which acts as proxy for temperature, salinity and water productivity, growth increments are more challenging to decipher due to the interplay of multiple physical and biological factors, with the contribution of each factor varying in proportion depending on the region. With *A. islandica* already established in the community as a versatile climate archive, which novel insights can be envisioned?

There is, for instance, an interest in exploring the spatial variability of environmental signals recorded by *A. islandica* master chronologies across diverse geographical regions. This attempt enables a more comprehensive understanding of the common growth signal and its relationship to large-scale climate phenomena. Spectral and correlation analyses have consistently revealed that *A. islandica* records decadal and multidecadal periodicities, often associated with natural oscillations that influence large-scale ocean circulation patterns such as the Atlantic Multidecadal Oscillation (AMO) and Pacific Decadal Oscillation (PDO), as well as atmospheric circulation patterns like the North Atlantic Oscillation (NAO). Given the ongoing state of climate change, characterized by increasingly frequent and potentially more intense extreme events compared to recent years, there is a burgeoning interest in assessing whether growth anomalies observed in marine organisms correspond to unusual climatic patterns. In my research, I define extreme growth as deviations in the 10^{th} and 90^{th} percentiles from the mean growth, and believe these can provide valuable insights into environmental stressors. The aim of this thesis and the results therein is to identify clues that can guide future research towards a deeper understanding of the complex large-scale climatic interactions shaping growth variability and extreme responses in *A. islandica*.

To extract the shared growth signal in the northern North Atlantic, I have compiled previously published centennial-long master shell chronologies in several bivalve-based networks, and applied distinct principal component analyses. It was interesting to see a higher degree of congruity in the low growth years across the networks and the methodological approaches, underscoring the robustness of the findings concerning bivalve extreme growth. To identify anomalous large-scale patterns in the sea surface temperature and sea-level pressure, I have relied on composite maps of growth extremes along with reanalysis data. The composite analyses revealed that years marked by reduced growth aligned with positive sea-surface temperature anomalies in the extratropical to polar North Atlantic

basin resembling multidecadal AMO mode, which paired with a coherent pattern in the North Pacific suggestive of a negative Pacific Decadal Oscillation. The bivalve networks further revealed that two chronologies from distinct areas – the northern Icelandic shelf and the German Bight in the southern North Sea – did not conform to the spatial patterns observed. Consequently, two case studies were conducted to investigate the unique characteristics of these locations.

Using the chronology from the northern Icelandic Shelf, based on *A. islandica* bivalves from a water depth of 81 to 83 meters, my approach specifically addresses why correlations with sea-surface temperature often lack the required statistical significance and are deemed inconclusive. In this example, I correlated the growth signal with a three-month running average of temperature and salinity data across various water depth layers, and found significant correlations with the subsurface waters starting at a depth of 56 meters during summer and autumn, whereas correlations with the surface temperature layers were lagged by two years. Additionally, by computing spatial correlation maps, I highlight the potential of *A. islandica* to track thermally similar water bodies at large-scale. Next, I used an unpublished growth chronology of *A. islandica* from Helgoland in the southern North Sea alongside composite maps, to investigate which atmospheric patterns are associated with extreme growth events. The results indicate that growth in *A. islandica* is reduced during years characterized by a positive polarity of the NAO in winter, followed by intensified atmospheric blocking over the British Isles in spring. Spring blocking might also be linked to winter blocking in the North Pacific. The regional atmospheric pattern impacts the timing of the spring phytoplankton bloom, leading to a delay in the availability of essential nutrients necessary for growth.

By bridging research gaps between the field of sclerochronology and climate dynamics, this thesis delves into different aspects of the *Arctica islandica*'s potential as a climate archive in the North Atlantic. Whether deciphering the common growth signal across bivalve networks (**Paper I**), or examining the spatial-depth relationship with subsurface temperature variations (**Paper II**), or uncovering links to atmospheric teleconnections and blocking frequency events (**Paper III**), each study adds exciting findings, holding relevance for both paleo- and future-oriented studies.

Zusammenfassung

In den Karbonatschalen von *Arctica islandica* (*A. islandica*) verbirgt sich eine Fülle von Informationen über vergangene Umweltbedingungen. Seit den 1980er Jahren erfreut sich diese Muschelart nicht nur zunehmender kommerzieller Beliebtheit, sondern wurde aufgrund ihrer jahrhundertelangen Lebensdauer im nördlichen Nordatlantik schnell zu einem der wichtigsten Klimaarchiv auf dem Gebiet der Sklerochronologie, welche sich mit Wachstumsmustern im Hartgewebe von Organismen befasst, die sich vermehren. Wachstumsschübe werden in der Regel jährlich abgelagert und können genau datiert werden, was die Querdatierung mehrerer Exemplare erleichtert. Somit können jahrhundertelange Gesamtchronologien und langfristige Umweltaufzeichnungen erstellt werden. Im Vergleich zur Isotopenzusammensetzung der Wachstumsbänder, die als Stellvertreter für Temperatur, Salzgehalt und Wasserproduktivität fungiert, sind Wachstumsinkremente jedoch aufgrund des Zusammenspiels mehrerer physikalischer und biologischer Faktoren schwieriger zu entschlüsseln, wobei der Beitrag der einzelnen Faktoren je nach Region unterschiedlich hoch ist. Welche neuen Erkenntnisse sind zu erwarten, nachdem sich *A. islandica* in der Forschung bereits als vielseitiges Klimaarchiv etabliert hat?

Es besteht ein Interesse daran, die räumliche Variabilität von Umweltsignalen zu erforschen, die von *A. islandica*-Masterchronologien in verschiedenen geografischen Regionen aufgezeichnet werden. Diese Arbeit ermöglicht ein umfassenderes Verständnis des gemeinsamen Wachstumssignals und seiner Beziehung zu großräumigen Klimaphänomenen. Spektral- und Korrelationsanalysen haben durchweg ergeben, dass *A. islandica* dekadische und multidekadische Periodizitäten aufzeichnet, die häufig mit natürlichen Oszillationen verbunden sind, welche großräumige Ozeanzirkulationsmuster wie die Atlantische Multidekadische Oszillation (AMO) und die Pazifische Dekadische Oszillation (PDO) sowie atmosphärische Zirkulationsmuster wie die Nordatlantische Oszillation (NAO) beeinflussen. Angesichts des fortschreitenden Klimawandels, der durch immer häufigere und potenziell intensivere Extremereignisse im Vergleich zu den letzten Jahren gekennzeichnet ist, wächst das Interesse an der Frage, ob bei Meeresorganismen beobachtete Wachstumsanomalien mit ungewöhnlichen klimatischen Mustern zusammenhängen. In meiner Forschung definiere ich extremes Wachstum als Abweichungen in den 10^{th}- und 90^{th}-Perzentilen vom mittleren Wachstum, welche wertvollen Erkenntnisse über Umweltstressoren liefern können. Das Ziel dieser Arbeit und der darin enthaltenen Ergebnisse ist es, Anhaltspunkte zu finden, die künftige Forschungen zu einem tieferen Verständnis der komplexen großräumigen klimatischen Wechselwirkungen führen können, die die Wachstumsvariabilität und die extremen Reaktionen von *A. islandica* beeinflussen.

Um das gemeinsame Wachstumssignal im nördlichen Nordatlantik zu extrahieren, habe ich zuvor veröffentlichte jahrhundertelange Muschelchronologien in verschiedenen Muschelnetzwerken zusammengestellt und verschiedene Hauptkomponentenanalysen durchgeführt. Es war interessant zu sehen, dass die Jahre mit geringem Wachstum in den verschiedenen Netzwerken und methodischen Ansätzen ein höheres Maß an Übereinstimmung aufwiesen, was die Robustheit

der Erkenntnisse über das extreme Wachstum der Muscheln unterstreicht. Um anomale großräumige Muster in der Meeresoberflächentemperatur und im Meeresspiegeldruck zu identifizieren, habe ich mich auf zusammengesetzte Karten von Wachstumsextremen zusammen mit Reanalysedaten gestützt. Die zusammengesetzten Analysen ergaben, dass Jahre reduziertem Wachstums mit positiven Anomalien der Meeresoberflächentemperatur im außertropischen bis polaren Nordatlantik einhergingen, die einem multidekadischen AMO-Modus ähneln, der sich mit einem kohärenten Muster im Nordpazifik paart, das auf eine negative dekadische pazifische Oszillation hindeutet. Die Muschelnetze zeigten außerdem, dass zwei Chronologien aus verschiedenen Gebieten – dem nördlichen isländischen Schelf und der Deutschen Bucht in der südlichen Nordsee – nicht mit den beobachteten räumlichen Mustern übereinstimmten. Daher wurden zwei Fallstudien durchgeführt, um die besonderen Merkmale dieser Gebiete zu untersuchen.

Anhand der Chronologie des nördlichen isländischen Schelfs, die auf *A. islandica*-Muscheln aus einer Wassertiefe von 81 bis 83 Metern basiert, befasst sich mein Ansatz speziell mit der Frage, warum Korrelationen mit der Meeresoberflächentemperatur oft nicht die erforderliche statistische Signifikanz aufweisen und als nicht schlüssig angesehen werden. In diesem Beispiel verglich ich das Wachstumssignal mit einem dreimonatigen laufenden Durchschnitt von Temperatur- und Salzgehaltsdaten in verschiedenen Wassertiefenschichten. Ich fand signifikante Korrelationen mit dem unterirdischen Wasser ab einer Tiefe von 56 m im Sommer und Herbst, während die Korrelationen mit den Oberflächentemperaturschichten um zwei Jahre verzögert waren. Zusätzlich habe ich durch die Berechnung räumlicher Korrelationskarten das Potenzial von *A. islandica* hervorgehoben, thermisch ähnliche Wasserkörper in großem Maßstab zu verfolgen. Als nächstes habe ich eine unveröffentlichte Wachstumschronologie von *A. islandica* aus Helgoland in der südlichen Nordsee gemeinsam mit zusammengesetzten Karten verwendet, um zu untersuchen, welche atmosphärischen Muster mit extremen Wachstumsereignissen verbunden sind. Die Ergebnisse deuten darauf hin, dass das Wachstum von *A. islandica* in Jahren mit einer positiven Polarität der NAO im Winter, gefolgt von einer verstärkten atmosphärischen Blockierung über den Britischen Inseln im Frühjahr, reduziert ist. Die Frühjahrsblockierung könnte auch mit der Winterblockierung im Nordpazifik zusammenhängen. Das regionale atmosphärische Muster wirkt sich auf den Zeitpunkt der Phytoplanktonblüte im Frühjahr aus und führt zu einer Verzögerung bei der Verfügbarkeit der für das Wachstum notwendigen Nährstoffe.

Durch die Überbrückung von Forschungslücken zwischen dem Gebiet der Sklerochronologie und der Klimadynamik werden in dieser Arbeit verschiedene Aspekte des Potenzials des *Arctica islandica* als Klimaarchiv im Nordatlantik untersucht. Ob die Entschlüsselung des gemeinsamen Wachstumssignals über Muschelnetzwerke hinweg (**Paper I**) oder die Untersuchung der Beziehung zwischen räumlicher Tiefe und unterirdischen Temperaturschwankungen (**Paper II**), oder die Aufdeckung von Verbindungen zu atmosphärischen Telekonnektionen und Blocking-Frequenzen (**Paper III**), jede Studie liefert spannende Erkenntnisse, die sowohl für paläo- als auch für zukunftsorientierte Studien relevant sind.

Contents

1

Introduction

With the aim of acquiring environmental data preceding the observational period (1850-present), researchers have relied on a variety of biotic and abiotic proxy data sources. These include biotic proxies such as microfossil assemblages (e.g, planktic and benthic foraminifera, ostracods, diatoms, radiolaria, dinoflagellates), corals, tree rings, mollusks, coralline algae, and fish otoliths, each providing unique insights into past environmental conditions either through their growth patterns and/or chemical compositions (i.e., isotopes and elemental ratios). Abiotic proxies retrieved from cave deposits such as speleothems, ice cores and sedimentary cores are attractive sources of paleoclimate information as these do not have a biological fingerprint, and can provide deep-time continuous records of past climate variations and abrupt climate shifts (e.g., Dansgaard et al., 1993; Bar-Matthews et al., 2000; Andersen et al., 2004; Lisiecki and Raymo, 2005; Jouzel et al., 2007; Wang et al., 2008; Barker et al., 2011; Ünal-İmer et al., 2015; Baker et al., 2015).

In marine paleoclimate research, sedimentary cores and foraminifera assemblages serve as primary sources of proxy data and information about paleotemperatures (Zachos et al., 1994; Dowsett et al., 2005; Pearson et al., 2007; Kim et al., 2008; Andersson et al., 2010; Leutert et al., 2020) and seawater composition (Lear et al., 2000; Waelbroeck et al., 2002). No proxy source is without its challenges, and one important caveat, among other, is the lack of high-resolution necessary for precisely identifying and understanding short-term climatic processes. On the other hand, corals, coralline algae and mollusks serve as excellent high-resolution proxy sources due to their inter- and intra-annual banding patterns in their carbonate-precipitated exoskeletons, which allow for precise dating and the detection of climate anomalies (e.g., Rimbu et al., 2003; Felis et al., 2009), and both short- and long-term internal modes of climate variability (Felis et al., 2000; Cobb et al., 2001; Rimbu et al., 2001; Schöne et al.,

2003a; Wanamaker et al., 2008; Felis et al., 2010; Halfar et al., 2011; Hetzinger et al., 2012; Lohmann and Schöne, 2013; Cobb et al., 2013; Mette et al., 2021). Additionally, coralline algae provides unique information about sea-ice variability on decadal to sub-decadal scales (Halfar et al., 2013) and primary production (Chan et al., 2017), whereas corals and mollusks can offer a detailed record of paleo-seasonality (Kobashi and Grossman, 2003; Ivany et al., 2004; Beierlein et al., 2015; Brocas et al., 2016; Mangerud and Svendsen, 2018). Hence, marine calcifiers have an inherent advantage over other proxy sources due to their ability to provide detailed and precise records about past oceanographic conditions.

In recent times, the interplay of natural climate variability and anthropogenic influences has accelerated the rise in global mean temperatures, leading to significant changes in ocean biogeochemistry (see Doney, 2010; Gruber, 2011). The current change in ocean conditions, as it is a crucial climate component responsible for absorbing one third of the anthropogenically-derived emissions (Sabine et al., 2004), poses a risk to carbonate-precipitating marine organisms and biodiversity through the effects of ocean warming, acidification and deoxygenation (Doney et al., 2009; Gruber, 2011; Heinze et al., 2021). Open ocean warming is becoming a global occurrence: the number of marine heatwaves has increased twofold for the satellite observation period 1982-2016 CE (Frölicher et al., 2018). Coastal areas are more profoundly affected by deoxygenation than the open ocean (Gilbert et al., 2010) due to factors such as warming, stratification, eutrophication, and microbial activity, leading to the global spread and increase of hypoxic regions (Diaz and Rosenberg, 2008).

A critical and classic example is the increase in frequency and magnitude of tropical coral reef bleaching events since the 1980s (Brown, 1997; Berkelmans and Oliver, 1999; Sully et al., 2019). The findings of Frieler et al. (2013) are concerning, suggesting that global warming should be limited to 1.1 to 1.4 °C above pre-industrial levels to protect at least 50 % of tropical coral cover from degradation. On the other hand, some modelling studies are more optimistic. These indicate that reducing wastewater pollution and other human activities can help coral reefs recover faster after a marine heatwave (Gove et al., 2023). Additionally, larger semidiurnal internal tides coupled with a shallower seasonal thermocline can enhance mixing with colder, deeper waters, providing thermal refugia in some regions (Storlazzi et al., 2020).

Tropical ecosystems are not the only ones susceptible to oceanic warming and seawater changes driving geographical shifts (e.g., Rodriguez-Ruano et al., 2023);

high-latitudes are also affected by this spatial reorganization of core habitats (Hodapp et al., 2023). Similar to coral reefs, the increased frequency and intensity of marine heatwaves and anomalously warm pools (e.g., Bond et al., 2015; Di Lorenzo and Mantua, 2016) in intertidal zones at higher latitudes have led to higher mortality rates among mollusks and other organisms that rely heavily on these ecosystems for survival (Soon and Zheng, 2019). Notably, ecological impacts and economic losses were observed during the North American West Pacific Blob of 2013-2015 (Cavole et al., 2016) and the 2012 northwest (NW) Atlantic heatwave (Mills et al., 2013).

The experimental study of Li et al. (2015) on *Mytilus edulis* – a bivalve species of economic and gastronomic importance – showed that increasing water temperatures exacerbate the impact of seawater acidification, corroborating Hiebenthal et al. (2012) observations on the same species. Specifically, a decrease of 0.3 pH units (from 8.1 to 7.8), coupled with an increase in temperature (e.g., from 19 °C to 22 °C and 25 °C), leads to significant changes in the biomineralization pathway of the organism. Such changes include a lower Ca/Mg ratio and calcification rate, as well as alterations in the crystallographic orientation within the shell microstructure. Additionally, these changes affect the shell's breaking force, making bivalves more susceptible to predators.

Amidst such climatic changes, there is an increased interest in researching resilient marine organisms capable of withstanding environmental pressures (see overview by Gazeau et al., 2013), while also providing reliable long-term records essential for paleoenvironmental reconstructions. In this context, *Arctica islandica* (*A. islandica*; Linnaeus, 1767) emerges not only as proven unique climate archive (Schöne, 2013), but also as a resilient one (see **A versatile and resilient bivalve species** section). This bivalve species serve a dual purpose by offering reliable reconstructions (e.g., seasonality, mean annual temperature, mean annual temperature range, salinity fluctuations and so on) from analogous past environments (e.g., Beierlein et al., 2015; Mangerud and Svendsen, 2018; Trofimova et al., 2021) and recent past (Wanamaker et al., 2008; Butler et al., 2013; Reynolds et al., 2017, 2018; Poitevin et al., 2019; Mette et al., 2021), while also capturing climatic signals and offering insights into the large-scale atmospheric and oceanic interactions. *Arctica islandica* is perhaps the most studied bivalve species of the North Atlantic region, and yet, very few studies have effectively connected growth records (see **Growth as environmental proxy records** section), including extreme growth events (notably Wanamaker et al., 2019) with large-scale oceanic and atmospheric modes of variability (Lohmann and Schöne, 2013)

and their corresponding spatial anomaly patterns (see **Motivation**).

Large-scale climate modes such as the Atlantic Multidecadal Oscillation (AMO) (Delworth and Mann, 2000; Dima and Lohmann, 2007), Pacific Decadal Oscillation (PDO) (Mantua et al., 1997), El Niño Southern Oscillation (ENSO) (Alexander et al., 2002), along with atmospheric teleconnections (Barnston and Livezey, 1987) like the North Atlantic Oscillation (NAO) (Hurrell, 1995) and the Pacific-North American (PNA) pattern (Wallace and Gutzler, 1981), operate on interannual, interdecadal to multidecadal time scales, influencing climatic trends and weather patterns. These modes of natural variability are particularly valuable for reconstructing past climates, regional climate anomalies, ecosystem responses, and understanding the interplay between them for forecasting future climate scenarios.

Our understanding of how natural variability interacts with anthropogenic forcing is also a complex and unclear topic. Swanson et al. (2009) have examined the role of natural climate variability during the 20^{th} century, and identified periods where interdecadal variability significantly influences global mean surface temperature. This underscores the importance of identifying markers of natural variability. The origin of an internal multidecadal oscillatory mode in the Atlantic basin is also debated (e.g., Mann et al., 2021), despite its observation in models and statistical methods (e.g., Delworth and Mann, 2000; Knight et al., 2005; Dima and Lohmann, 2007, 2010; Dima et al., 2022) as well as terrestrial (e.g., Gray et al., 2004; Knudsen et al., 2011; Wang et al., 2017) and marine proxy data (Moore et al., 2017; Mette et al., 2021).

Swanson et al. (2009) also noted that numerical models cannot reproduce the spatial extent and magnitude of internal circulation modes (e.g., Mann et al., 2020), although Hausfather et al. (2020) found that the majority of models starting from the 1970s were quite accurate in their projections. Recent advancements in modeling, as demonstrated by Su et al. (2018), reveal that incorporating submesoscale turbulence enhances vertical heat transport, leading to surface warming increases ranging from 0.06 to 0.3 °C in extratropical regions. Similarly, Busecke and Abernathey (2019) found that enhancing surface diffusivity in models strengthens the connection to major climate modes such as ENSO, NAO, PDO, and the Dipole Mode Index in the southeast (SE) Indian Ocean. An eddy-resolving ocean model significantly enhances the accuracy of heat fluxes along the trajectory of the North Atlantic Current and offers insight into a lagged subdecadal ocean response to NAO (Huo et al., 2024).

The model advancements mentioned are definitely essential for capturing natural climate variability and improving the accuracy of future projections by more rigorous means (e.g., Jain et al., 2023). Marine proxy records provide additional and valuable insights into ocean circulation patterns, anomalies, and relevant periodicities, which hold the potential to expand our understanding of large-scale anomaly patterns in the natural environment. The native habitat of *A. islandica* in the North Atlantic basin renders it an enticing bio-archive for investigating large-scale climate phenomena that leave a distinct imprint on the North Atlantic climate, and ultimately its growth patterns.

1.1 A versatile and resilient bivalve species

Arctica islandica, also known as the ocean quahog, is a bivalve species (Order: *Venerida*) native to the northern North Atlantic basin, stretching from Nova Scotia to South Carolina on the western margin, and from the Celtic Sea to the Barents Sea and the White Sea on the eastern margin (Figure 1.1A). As the sole surviving species of the *Arcticidae* family (Nicol, 1951), *Arctica islandica* dates back to the Cretaceous period (145-66 Myr; Morton, 2011). This long-term record provides an exceptional opportunity for investigating climatic fluctuations over geological timescales, serving as a significant biogeostratigraphic marker in coastal sedimentary deposits (e.g., Raffi, 1986; Crippa and Raineri, 2015). *Arctica islandica* precipitates aragonite, a metastable calcium carbonate polymorph that is more prone to diagenetic alternations with burial. Casella et al. (2017), in their experimental study, emphasize its resilience up to 175 °C during burial. The oxygen isotopic composition of unaltered sub-fossil samples of *Arctica islandica* is an excellent proxy for seasonal temperature reconstructions (Beierlein et al., 2015; Mangerud and Svendsen, 2018; Trofimova et al., 2021). For instance, during the Holocene Climate Optimum warm period (∼ 10.5-8.2 kyr BP; Dahlgren et al., 2000) *A.islandica* sub-fossil samples reveal a seasonal amplitude of ∼ 12 °C at approximately 30-m depth in a fjord from Svalbard (Beierlein et al., 2015), which is double compared to the present, and 4.5 °C at about 45-50-m depth from Viking Bank, North Sea (Trofimova et al., 2021), closely aligning with present ranges.

Arctica islandica is an adaptable species for inhabiting surface waters (e.g., 5-m depth) to several hundred meters below the thermocline (>100 m) of the coast and continental shelves. *A. islandica* is primarily found in water depths of 25 to 60 m (Nicol, 1951; Dahlgren et al., 2000; Morton, 2011), which may account for the predominance of recent live-collected specimens in this range (for example BOX 1). In the southern parts of the North Sea, *A. islandica* is limited to below 30-40 m depth (Witbaard and Bergman, 2003), where the summer temperatures do not exceed the thermal tolerance of 16 °C for adults (Hiebenthal et al., 2012) and ∼ 20 °C for larvae and juveniles (Mann and Wolf, 1983). The species has adapted to a warmer habitat such as the German Bight, where summer temperatures exceed 16 °C (Witbaard and Bergman, 2003; Epplé et al., 2006). However, a further widening of the temperature tolerance window in the German Bight renders the clam more vulnerable and reduces the presence of spat and juveniles (Witbaard and Bergman, 2003; Basova et al., 2012). Basova et al. (2012)'s research indicates that populations adapted to a broader temper-

ature and salinity range show less thermal stress compared to locations with a narrow temperature window. In such locations (e.g., Kiel Bay, Kattegat and White Sea), the *Arctica islandica* bivalves show minimal response to increasing temperatures, but generally express a higher metabolic rate, and higher concentrations of a cellular stress marker, lipofuscin (Begum et al., 2009; Basova et al., 2012, 2017). The metabolic respiration is lower in *Arctica islandica* compared to other bivalve species (Begum et al., 2009), even in warm-adapted populations of the German Bight (Basova et al., 2012, 2017).

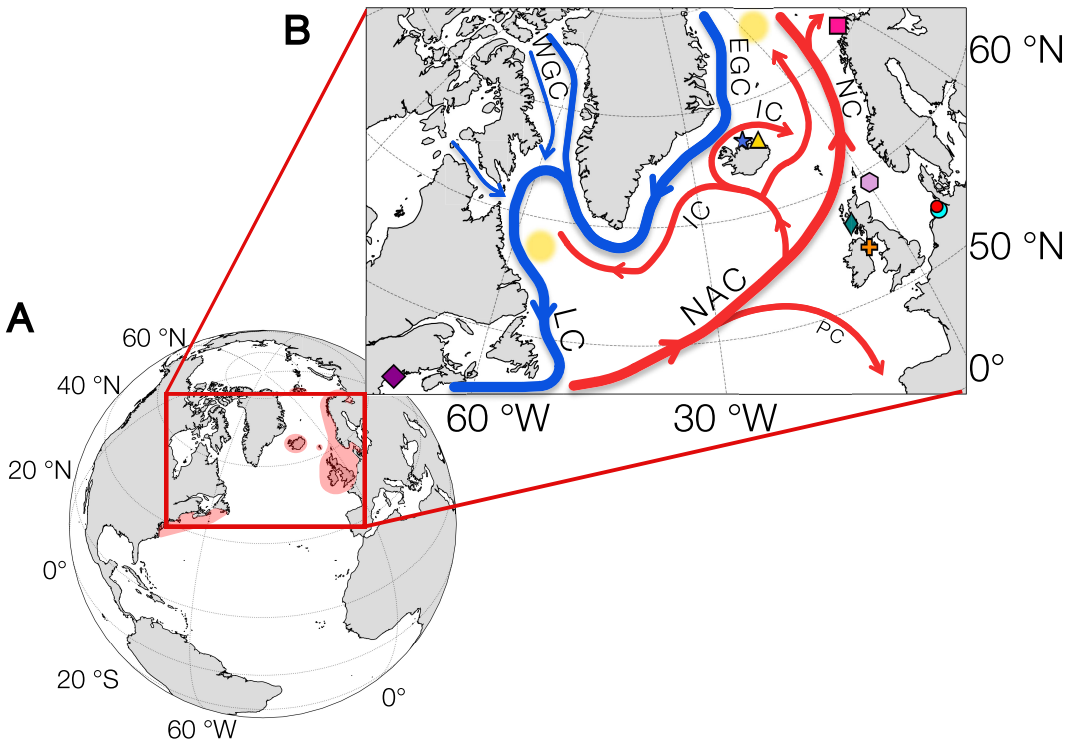

Figure 1.1. Map of the North Atlantic region showing **(A)** present-day abundance (red shade) of *A. islandica* clam species (after Dahlgren et al., 2000; Schöne, 2013) and **(B)** nine multi-centennial growth records (colorful symbols; see BOX 1 and Figure 2.2 for more information about each chronology) used in this research. Dominant ocean currents are shown in panel B. Cold and fresh oceanic currents are highlighted in blue (**EGC**: East Greenland Current; **WGC**: West Greenland Current; **LC**: Labrador Current), whereas warm and saline currents in red (**NAC**: North Atlantic Current; **NC**: Norwegian Current; **IC**: Irminger Current; **PC**: Portugal Current).

The spatial distribution of *Arctica islandica* populations, including those that have become extinct in certain regions, can be explained by factors such as latitude and temperature. Sub-fossil specimens also indicate a broader spatial extent compared to modern specimens (Fig.1 in Dahlgren et al., 2000), with Holocene deposits located in the northern coastal parts of Newfoundland

and Labrador, SW Greenland (Funder and Weidick, 1991), northern Siberia, and Svalbard (Beierlein et al., 2015; Mangerud and Svendsen, 2018). Populations from the Mediterranean region are thought to have become extinct during Holocene Climate Optimum ($\sim$ 9.8 kyr), when the late summer arctic temperatures were about 6 °C higher than present (Mangerud and Svendsen, 2018). At present, the species is commonly found in the shelf areas surrounding Iceland (Thórarinsdóttir and Einarsson, 1996; Butler et al., 2013; Lohmann and Schöne, 2013; Marali and Schöne, 2015; Mette et al., 2023), the Faeroe Islands (Bonitz et al., 2018), the North Sea (Witbaard et al., 1994; Witbaard and Bergman, 2003; Schöne et al., 2005d), Western Baltic (Brey et al., 1990; Stemmer et al., 2013), White Sea (Isachenko et al., 2013) and more recently, around Svalbard (Dahlgren et al., 2000, and references therein), showcasing the warming aspect of the present climate.

Salinity has a lesser effect on growth and metabolic processes as long as oceanic conditions prevail, and temperature remains in the optimal range of 5-12 °C (Witbaard et al., 1998; Hiebenthal et al., 2012). Adult and juvenile specimens showed resistance to ocean acidification conditions in experimental studies (Stemmer et al., 2013; Liu et al., 2023). However, the experimental observations by Hiebenthal et al. (2012) and Begum et al. (2010) indicate that mortality increases with decreasing salinity ($<$ 15 PSU), particularly in cold waters (4 °C). In regard to alkalinity conditions, an increase in CO_2 partial pressure, i.e lower pH, is more prominent during summer-autumn months, when surface waters are well-stratified. Yet, laboratory experiments indicate that *A. islandica*'s growth rate and shell microstructure are unaffected by the low pH (Stemmer et al., 2013). In fact, *A. islandica* from the western Baltic is well adapted to these challenging conditions, such as those at a 15-meter depth below the halocline in Kiel Bay (Brey et al., 1990), albeit at the expense of their longevity (Basova et al., 2012).

The clam feeds on suspended material and phytoplankton, as well as organic-rich material found at the interface between sediment – coarse to fine sand, muddy sands – and water (Morton, 2011; Schöne, 2013). *Arctica islandica* is known for its burrowing behaviour of a few days to a week (Taylor, 1976; Abele, 2002) and prolonged anaerobic respiration. Burrowing is possibly a pre-adaptation to inhospitable conditions (e.g., anoxia) and seasonal food input, as well as a factor that contributes to *A. islandica*'s slow metabolism and exceptional ages (Abele, 2002).

Arctica islandica demonstrates resilience under the aforementioned conditions but has been endangered by increased human disturbance of the ocean floor over the past few decades. Demersal fish species that are largely exploited for human consumption, such as Atlantic cod *Gadus Morhua*, among others, feed on the ocean quahog (Brey et al., 1990). Fishing activities by bottom trawling damage and scar the posterior ventral sides which are typically found at the sediment-water interface (Witbaard, 1994; Ragnarsson et al., 2015). Consequently, over-fishing since mid-1970s in the southern North Sea (e.g., Oyster Ground; Witbaard and Bergman, 2003) has reduced *A. islandica* adult and juveniles populations (Witbaard, 1994). Juvenile populations are also more scarce in the Western Baltic Sea as documented by Brey et al. (1990) and Basova et al. (2012), possibly due to the effects of beam trawler fishery and fluctuating environmental conditions. Cyclonic conditions also add to factors causing physical disturbance. Thórarindsóttir et al. (2009) documented a mass mortality event among *Arctica islandica* population from Lonafjördur in the northeast (NE) Iceland due to a storm in 2006. The shells were displaced from deeper waters with soft-sediment substrate to shallower areas with hard-bottom substrate, rendering the ocean quahog more vulnerable to predators.

1.2 Growth as environmental proxy records

Rob Witbaard entitled his dissertation „Tree of Sea“ in 1997 – a term originally coined by Thompson and Jones (1977) – to highlight the well-defined growth increments of *Arctica islandica*, resembling the growth rings commonly observed in tree bark cross-sections. The species gained popularity in the 1980s by becoming a commercially important species on the western margin of the North Atlantic (see Figure 1.1A), and also a focal point of research. Initially, research involved counting the external grooves (e.g., Figure 1.2A); however, this method quickly became unreliable as older specimens exhibited crowded and indistinguishable lines, especially toward the ventral margin (see Figure 1.2B). The following decades focused on improving the reliability of dating and cross-dating *Arctica islandica* (Ropes et al., 1982; Schöne et al., 2005a; Scourse et al., 2006; Surge and Schöne, 2013; Black et al., 2019), and debunking the theory that shell growth is unrelated to environmental parameters (e.g., Thompson et al., 1980).

Bivalve growth and development is temperature dependent (Cargnelli et al., 1999). Although spawning occurs consistently throughout the year, without distinct seasonal patterns (see discussion in Schöne, 2013), larval density peaks during late summer and early autumn (Mann and Wolf, 1983). Larval growth rate increases with temperature, requiring a minimum temperature of 11-12 °C, and reaching optimal levels of 14.5 °C (Lutz et al., 1982; Mann and Wolf, 1983). Bivalve larvae exhibit vertical movement to locate the optimal temperature for development (Mann and Wolf, 1983) and drift with the ocean currents before settling into sediment and undergoing metamorphosis into spat.

Biomineralization takes place at the ventral margin, where the mantle tissue (comprising inner and outer epithelium and inner tissue), periostracum, and shell material, derived in the form of ions from the extrapallial space and its fluid, come together (Figure 1.2B). In the early larval stages, the organic periostracum layer is first formed for protection and camouflage providing a template for mineralization, whereas the initial shell layer is composed of granular amorphous calcium carbonate (Marin, 2012). With growth, the shell layer develops into a prismatic outer layer and a nacreous inner shell layer (Figure 1.2B) composed of aragonite. Studies have shown that there are specific epithelial cells which secrete the prismatic and nacreous aragonite layers (Marin, 2012), and that temperature variations impacts the crystallographic orientation (Milano et al., 2017) and size of the biomineral units in *A. islandica* microstructure (Höche et al., 2021, 2022). Bivalves grow their shells by extracting the bicar-

bonate anions and Ca^{2+} cations required for calcification from filtering water, digested food and metabolism, and storing them in the outer epithelium and extrapallial fluid. The inner epithelium of the mantle tissue is in contact with the ambient seawater, whereas the outer epithelium is adjacent to the shell layer (Marin, 2012), and together with the extrapallial fluid supersaturated in Ca^{2+}, HCO_3^- and other ions, are responsible for secreting new shell layers (see eq. (1.1)). Bivalves also secrete an organic protein-based template which guides the build-up of aragonite biomineral units (Saleuddin and Wilbur, 1983). Growth lines (Figure 1.2B) are deposited in late autumn and winter, depending on bivalve location relative to the thermocline after seasonal temperature maximum (Schöne, 2013), and commonly reflect annual periodicities, although sub-annual periodicities have also been observed (Schöne et al., 2005c). The space between two growth lines (dark delineations under the microscope) is referred to as a growth increment or a growth band. The rate of growth, as observed through growth increments, reflects whether environmental conditions are beneficial or not, with narrower growth increments indicating less favorable environmental factors.

$$Ca^{2+} + HCO_3{}^- \longrightarrow CaCO_3 + H^+ \tag{1.1}$$

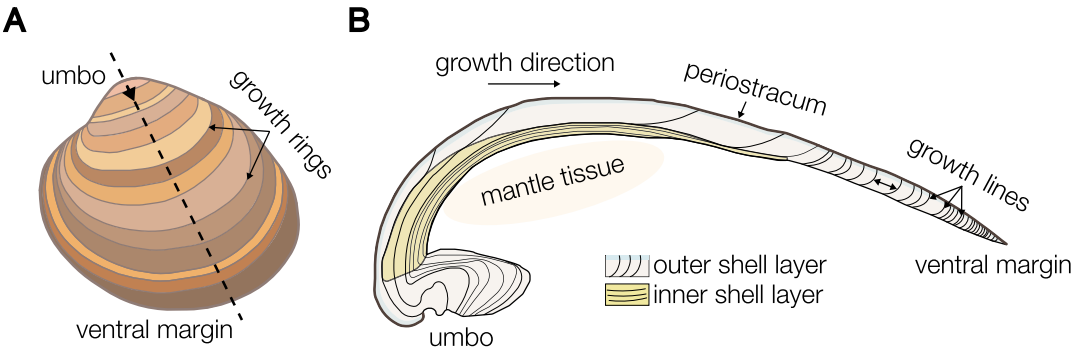

Figure 1.2. Shell morphology of *Arctica islandica*. **(A)** Illustration of the anterior left valve showing the external grooves and growth rings and its specific brown colouring. The umbo represents the older section, whereas the ventral margin is the youngest portion of the shell. The dashed line shows the axis of maximum growth, typically used to cut the valve. **(B)** Schematic drawing of the aragonite shell layer in *Arctica islandica* as seen from a cross-section. The outer shell layer and hinge plate are used in the field of sclerochronology to determine growth patterns and the isotopic composition of the carbonate. After Schöne (2013).

After field collection, the mantle tissues are removed, and the aragonite shell valves are cleaned, dried, embedded in epoxy and sectioned along the maximum growth axis (Figure 1.2A). Extraction of carbonate material for isotopic analyses is performed by micro-milling and/or micro-drilling the outer shell layer

and hinge plate (the area with the umbo; see Figure 1.2B). For visual inspection under a polarizing light microscope of the annual growth layers, growth increments, and other micro-growth structures, the embedded shell is either stained in Mutvei's solution (Schöne et al., 2005a) and/or the surface is etched and acetate peels are taken (Ropes, 1984). Sub-fossil specimens in which the time of death is unknown are dated by radiocarbon dating (e.g., Stott et al., 2010; Scourse et al., 2006) and amino-acid racemization techniques (Miller and Brigham-Grette, 1989; Marchitto et al., 2000; Demarchi et al., 2011).

The resulting growth chronologies are detrended to remove the ontogenic growth, allowing a clearer analysis on the environmental factors influencing growth rate (examples of detrending functions commonly used can be found in section 2.1 and Figure 2.2 of Paper I), and averaged and standardized (see example in section 3.1 of Paper III). However, detrending can affect the lower frequency amplitudes in the frequency domain, potentially removing or distorting information about slow periodic processes in bivalves and climate signals (Cook et al., 1995). Afterwards, the individual chronologies are stacked and aligned temporally using software products (e.g., Grissino-Mayer, 2001) for cross-dating (Black et al., 2008, 2016). The resulting composite chronology is checked for robustness (EPS>0.85) using the Expressed Population Signal (EPS) and Rbar (the average of inter-series correlation) by Wigley et al. (1984).

Additional information on the bivalve biomineralization processes are found in Saleuddin and Wilbur (1983) and Marin (2012) and composite chronology construction in Schöne (2013).

1.3 Motivation

A substantial effort is dedicated to preparing live-collected and sub-fossil bivalve shells for the counting of growth increments across multiple specimens, cross-dating and constructing master chronologies. These processes, as described by Thompson et al. (1980), are "time-consuming", often constraining research to local and regional reconstruction of environmental parameters, with insufficient time allocated for exploring large-scale climatic patterns. Thanks to the efforts of many researchers and their working groups, master chronologies of *Arctica islandica* spanning centuries have become readily accessible. By leveraging existing resources, I embark on further research by revisiting long-term chronologies, now directing the focus towards extremes and large-scale climate phenomena. In BOX 1, the reader can find an overview of the master chronologies used in my research. The visual representation is found in Figure 2.1.

BOX 1. The location, water depth and chronology span of *Arctica islandica* records (map symbols) used in this thesis

#	Lon**	Lat**	Water depth (m)	Location	Period	Reference	Thesis location
■	24.09	71.06	5-10	Ingøya island, N Norway, southern Barents Sea	1449-2012	Mette et al. (2016, 2021)	Chapter 2
●	7.75	53.8	15-20	Spikeroog island, German Bight, North Sea	1840-2002	Epplé et al. (2006)	
*♦	-6.4	56.63	25-55	Tiree Passage, NW Scotland	1805-2010	Reynolds et al. (2013)	
▲	-14.92	66.27	~ 30	NE Iceland	1495-2003	Lohmann and Schöne (2013)	
✚	-5.5	54.2	35-70	Irish Sea	1516-2004	Butler et al. (2009b, 2010)	
◆	-69.75	43.71	38	Gulf of Maine, NW Atlantic Ocean	1762-2013	Griffin (2012); Wanamaker et al. (2019)	
●	7.79-7.82	54.15	40	Helgoland island, German Bight, North Sea	1767-2004	Bauer (2011)-unpublished	Chapter 4
✖	-69.48	40.47	66	Nantucket Shoals (site 315)	1888-1992	Marchitto et al. (2000)	Chapter 2
★	-18.19	66.53	81-83	Grimsey island, N Iceland	649-2005	Butler et al. (2013)	Chapter 2,3
⬢	0.29	58.99	> 125	Fladen Ground, North Sea	1545-2001	Butler et al. (2009a); Estrella-Martínez et al. (2019)	Chapter 2

* Species: *Glycymeris glycymeris* ** The longitude (- for °W; + for °E) and latitude (°N) are given in decimal degrees.

One of the key motivations behind integrating centennially-long chronologies was to achieve a comprehensive overview over the collective growth signal across the northern North Atlantic basin. This would allow for understanding whether the collective growth-climate signal is spatially and temporally coherent, and what large-scale oceanic and atmospheric patterns and teleconnections are associated with the extreme indices obtained. The network idea was conceived while keeping in mind the framework of the PALEX project, and specifically aimed at addressing the absence of bivalve growth-based networks in the field of sclerochronology. This synthesis **(Paper I/ Chapter 2)** was intended to address inquiries raised by Trofimova et al. (2020) concerning large-scale ocean-atmosphere interactions and the potential integration of sclerochronological data

in paleoclimate reanalyses and proxy-based assimilation approaches.

The synthesis paper showed that while most chronologies adhere to the common growth signal obtained, two chronologies from specific regions – namely, the deeper waters in northern Iceland and the shallow environment of the German Bight in the southern parts of the North Sea – stood out notably, being characterized by negative loading indicators (further details provided in **Chapter 2**; see Figure 2.3). An interesting aspect about the chronology from a water depth of 81-83 meters in the North Icelandic shelf (Butler et al., 2013) was that it contrasted with the chronology of Lohmann and Schöne (2013). The latter chronology was based on bivalves collected from a nearby region, albeit at a shallower water depth (i.e., 30-m). Hence, I was curious to investigate the sensitivity of the *Arctica islandica* growth signal to potentially depth-dependent temperature and salinity variations, which eventually led to the study described in **Paper II/ Chapter 3**. Although the concept itself may seem intuitive, the research findings contributed to a deeper understanding of why certain correlations often fail to attain significance with sea-surface temperature, thereby enriching the rationale behind such occurrences.

For the second region, I turned to an unpublished chronology of *Arctica islandica* from the Helgoland waters created by Florian Bauer in his bachelor study of 2011. Similar to the Spikeroog chronology of Epplé et al. (2006) from southern North Sea (used in **Chapter 2**; BOX 1), the Helgoland chronology presented well-defined growth increments of 5 to 8-year periodicity which unmistakably resonates with the NAO periodicity. Such periodicity is often reported in various studies from the North Sea in the form of a correlation coefficient with NAO and spectral analyses, however without delving deeper. In **Paper III/ Chapter 4**, I explicitly explore the connections between growth and atmospheric anomalies, as well as their relationship with atmospheric teleconnection indices, with the aim of extracting information that may not be readily accessible through other proxies and observational data. In BOX 2, the reader can find the research questions tailored for each of the three studies comprising this doctoral thesis.

BOX 2. Research Questions

RQ.1	Which large-scale climatic phenomena are associated with the common growth signal of a bivalve-based network from the northern North Atlantic? Which large-scale phenomena particularly stand out when analyzing extreme growth indices?	Chapter 2/ Paper I
RQ.2	Does *Arctica islandica* exhibit a depth-dependent growth response to seasonal fluctuations in subsurface water temperature and salinity, necessitating consideration in correlation analyses? And if so, is it intertwined with large-scale oceanic circulation patterns?	Chapter 3/ Paper II
RQ.3	Is there a discernible connection between the extreme growth indices observed in *Arctica islandica* and large-scale atmospheric patterns, particularly synoptic atmospheric blocking, in a region prone to such influences as the North Sea?	Chapter 4/ Paper III

2

Paper I

Unveiling extreme growth responses from a marine network of *A. islandica* shell growth records

RQ.1	Which large-scale climatic phenomena are associated with the common growth signal of a bivalve-based network from the northern North Atlantic? Which large-scale phenomena particularly stand out when analyzing extreme growth indices?

This research study has been submitted to the *Palaeogeography, Palaeoclimatology, Palaeoecology* journal and is currently *under review pending major revisions.*

The supplementary material accompanying this paper is found in **Appendix A**. The manuscript version is found below.

Author contributions:

DEC designed the study, conducted statistical analyses, wrote the manuscript and produced all figures. TB, GL and MI contributed with manuscript feedback. MI supervised.

Paper I

Unveiling extreme growth responses from a marine network of *A. islandica* shell growth records

Diana E. Caldarescu[1], Thomas Brey[1,2,3], Gerrit Lohmann[1,4] and Monica Ionita[1,5,6]

[1]Alfred Wegener Institute, Helmholtz Centre for Polar and Marine Research (AWI), Bremerhaven, Germany [2]Helmholtz Institute for Functional Marine Biodiversity, University of Oldenburg (HIFMB), Oldenburg, Germany [3]Department of Functional Ecology, University of Bremen, Bremen, Germany [4]Department of Environmental Physics, University of Bremen, Bremen, Germany [5]Emil Racovita Institute of Speleology, Romanian Academy, Cluj-Napoca, Romania [6]Faculty of Forestry," Stefan cel Mare" University of Suceava, Suceava, Romania

Abstract

The longevity and well-defined growth increments of the bivalve species *A. islandica* make it a reliable source for high-resolution environmental reconstructions. However, only a limited number of studies employ networks of bivalve-based proxy records to investigate the connection between growth and climate on a large-scale rather than at a regional level, and even fewer explore extreme growth responses within a climatic context. In this study, we seek to understand if the shared growth signal in bivalve networks from the northern North Atlantic region is clear enough among the principle component analysis (PCA) strategies employed, and whether the years with extreme growth are related to large-scale climatic anomalies. The PCA strategies show a coherent leading time component, relatively stable in time and space, however, some incongruities do occur, either due to methodology or from strong regional influences in some chronologies. The low extremes in the shared growth signal exhibit greater consistency compared to the high extremes. They are typically associated with long-term positive temperature anomalies in the North Atlantic, which extend into subtropical regions and are complementary to cyclonic conditions in the central areas of the northern North Atlantic basin. Although these features are generally consistent across the networks and time frames used, we notice that in the North Pacific, the temperature anomalies change patterns in the 1900-2001 period. We conclude that growth extremes in *A. islandica* bivalve specimen are linked to coherent large-scale climate modes, and show potential for obtaining information beyond the instrumental period.

Keywords: *A. islandica*; growth record; growth extreme; Atlantic Multidecadal Oscillation; Pacific Decadal Oscillation; North Atlantic.

1. Introduction

Sclerochronology can be used to retrieve meaningful climatic signals from multi-species, multi-proxy records across a vast geographical area (Trofimova et al., 2020). Although the idea of multi-proxy network is interesting, and it shows its potential, in particular for regional-scale reconstructions and for identifying local climate drivers (e.g., Black, 2009; Black et al., 2009, 2014), it is yet difficult to create one without having a complete understanding about the large-scale signal captured by each species' group or proxy's type. Discrepancies can occur, for instance, between tree- and shell-rings in locations where oceanic conditions are strongly present on land (e.g., Piermattei et al., 2017).

With the exception of a couple of studies (e.g., Butler et al., 2009; Holland et al., 2014; Reynolds et al., 2018; Peharda et al., 2019), bivalve-based proxy networks are limited in number compared to, for example, tree-ring (e.g., Cook et al., 1998, 2002; D'Arrigo et al., 1999, 2001; Gray et al., 2004; Frank and Esper, 2005; Klippel et al., 2019; Balting et al., 2021) and coral (e.g., Charles et al., 2003; Tierney et al., 2015) networks. Moreover, networks of composite chronologies that target shell growth increments are greatly underrepresented. It is often the case that internal modes of oceanic variability are often reconstructed from terrestrial-based networks (e.g., D'Arrigo et al., 1999; Biondi et al., 2001; Gray et al., 2004; Wang et al., 2017) instead of marine-based ones.

The North Atlantic basin is, undoubtably, a key region for developing bivalve-based networks for instance using *Arctica islandica* (*A. islandica*; Linnaeus, 1767) species. Because *A. islandica* is abundantly distributed and reaches multi-centennial lifespans in the polar and subpolar waters of the North Atlantic region (e.g., $>$ 500 years; Butler et al., 2013), it yields the longest composite growth chronologies. The North Atlantic basin is also prone to large-scale ocean circulation changes such as the Atlantic Meridional Overturning Circulation (AMOC) (Rahmstorf et al., 2015; Dima et al., 2021), poleward shift of subtropical and subpolar ocean gyres (Yang et al., 2020; Dima et al., 2022), and substantial sea ice decline starting with 1970s (Walsh and Chapman, 2001). Considering this dynamical aspect, a marine proxy network might be able capture a large-scale climatic signal beyond pre-industrial period, which, in turn, it would allow for a coherent common signal to be retrieved and, ideally, used to evaluate extreme responses to past conditions.

In the Gulf of Maine, a region undergoing rapid warming, shell growth reduc-

tion in the *A. islandica* was associated with a negative Pacific Decadal Oscillation (PDO) phase, and to some extent the variability of El Niño-Southern Oscillation (ENSO) (Wanamaker et al., 2019), while an Atlantic Multidecadal Oscillation (AMO) fingerprint has been observed in other sclerochronological studies (Wanamaker et al., 2008; Holland et al., 2014; Poitevin et al., 2019). A more recent study by Mette et al. (2021) has revealed that *A. islandica* records from the southern Barents Sea captures the AMO signal for the past five centuries. In another example, Caldarescu et al. (2021) have shown that *A. islandica* growth links water bodies of similar thermal properties at large-scale, suggesting a shared response to intrinsic modes of variability. All the aforementioned studies indicate that there is a high potential in *A. islandica* for detecting oceanic circulation patterns and environmental signals.

Our study relies on long-term growth records primarily of the *A. islandica* bivalve species. Depending on the chronology length, we combine these records to create spatial networks that cover both an extended period (1764-2001 CE) and a more recent time frame (1900-2001 CE). Using nested principle component analysis and adopting similar strategies as those employed by Reynolds et al. (2018), our objective is to evaluate the clarity of the shared growth signal across various strategies and networks, assessing its ability to coherently depict anomalies in atmospheric-oceanic interactions. It is essential to explore the large-scale aspect behind such anomalies, not only because growth signal is complex and often linked to regional climate influences, but also because it can conceal valuable information. This study provides a synthesis of the shared growth signal in bivalve shells from the northern North Atlantic, shedding light on the possible large-scale anomalies in the sea surface temperature and pressure associated with extreme growth responses.

2. Materials and Methods

2.1. Composite chronologies

Composite chronologies or master shell chronologies are created by using the growth increments of multiple bivalve shells from the same species, collected from the same or different depths at a single location and cross-dated. In this study, we primarily used annually-resolved growth chronologies based on *Arctica islandica* species because of its prolonged lifespan allowing oceanographic reconstructions in key locations of the northern North Atlantic (Figure 2.1, Figure 2.2), i.e. along pathways of major ocean currents: warm, nutrient-rich North Atlantic Current controlling the east Atlantic climate, and cold, fresh Labrador

Current influencing the Iceland region and western side of the Atlantic.

We have also considered shorter composite chronologies (marked with an asterisk in Figure 2.2) in the same geographical region to increase the number of chronologies in the observational period 1900-2001. One of these shorter chronologies is based on a different bivalve species, *Glycymeris glycymeris* (Linnaeus, 1758), deemed equally advantageous in reconstructions akin to *A. islandica* (Brocas et al., 2013; Reynolds et al., 2013, 2017). Another chronology, namely the Nantucket Shoals chronology terminates in 1992, and as such, its use is limited (see more details in section 2.3). Because we want to incorporate as many chronologies as possible, we included the German Bight chronology for the observational period in spite of its decreased population strength and lack of coherent climate signal (Epplé et al., 2006).

These chronologies not only vary in length, location and depth, but also preprocessing methodology (Figure 2.2). Detrending methods such as negative exponential function (NE), spline smoothing (Sp) or regional curve standardization (RCS) are commonly used to remove the ontogenic growth present in the first few years of bivalves' life. As a consequence, the detrending method used hampers the recoverable long-term climatic signal whilst removing the low frequency biological noise. At this point, we have no compelling evidence to suggest that the detrending method plays a significant role in detecting the overall climatic signal. For instance, Lohmann and Schöne (2013) generated spline and power detrended chronologies, and while spline-detrended captured more high-frequency variance, the climatic fingerprint remained similar. In this paper, we relied on the power-detrended chronology for its decadal variability. Additionally, we utilized regional curve standardization-detrended chronologies, where available, such as for the Irish Sea and Grimsey Island series, due to their ability to preserve multi-centennial signals (Esper et al., 2003).

All datasets chronologies used in this study are publicly available from the NOAA's National Climatic Data Center and PANGAEA database.

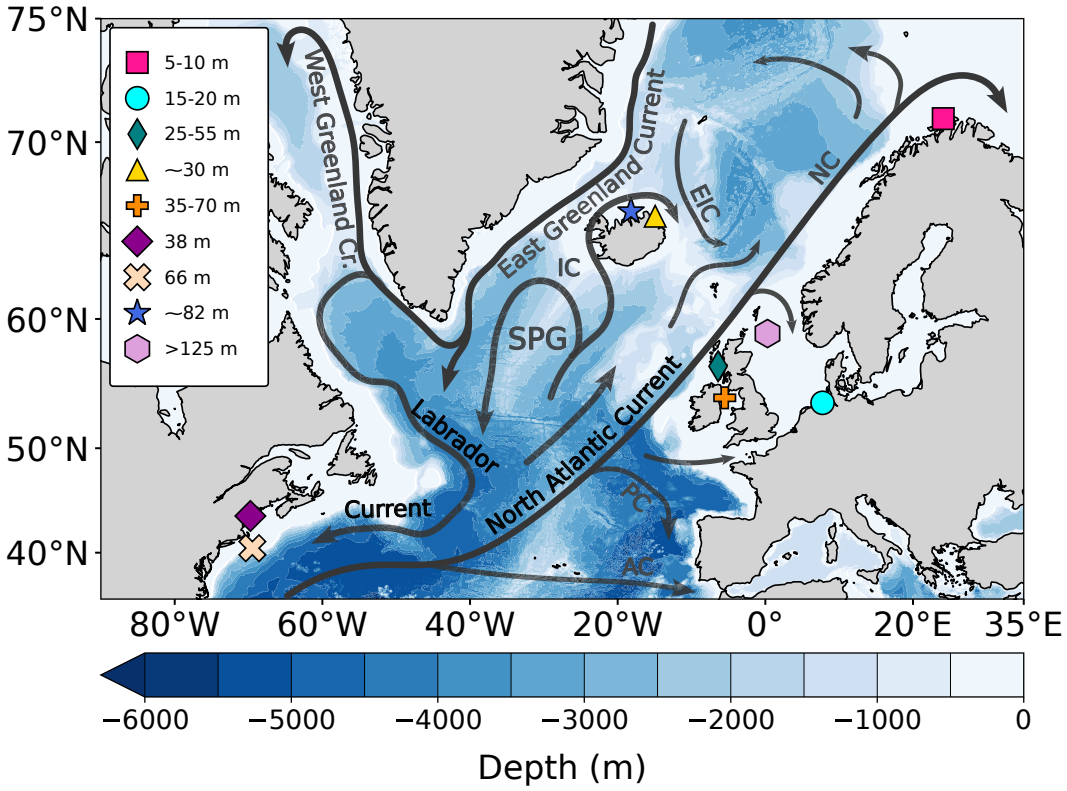

Figure 2.1. Bathymetric map of the northern North Atlantic basin (35°N – 75°N, 90°W – 35°E). The symbols show the sampling site and water depth of each master chronology used in this study (see more details in Figure 2.2). Major warm water currents are marked, including the North Atlantic Current and its branches: **AC** (Azores Current), **PC** (Portugal Current), **IC** (Irminger Current), and **NC** (Norwegian Current). Cold-water currents are also indicated: the East Greenland Current with its eastern branch, East Icelandic Current (**EIC**), as well as the West Greenland Current and the Labrador Current. **SPG** refers to the subpolar gyre. Gridded bathymetric data was obtained from The General Bathymetric Chart of the Oceans (GEBCO).

	Collection Site			Period	Detrending method	Reference
	Water depth (m)	*Location*	*Nr. of specimens*			
	5-10	Ingöya island, northern Norway, southern Barents Sea	5 live-collected and 34 dead specimens of *A. islandica*	1449-2012	negative exponential function	Mette et al. (2016, 2021)
*	15-20	German Bight, southern North Sea	8 live-collected specimens of *A. islandica*	1840-2002	7-yr moving average filter and single exponential smoothing	Epplé et al. (2006)
*	25-55	Tiree Passage, NW Scotland	14 live-collected specimens of *Glycymeris Glycymeris*; 188 dead valves	1805-2010	adaptive power transformation in combination with negative exponential detrending	Reynolds et al. (2013)
	~ 30	NE coast of Iceland	11 live-collected specimens of *A. islandica*	1495-2003	power function and cubic smoothing spline	Lohmann and Schöne (2013)
	35-70	Irish Sea	109 shells of *A. islandica*	1516-2004	adaptive power transformation in combination with negative exponential function, cubic smoothing spline and regional curve standardization (comparison)	Butler et al. (2009b, 2010)
	38	Seguin Island, Gulf of Maine, NW Atlantic Ocean	over 200 live- and dead-collected specimens each of *A. islandica*	1761-2013	smoothing spline	Griffin, (2012); Wanamaker et al. (2019)
**	66	Nantucket Shoals (site 315)	7 live-collected specimens of *A. islandica*	1888-1992	smoothing spline	Marchitto et al. (2000)
	81-83	Grimsey island, North Icelandic Shelf	29 live and dead specimens of *A. islandica*	649-2005	negative exponential function and regional curve standardization (comparison)	Butler et al. (2013)
	>125	Fladen Ground (site B), northern North Sea	16 specimens (5 adults from Butler et al. (2009a)) and two juveniles	1545-2001	adaptive power transformation and smoothing spline	Butler et al. (2009a); Estrella-Martínez et al. (2019)

Figure 2.2. Sampling location and further details about the annually-resolved composite chronologies used in this study. NB. (*) refers to two shorter composite chronologies used in the PCA analysis for the 1900-2001 CE period.(**) The Nantucket Shoals chronology is the shortest (until 1992), and used only for validating the PCA analysis in the 1900-2001 analysis period.

2.2. Climate data

Gridded climate reconstructions prior to 1900 are scarce, however Tardif et al. (2019) introduced a paleo-reanalysis project (Last Millennium Reanalysis; LMR) in which annually-resolved climate field reconstructions are based on proxy data assimilation methodology, thus combining various proxy records (e.g., Emile-Geay et al., 2017), climate models and proxy system models. Here we specifically relied on annually-resolved sea-surface temperature (SST) and sea-level pressure (SLP) reconstructions of 2° x 2° resolution from the LMRv2.1 (Tardif et al., 2019) for our analyses. For the observational period (1900-2001), we used SST at 2° x 2° grid resolution from ERSSTv.5 dataset (Huang et al., 2017), subsurface temperature from the EN4.2.1 dataset (Good et al., 2013) and SLP data with 1° x 1° resolution from NOAA's 20^{th} Century Reanalysis V3 (Slivinski et al., 2019).

Another rationale is to consider available SST-based climate indices to investigate whether coherent patterns of variability are captured by the growth network. For this we considered two important monthly-resolved indices which impact the climate in the Northern Hemisphere on decadal to multidecadal timescales: the Atlantic Multidecadal Oscillation (AMO_{obs}) index based on HadlSST1 dataset starting from 1870 (Rayner et al., 2003) and the Pacific Decadal Oscillation (PDO_{obs}) index spanning from 1900 to present (Mantua et al., 1997).

For reconstructed climate indices, we used the PDO index by Tardif et al. (2019) (PDO_{Tardif}) from the LMR dataset and Biondi et al. (2001) index based on a network of six pine and fir tree-ring records from California. Wang et al. (2017) reconstructed a 1200-year annually-resolved Atlantic Multidecadal Variability (AMO/AMV) index (AMO_{Wang}) based on 46 terrestrial proxy records (tree-rings, ice-cores, historical documents) from the circum-North Atlantic region. We also considered tree-ring and coralline algae AMO reconstructions by Gray et al. (2004) and Halfar et al. (2013), respectively.

2.3. Data analysis

We constructed two bivalve-based networks depending on the number of overlapping composite chronologies (Figure 2.2). The first network (N_{1764}) combines six growth chronologies of *A. islandica* over in the common period 1764-2001. We did not start the network with coeval year 1761 (Figure 2.2) mostly in our

attempt to reduce uncertainties. For instance, Estrella-Martínez et al. (2019) have reported a reduced expressed population signal (>0.85; Wigley et al., 1984) before 1764, attributed to a notable decline between 1752 and 1763. This decline may be due to a decreased abundance of shells and the presence of juvenile specimens, which may have counteracted the signal.

The second network (N_{1900}) comprises eight composite chronologies, six from N_{1764} supplemented by two additional ones (section 2.1; Figure 2.2) in the most recent period 1900-2001 CE. The Nantucket Shoals chronology by Marchitto et al. (2000) was added to N_{1900}, limiting the analysis period to 93 years (referred as N_{1900*}), and as such, it was used only for verifying the N_{1900} signal. The composite chronologies building up the networks are z-normalized/standardized (mean=0, SD=1) according to the analysis period prior to principal component analysis.

The PCA or empirical orthogonal function (EOF) analysis is a common statistical approach used in meteorological and climate studies to linearly reduce the dimensionality of data into a new set of data explaining dominant spatio-temporal modes of variability (Jolliffe, 2005; Wilks, 2019). Here the spatial mode of variability is given by the loading (EOF coefficients; Jolliffe, 2005) of each composite chronology at their respective geographical location (see Figure 2.3) so that a coherent spatial structure is obtained. The resulting time series stemming from each spatial mode, i.e. principle components (PCs), describe the temporal domain (Deser et al., 2010). The selection of appropriate time components for analyses is performed by the highest percentage of explained variance, usually the first EOF modes. However, the time components deemed valid must fulfill the criteria that their eigenvalues are well-separated according to North's Rule (North et al., 1982), and that the separation is significant for an eigenvalue higher than 1 (e.g., Wang et al., 2017; Reynolds et al., 2018).

Reynolds et al. (2018) used a nested PCA approach to extract the large-scale oceanographic conditions by compiling stable oxygen isotope ($\delta^{18}O$) chronologies. Following the recommendations by Reynolds et al. (2018), we apply three nested PCA strategies to the N_{1764} and N_{1900}, respectively. The first strategy (S_1) accounts for the entire analysis period, whereas for the second strategy (S_2) we split the analysis period into two non-overlapping bins of equal lengths, and performed PCA on each half. For the third strategy (S_3), we applied PCA on individual bins of 30-years with 20 years of overlap. Thereafter, the overlapping periods were averaged to create a single time series.

To assess the climatic signal behind extreme growth indices, the leading principle component (PC1) is selected. Extreme high indices are defined as years in which PC1 values were above 90 % of the data (90^{th} percentile), whereas low indices fell below 10 % of the data (10^{th} percentile) (following e.g., Wanamaker et al., 2019). Composite maps of climate data fields were based on years of extreme low and high values according to each network.

To assess the linear relationship between the principle components, as well as with climate indices, we relied on the Spearman correlation coefficient (r_s). To account for autocorrelation (lag-1) in the series when performing statistical significance test, we calculated the effective degrees of freedom (N_{eff}) following the recommendation by Bretherton et al. (1999) and Dima et al. (2005):

$$N_{\text{eff}} = N\frac{1 - r_1 r_2}{1 + r_1 r_2} \tag{2.1}$$

where N is the sample size, and $r_1 r_2$ is the product of the autocorrelation coefficients at lag-1 for the time series used. The statistical significance of the correlations was obtained by considering the N_{eff} and correlation coefficient (r_s), and performing a student's t-test under the null hypothesis of no correlation:

$$t = r_s\sqrt{\frac{N_{\text{eff}} - 2}{1 - r_s^2}} \tag{2.2}$$

All gridded data products used in this study are z-normalized, whereas the SST data is additionally linearly detrended. We calculate the grand mean by averaging the ensemble mean values of the LMR data, which consist of 20 individual ensemble means. All statistical analyses were performed in R and Python. The PCA analysis was performed using "scikit-learn" package in Python and "factoextra" package in R.

3. Results

3.1. Networks' spatio-temporal coherence

The EOF analysis applied to the N_{1764} marine network yields an EOF pattern explaining 24.8 % of the variance (Figure 2.3A). The leading mode (EOF1) resulting from strategy S_1 describes a seemingly quasi-monopolar structure, with one strong negative loading centered north of Iceland (the weaker loading is not significant), and four positive loadings arched from the eastern margin of North

America to the western margin of Europe (Figure 2.3A).

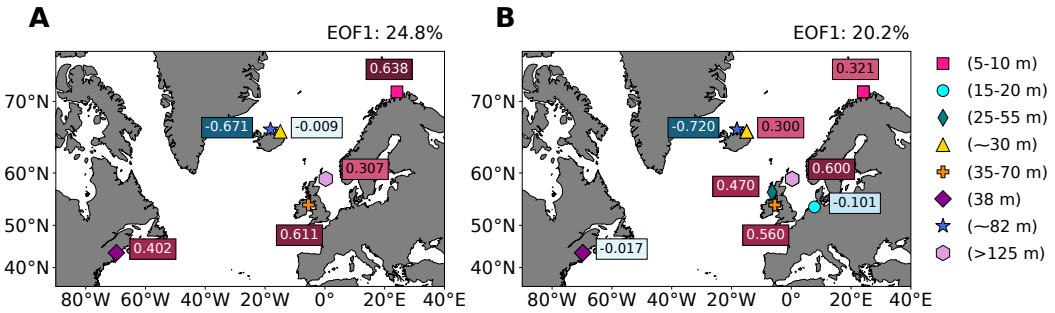

Figure 2.3. Geographical distribution of EOF coefficients (loadings) and their signs for **(A)** N_{1764} and **(B)** N_{1900} using the first strategy (S_1). The numbers indicate the loading contribution of each chronology, whereas the colors highlight the strength of the loading, i.e. positive (red shades) and negative (blue shades).

The shorter network of eight growth chronologies, namely N_{1900}, reveals a similar EOF pattern (Figure 2.3B) and variance to the one obtained with N_{1764}, apart from the 30-m depth chronology from NE Iceland and Gulf of Maine chronology changing loading signs in the 1900-2001 period. The EOF1 pattern of N_{1900*}, explaining 19.8 % of variability, showed that with the addition of the Nantucket Shoals chronology, the Gulf of Maine region retains its positive loading observed with N_{1764} (Figure 2.3A), whereas the loadings from Iceland region and German Bight remain unchanged as observed with N_{1900} in Figure 2.3B. Hence, with the exception of Grimsey and German Bight chronologies yielding opposite signs, the majority of chronologies are homogeneous in a SW-NE direction.

The networks processed under three different PCA strategies yield corresponding PC1 time series which show strong agreement with one another (Figure 2.4). For example, $PC1_{S1}$ is temporally coherent with $PC1_{S2}$ (r_s=0.904; p<0.05; N_{eff}=108), yet it shares only 34 % of variability with $PC1_{S3}$ (r_s=0.582; p<0.05; N_{eff}=144). The variance improves to $\sim$ 41 % when $PC1_{S2}$ and $PC1_{S3}$ are compared (r_s=0.643; p<0.05; N_{eff}=152). For N_{1900} and N_{1900*}, the difference in strategy choice is negligible (r_s<0.8), aside from some minor amplitude offsets.

3.2. Extremes of the common signal

By using S_1 and S_2, the PC1s display a pronounced decadal to multidecadal trend compared to S_3 (Figure 2.4). This feature is reflected in the distribution of extremes, with increased clustering for certain periods of time. There were identified 24 extreme events for N_{1764}, and 11 events, for N_{1900}, respectively (see

Appendix A, Table A1). Across each of the three strategies and networks, we found an increased number of overlapping low indices rather than high ones (Table 2.1). Moreover, 80 % of the low indices occurring in N_{1900} are also recognized in N_{1764}. By looking solely at 1764-1899 CE period, the overlay of extreme low indices between strategies improves only with two additional years: 1800 and 1839, respectively. In general, we notice, partly due to the nature of analysis, that extremes overlap better between S_1 and S_2. The most mismatched period in terms of extremes among all strategies is from 1764-1800 where high extremes are highlighted only in S_3 (see Figure 2.4).

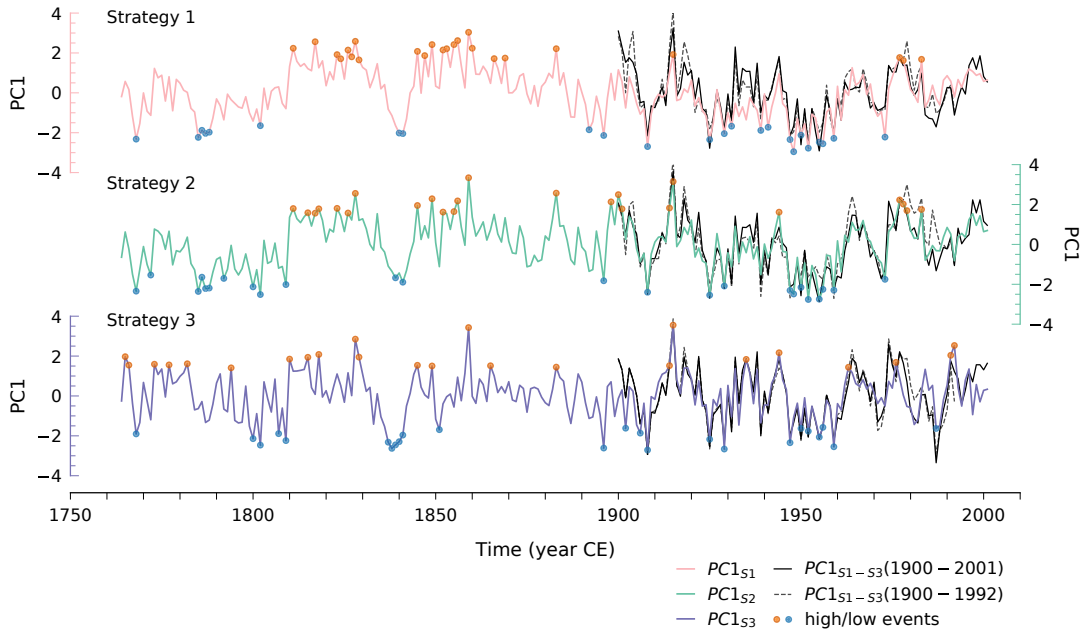

Figure 2.4. The principle component time series for the N_{1764} network, using three different nesting strategies: S_1 (pink line), S_2 (green line) and S_3 (purple line), respectively. The corresponding PC1s for the N_{1900} (black line) and N_{1900*} (dashed black line) using each strategy are also shown. The extreme high (orange filled circles) and low (blue filled circles) indices are highlighted for the long N_{1764} network.

Spectral analysis indicates that $PC1_{S2}$ has two significant peaks of 16 years (90 % Cl, i.e. confidence level) and 43 years (95 % Cl; see **Appendix A**; Figure A1), respectively. Similar peaks are found for $PC1_{S3}$ at 17 years (90 % Cl) and 48 years (95 % Cl), respectively, whereas $PC1_{S1}$ shows a significant peak (95 % Cl) with a 68-year period. Given the decadal to multidecadal component observed, the PC1s time series can be compared with indices of long-term SST anomalies typical for Northern Hemisphere basins (i.e., AMO and PDO). The correlation with AMO_{Wang} reconstruction is significant for strategy S_1 (r_s=-0.221; $p<0.05$; N_{eff}=120) and S_2 (r_s=-0.207; $p<0.05$; N_{eff}=130), respectively. By using N_{1900}, the PC1 of neither strategy exhibited a correlation with AMO_{Wang} and AMO_{obs}

Table 2.1. Common extreme years in PC1 time series across each strategy for N_{1764} and N_{1900}, respectively. The overlap years between networks are highlighted in bold.

Network	*Low indices*	*High indices*
$\mathbf{N}_{1764}$	1768, 1802, 1841, 1896, **1908, 1925, 1929, 1947, 1950, 1952, 1955**, 1956, **1959**	1828, 1845, 1849, 1859, 1883, **1915**
$\mathbf{N}_{1900}$	1908, 1925, 1929, 1947, 1948, 1950, 1952, 1954, 1955, 1959	1900, 1915, 1918, 1977

due to reduced degrees of freedom, less than the 60-80-year periodicity of the AMO (Schlesinger and Ramankutty, 1994). Because AMO_{obs} series starts with 1870 CE, we used the N_{1764} to re-assess the relationship and increase, albeit marginally, the degrees of freedom. As a result, the significance and magnitude of the correlation increases for $PC1_{S1}$ (r_s=-0.341; p<0.05; N_{eff}=63) and $PC1_{S2}$ (r_s=-0.300; p<0.05; N_{eff}=66). We observed that $PC1_{S1}$ and $PC1_{S2}$ indicate significant inverse relationships also with AMO_{Wang} and AMO_{Tardif} in the range of 0.2-0.3 (N_{eff}=85-98) starting from 1840 CE, and with coralline algae-based AMO reconstruction of Halfar et al. (2013) from 1770 CE ($PC1_{S1}$ only). Neither $PC1_{S1}$, nor $PC1_{S2}$ have shown any relationship to the tree-ring based proxy AMO index of Gray et al. (2004) in the 1764-1985 period. A weak significant correlation (r_s=-0.199; p<0.05; N_{eff}=101) is similarly observed between $PC1_{S1}$ and the PDO_{Tardif} index, but not with the tree-ring based PDO reconstruction of Biondi et al. (2001). No significant relationship is found between N_{1900} and PDO_{obs}.

$PC1_{S1}$'s extreme highs and lows coincide with some major long-term SST anomalies in spite of weak correlations (Figure 2.5). For instance, low indices at the end of 18^{th} century and beginning of 19^{th} century covary with a positive AMO and PDO phase. Thereafter, extreme high indices are subsequently clustered between 1811 and 1862 CE (Figure 2.4; Figure 2.5) concurring with the last phase of the Little Ice Age (LIA) in the Northern Hemisphere (Masson-Delmotte et al., 2013) and strong, negative AMO and PDO phases (Figure 2.5). After 1860-1870 CE, $PC1_{S1}$ and $PC1_{S2}$ indicate a slight decreasing trend toward lower values (Figure 2.4). In contrast, $PC1_{S3}$ reflects a period of reduced variability until the 1900s (Figure 2.4). In the beginning of the 19^{th} century, the PC1 indices are low (e.g., minimum recorded at 1908 CE; see Table 2.1), followed by a sharp a positive peak at 1915. Extreme low years culminate in the 1920s-1960s pe-

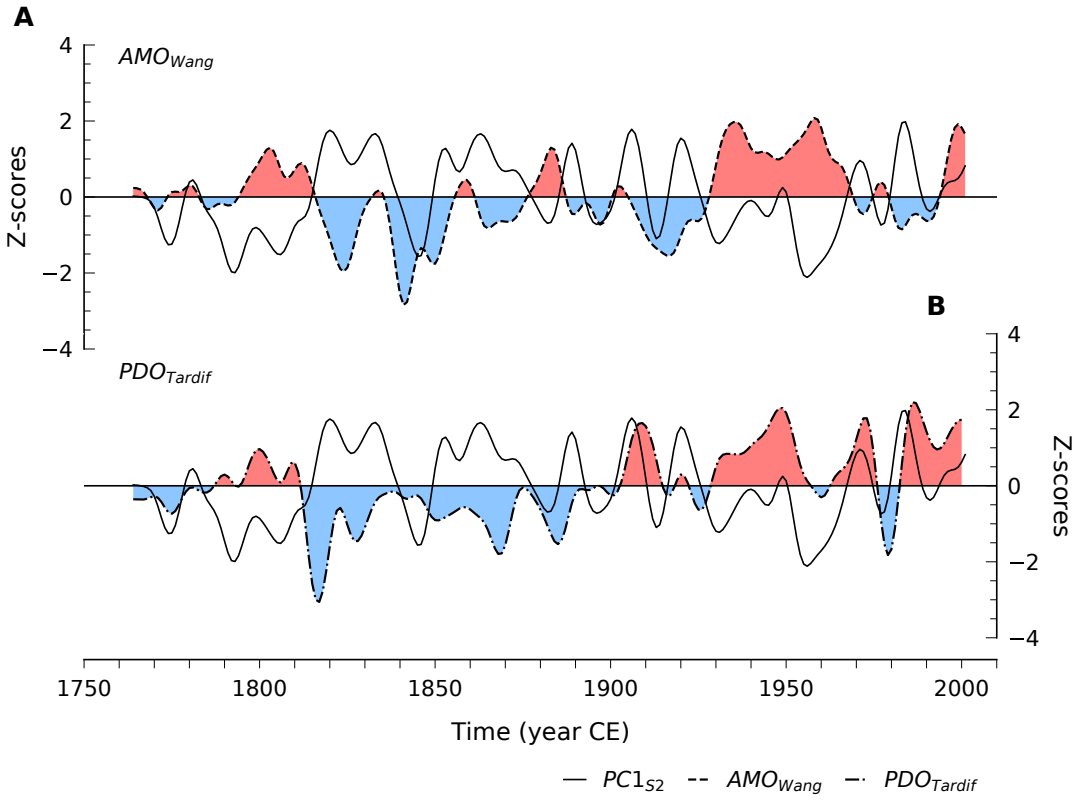

Figure 2.5. Phase shifts of **(A)** Atlantic Multidecadal Variability (AMO_{Wang}) proxy reconstruction of Wang et al. (2017) and **(B)** Pacific Decadal Oscillation (PDO_{Tardif}) of (Tardif et al., 2019) in comparison with the principle component time series of N_{1764} network using the second strategy S_2 (i.e, $\mathrm{PC1}_{S2}$; green line in Figure 2.4). The data are presented with a 10-year low-pass filter. Positive (above 0) and negative (below 0) phases are highlighted in red and blue, respectively.

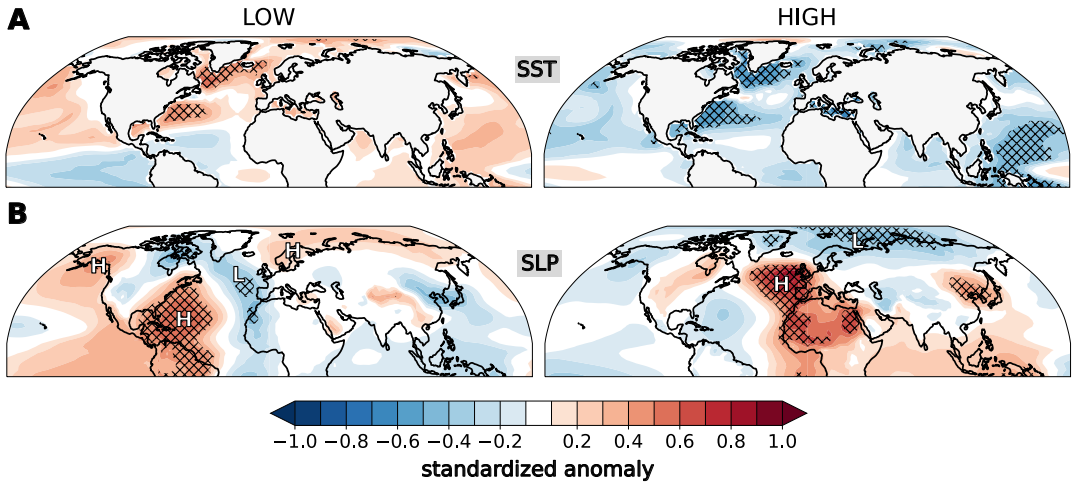

Figure 2.6. **(A)** Annually-resolved sea-surface temperature and **(B)** sea level pressure data from Tardif et al. (2019) indicating anomalies when $PC1_{S2}$ indices are above the 90^{th} percentile (high) and below the 10^{th} percentile (low) threshold, respectively. The capital letters "H" (i.e., positive anomalies) and "L" (i.e., negative anomalies) show high- and low-pressure centers, respectively. The analysis covers the period from 1764 to 2000 CE using the N_{1764} network of this study. Significance at p¡0.05 is indicated by hatches. For PC1s obtained with strategies S_1 and S_3, see Figure A2 in the **Appendix A**.

riod coinciding with the strongest positive AMO phase in the observational data.

The anomaly patterns for extreme high and low PC1 indices in the gridded annually-resolved sea-surface temperature and sea level pressure reconstructions by Tardif et al. (2019) exhibit similar geographical anomaly distributions for strategies S_1 (Figure A2.A) and S_2 (Figure 2.6). However, this similarity does not extend to strategy S_3, where anomalies are rather bounded between ± 0.2 SD and lack a clear outline (for strategy S_3, see Figure A2.B in the Supplementary Material). The $PC1_{S1}$ and $PC1_{S2}$ indicate a homogeneous spatial pattern associated with warmer (colder) Atlantic and Pacific surface water anomalies for low (high) indices (Figure 2.6A). These spatial structures are confirmed by the N_{1900} network (Figure 2.7A). Furthermore, certain anomalies exhibit more pronounced and distinct features than those in Figure 2.6A, showcasing a more defined regional perspective. One clear difference is, for instance, the SST dipole present between the eastern and central North Pacific. Composite maps of sea level pressure (SLP) anomalies reveal persistent anomaly centers arising from jet stream latitudinal fluctuations, thereby highlighting (tele)connections between the Atlantic and Pacific basins (Figure 2.6B; Figure 2.7B). More noticeably, the coherence of extreme low $PC1_{S2}$ indices in both networks reveals a distinct tripole structure. This structure comprises a high-pressure system in the

high-latitudes of the North Pacific, coupled with a positive center in the western regions of the central North Atlantic and a negative center situated to the south of the Greenland and Labrador Sea area (Figure 2.7B). Additionally, the negative anomaly center extends to the central eastern parts of the North Atlantic, albeit with reduced magnitude (Figure 2.6B). On the other hand, we observed that extreme high $PC1_{S2}$ indices lack a consistent preferred structure, with anomalies and their magnitudes differing between N_{1764} (Figure 2.6B) and N_{1900} (Figure 2.7B) networks (refer also to Figure A2 and Figure A3 for the use of other strategies). Despite this, there are signs of a persistent high-pressure system in the central northern North Atlantic, covering the British Isles (Figure 2.6B), albeit only for $PC1_{S1}$ and $PC1_{S2}$.

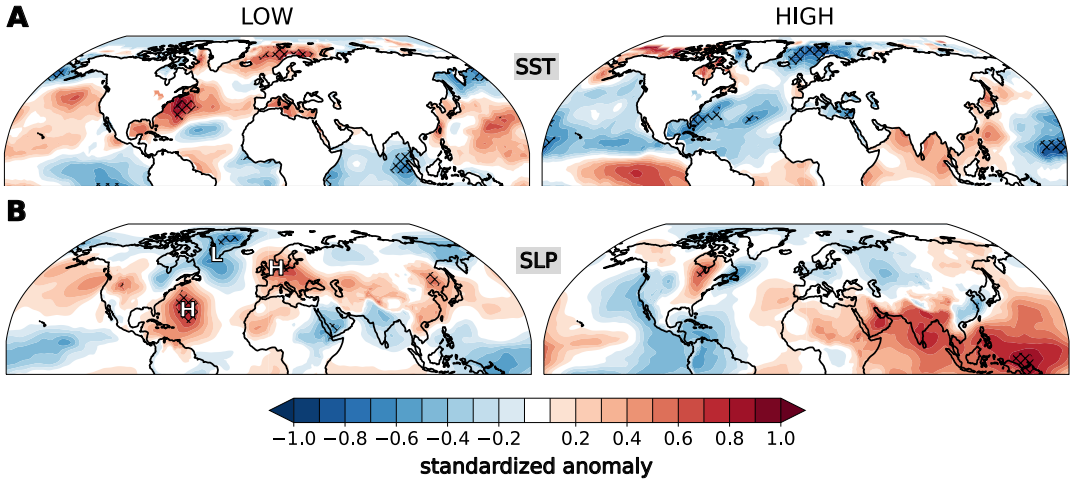

Figure 2.7. **(A)** Annually-resolved sea-surface temperature from ERSSTv.5 dataset (Huang et al., 2017) and **(B)** spring (MAM) sea level pressure data from 20^{th} Century Reanalysis V3 (Slivinski et al., 2019) indicating anomalies when $PC1_{S2}$ indices are above the 90^{th} percentile (high) and below the 10^{th} percentile (low) threshold, respectively. The capital letters "H" (i.e., positive anomalies) and "L" (i.e., negative anomalies) show high- and low-pressure centers, respectively. The analysis covers the period from 1900 to 2001 CE using the N_{1900} network of this study. Significance at p¡0.05 is indicated by hatches. For PC1s obtained with strategies S_1 and S_3, see Figure A3 in the **Appendix A**.

4. Discussion

The bivalve-based networks employed in this study are focused on the northern North Atlantic basin, sharing key locations such as the northern Icelandic shelf, northern Norwegian shelf, Gulf of Maine and Irish Sea (Figure 2.1, Figure 2.2) with the network of Reynolds et al. (2018). In contrast to the mentioned study, we expanded the network by targeting growth records rather than stable oxygen isotope ($\delta^{18}O$) series while maintaining the same nested PCA approach. Acquiring a consistent shared growth signal poses a more intricate challenge, given that growth records do not follow a straight-forward function of temperature and the isotopic composition of seawater. Owing to the fact that bivalve molluscs are ectotherms, ambient temperature modulates growth, making subsurface temperature anomalies detectable in local water bodies and at large-scale. Significant influence on growth is discerned through the availability and quality of phytoplankton (e.g., Ballesta-Artero et al., 2018; Bonitz et al., 2018), which in turn is being modulated by winter atmospheric anomalies (e.g., Lohmann and Wiltshire, 2012; Lohmann and Schöne, 2013) during the bivalve's growth period, i.e., boreal spring and summer. Bivalve growth-climate relationships, if proven and demonstrated to be consistent with observational data, provide an opportunity to reconstruct anomalies beyond the instrumental period.

4.1. The climatic coherence of the leading component

4.1.1. The general representation of SST anomalies

In this study, the extremes of the leading time component for the data-rich N_{1900} network and, by extension, the N_{1764} network provide robust evidence of a consistent, large-scale subsurface temperature signal across the Pacific and Atlantic basins (Figure 2.6A; Figure 2.7A). In broad terms, extreme low indices are linked to positive anomalies in water bodies, whereas extreme high indices are associated with colder waters. By using seasonally-averaged subsurface temperature data from products such as EN4.2.1 (Good et al., 2013), we observe persistent pools of positive temperature anomalies in the Labrador Sea, north of Iceland, and the polar regions of the North Atlantic during the boreal winter and spring (Figure A4.B). This signal is similar to the one at 5-m depth (Figure A4.A), but unlike the ERSSTv.5 data (Figure 2.7A), it remains bound to the extratropical region. In the Atlantic Ocean, a subtropical signal suggests an enhanced northward transport of anomalously warm Atlantic water, and an enhanced meridional heat transport is suggestive of a strong AMOC (Dima and Lohmann, 2010) and a positive phase in the multidecadal component, i.e. AMO.

Reynolds et al. (2018) have found this latitudinal expansion to be an expression of the S1 strategy because it retains centennial periodicities compared to the other two strategies, and to be indicative of long-term coupling between the tropical Atlantic and the subpolar gyre. Besides centennial time-scales to be representative of the air-sea coupling in combination with solar variability, Black et al. (1999) have suggested that a 12-13-year periodicity to be a natural interdecadal signature of tropical Atlantic at least since 1300s as found in planktonic foraminifera records. We found a significant interdecadal peak (Figure A1) which might relate to this periodicity (16-17 years), but given the distance, it may occur with a lag. However, this is an uncertain hypothesis, because this peak could also relate to the PDO periodicity (Mantua et al., 1997), a delayed coupling between the AMO and PDO opposite-sign phases (e.g., Karmouche et al., 2023) and perhaps, more likely, a subpolar air-sea interaction similar to the one found in the Pacific (Latif and Barnett, 1994). The PDO-like pattern in the North Pacific is clear with the N_{1900} network in the 1900-2001 period (Figure 2.7A), where low (high) indices are associated a negative (positive) PDO and positive (negative) AMO polarities. This pattern is not apparent in the 1764 and 2000 analysis period (Figure 2.6A), where, as described previously, there is a rather homogenous structure encompassing the north hemisphere basins. However, by using the longer $PC1_{S2}$ time series in the 1764-1899 period, the resulting pattern is, in fact, inverted (Figure A5). It may be that the polarity opposites obtained in Figure 2.7A represent a signature of the 20^{th} century, with longer out-of-phase polarity between AMO and PDO as indicated in Karmouche et al. (2023) analysis covering the period from 1900 to 2014.

It is worth highlighting that these phase shifts can be captured through composites of low extremes in *A. islandica* bivalves. Nevertheless, a persistent observation is the stability of sea surface temperature (SST) anomalies within the Atlantic region when associated with low PC1 indices. In connection with the quasi-monopole structure of the EOF1 pattern (Figure 2.3), positive temperature changes associated with a warm AMO state might lead to a growth reduction in the majority of *A. islandica* ((Figure 2.5A)). However, we must point out that every bivalve species has a particular, genetically determined temperature window it can survive in (overview in Cargnelli et al., 1999). Growth is best at the optimum temperature (4-16 °C) and decreases towards the lower and the upper temperature limit (Witbaard et al., 1998; Hiebenthal et al., 2012). Marine heatwaves, for instance, can reach the upper tolerance limit of *Arctica islandica* and may cause a decrease in shell growth. With our type of analysis, we cannot

detect synoptic-scale extremes such as heatwaves, but we do observe that the time frame associated with extended lower growth (late 1920s to late 1950s) is similar to the period 1925-1954 CE in which several global SST datasets indicate an increase in marine heatwaves' frequency and duration (see Figure 5 in Oliver et al., 2018). For the northern North Atlantic basin, these marine heatwaves have been linked with a positive AMO state (see Figure 6 in Oliver et al., 2018). Suppressed shell growth in the 1920-1960s has been observed also in bivalve-based chronologies from Scotland (Stott et al., 2010) and NE Iceland (Marali and Schöne, 2015). Westward, the warming of the Labrador Current enhanced coralline algae growth (Halfar et al., 2011) and shell growth (Poitevin et al., 2019).

4.1.2. The general representation of SLP anomalies

For the Northern Hemisphere, the strength, latitudinal migration and waviness of the polar jet stream influences the weather systems across North American and European continents on synoptic timescales (Rimbu et al., 2014; Trouet et al., 2018). In a similar manner as with the SST anomalies, we suggest that the sea level pressure (SLP) anomalies observed are long-lived (persistent or more frequent) atmospheric structures. The tripole pattern observed over the Pacific and western-Atlantic (Figure 2.6B; Figure 2.7B) resembles a negative Pacific/North American (PNA) phase typically observed in the 500hPa geopotential height anomalies. Lower than average SLP levels tend to prevail in the central regions of the northern North Atlantic when associated with low PC1 indices. However, unlike the typical dipole observed with positive phases of North Atlantic Oscillation (NAO) (Hurrell and Deser, 2010) and Arctic Oscillation (AO), we did not find a strong positive center. During the analysis period from 1900 to 2001 (Figure 2.7B) the low-pressure center is particularly concentrated over the Greenland region. Prevalent cyclonic conditions over the Atlantic (i.e., increased wind movement, precipitation, wave activity and turbidity) in association with warm Atlantic waters are not favorable for a proper growth. Although positive SST anomalies, increased precipitation and riverine discharge enhance stratification and can decrease growth performance, stormy conditions particularly crucial for shallow-water bivalves due to physical disturbance of their habitat (e.g., Thórarindsóttir et al., 2009). In another example, Komagoe et al. (2018) have shown that decreased shell growth in *Tridacna maxima* occurs during typhoon activity at Okinotori atoll, Japan. We may even consider that stormy conditions are able to reduce inter-series synchronicity (e.g., North Sea Epplé et al., 2006).

Schöne et al. (2003b) have found that large-scale atmospheric anomalies induced oceanographic and implicitly food-related changes which in turn affect shell growth. For example, a positive winter NAO phase amplifies wind-driven mixing, thereby augmenting the flux of nutrients and fostering increased shell growth in a chronology from the central North Sea (Schöne et al., 2003b). The dipole observed over the Atlantic region during high PC1 indices bears some similarity with a positive NAO phase (Figure 2.6B). The position of the anticyclonic system defines where the westerlies intensify, positively affecting the degree of winter and spring upwelling and nutrient input. It may be critical when and where this anticyclonic blocking over the eastern Atlantic takes place. For instance, it is plausible that shell growth enhanced in some coastal regions during the last phase of the Little Ice Age when both AMO and PDO were in their negative phases. Interestingly, on land, the combination of lower solar activity such as Dalton Minimum (1770–1840 CE), cold SST anomalies over the Atlantic and blocking activity over the British Isles are found to be the prerequisites for megadroughts occurrence over Europe (Ionita et al., 2021). Therefore, it appears that our pattern (Figure 2.6B), based on the N_{1764} bivalve network spanning this period, align with the findings from Ionita et al. (2021).

4.2. Limitations of the bivalve network

Here networks with varying amounts of chronologies tested at two different analyses periods maintain the overall spatial and temporal structure (Figure 2.3), and as discussed previously, the extremes in the shared growth signal are associated with climatic conditions. Pronounced mismatches are more frequently observed when comparing the extremes between $PC1_{S1}$ and $PC1_{S2}$ with $PC1_{S3}$ in the 1764-1799 CE period, with the latter exhibiting more high extremes (Figure 2.4). However, it is important to note that these mismatches are an artefact of the S_3 strategy for that period. In fact, when comparing the PC1s within that time frame, they exhibit no significant discrepancies (as shown in Figure A6).

The signal of the three nested-PCA strategies is, nevertheless, more coherent in terms of extreme low indices rather than high PC1 indices (Table 2.1). The resulting extreme years also overlap best between N_{1900} and N_{1764}, pointing towards a clear low growth signal. On the other hand, high PC1 indices (higher growth in most chronologies) converge to the same pattern (e.g., Figure 2.6A) only when using $PC1_{S1}$ and $PC1_{S2}$ time series from N_{1764} and $PC1_{S2}$ time series from N_{1900} network. The $PC1_{S3}$ patterns are consistent only for N_{1900} at low

indices. Since no specific high indices composite pattern is obtained for $PC1_{S3}$, it may be that the constraint arises from the methodology approach used for the S_3 strategy. A plausible hypothesis is that while the chronologies used in the network are able to withhold information at lower frequencies, the time slice of 30 years for a nested PCA is thereby too short to converge the environmental signal. It is important to note that there is an inherent limitation on the low frequency that can be achieved, determined by the shortest length of the growth record contributing to the chronology construction (Cook et al., 1995). This "segment length curse" as coined by the authors, can be mitigated by other detrending techniques, such as the regional standardization curve (Esper et al., 2003). It is true that most chronologies used in this study have been ontogenically detrended by negative exponential functions or smoothing curves. However, very long chronologies, such as those from Grimsey Island and the Irish Sea, have been processed with the RCS method. In this analysis, they not only show robust loading signals across two time periods but also retain lower frequencies.

A second explanation is that above average growth in most chronologies might in fact relate to regional hydrography, leading to a diffused signal. Variable conditions seem to be at interplay also because the blocking over the British Isles observed in the high composite SLP map (Figure 2.6B) is rather absent over in the 1900-2001 period (Figure 2.7B). It remains unclear why chronologies in the area do not exhibit a more pronounced reflection of this anomaly, warranting further investigation in future research. However, the same pattern might not be applicable in this period due to the general warming ocean trend (Tierney et al., 2015), and limited cold conditions starting with the 1900s. Despite the lack of a congruent atmospheric pattern to understand the dynamics, high growth remains bound to the same water temperature conditions, with a notable enhancement during the early 1900s and a peak in 1914-1915, coeval with a negative phase of the AMO (Figure 2.5). Anomalous cold SST conditions were observed in the 1968-1977 CE period (Hansen and Bezdek, 1996) concurrent with climatic changes in the North Pacific: negative SLP anomalies over the Aleutian Low during 1976-1977 CE (Deser and Phillips, 2006) and a negative PDO polarity (Figure 2.5B).

By having a limited number of chronologies in a network compared to, for instance, tree-derived proxies, may come with caveats regarding the spatial stability of the growth signal. The N_{1764} network is complemented by two and three additional chronologies for the periods 1900-2001 and 1900-1992, respectively.

However, having an adjacent chronology does not always help with the interpretation, even though, intuitively, one would expect that chronologies from the same region would carry the same loading sign. For instance, the Nantucket Shoals chronology from 66-m depth showed in our analysis for the 1900-1992 CE period (N_{1900*}) a positive loading compared to the 38-m one from Gulf of Maine. Another example is the opposite signs found in the north of Iceland between 82-m and 30-m derived chronologies (Figure 2.3B).

Witbaard (1996) conducted an analysis between 1970-1990 CE and found that two proximal locations in the Fladen Ground, North Sea, indicate very contrasting influences: the northmost one related positively to an eastward branch of the North Atlantic Current, whereas the southern one was inversely proportional to another branch. By analyzing shell microstructures, Höche et al. (2022) determined that temperature dependence on the size of biomineral units is strongest in shells from NE Iceland as compared to the Norwegian Trench. In our study, it may explain the opposing loading signs between the chronology of Butler et al. (2013) from the northern Icelandic shelf and that of Butler et al. (2009) from northern North Sea, even more so considering the similar water depths. One of the additional composite chronologies from the German Bight, North Sea, does not contribute significantly to the common signal (Figure 2.3B). Epplé et al. (2006) found that low synchrony in the studied specimens' growth was potentially due to strong local environmental variability in a shallow setting. In a similar manner, Stott et al. (2010) found that cross-dating becomes more difficult in shallow water environments and also during periods of prolonged stress.

Considering these factors, the inclusion of shallow-water chronologies from extratropical regions or regions exhibiting a pronounced warming trend, as seen in the southern North Sea (e.g., Wiltshire et al., 2010), could potentially introduce complications into reconstructions due to environmental biases, such as excessive warmth or the interplay of dynamical factors. Therefore, it becomes evident that local hydrology plays a crucial role in moderating growth, and it is plausible that the growth response is influenced by the frequency-dependent nature of the environment (Stott et al., 2010). These intertwined factors may not be easily disentangled.

4.3. Potential applications

In this study, we primarily used N_{1764} and N_{1900} bivalve-based networks in their respective reference periods to evaluate the shared growth signal and its extremes

(10-90th percentile) in a large-scale climate context. However, some chronologies extend beyond the analysis periods, and it may be possible to integrate them in other networks. For example, three additional networks can be formed: N_{1495}, covering the period from 1495 to 2003 and incorporating chronologies from depths of 6-, 30-, and 82-m (as detailed in Figure 2.2). We also included the Irish Sea chronology, commencing in 1516 CE, to create N_{1516}, as well as the Fladen Ground chronology, starting in 1545 CE, forming the N_{1545} network. The $PC1_{S1}$ of N_{1516} and N_{1545} are highly correlated (r_s = 0.94; N_{eff} = 298; p<0.05), whereas the $PC1_{S1}$ of N_{1495} is not significantly correlated with any of the above chronologies, only in the 1764-2001 period. We, however, refrain from using the N_{1495} because it is based on solely three chronologies, and the signal is dominated by the opposing loading signs from 30-m and 82-m depth from northern Iceland. The resulting EOF1 spatial pattern of N_{1516} and N_{1545} is similar to that of N_{1764} (Figure 2.3A), with positive loadings for the NE Atlantic chronologies and negative loadings for both Iceland chronologies. This result is expected as the agreement with the N_{1764} network is very good (r_s>0.8; p<0.05). The 30-m depth chronology from Iceland seems to change the loading sign in the 1900-2001 period (Figure 2.3B), indicating a potential broadening of the Irminger Current and hence more pronounced Atlantic waters. Both networks indicate higher frequency variability up to 1650 CE (Figure A7). We found that the correlation with AMO_{Wang} index is positive in the 1516-1763 period (r_s = 0.165; N_{eff} = 192; p<0.05), contrary to our observations for the 1764-2000 period. Interestingly, the low extremes in the LIA period, here better covered with the N_{1516}, are associated with significantly colder conditions in the Atlantic Ocean as compared to the 1900-2000 observational period (Figure A8.A). The high extremes in the 1516-1763 period are associated with warmer water bodies in the Northern Hemisphere, in reference to the entire analysis period. This may complicate future reconstructions based on extremes, however, we underline that either extreme of water temperature can reduce growth. Considering the negative temperature anomalies of the Little Ice Age in the Northern Hemisphere (Mann et al., 2009), this particular result is not surprising. Moreover, positive SLP anomalies in the Greenland and subpolar regions are present for the both high and low extremes in the 1516-1763 period, indicating persistent anomalies associated with a negative Arctic Oscillation (Figure A8.C). Such pattern has been previously observed in reconstructions and models (e.g., Mann et al., 2009, and references therein). No significant relation to PDO_{Tardif} was observed, although the Pacific dipole is a prominent feature in the composite maps (Figure A8.A and Figure A8.B).

Tierney et al. (2015) reconstructed tropical SSTs in the Western Atlantic and Eastern Pacific regions from coral-based proxy networks (e.g., δ^{18}O, Sr/Ca and growth increments), reconstructions which extend to 1552 CE and 1607 CE, respectively. We did not find any significant correlations with the tropical SSTs until the 19^{th} century. There is an inverse relationship with the reconstructed SSTs anomalies in the Western Atlantic region between 1800-1960 (r_s = -0.341; N_{eff} = 65; p<0.05) which improves after 1900 CE by using $PC1_{S2}$ from N_{1900} (r_s = -0.414; N_{eff} = 31; p<0.05). Positive correlations with the Eastern Pacific region are found only after 1870 CE (r_s = 0.240; N_{eff} = 79; p<0.05). These results, do not only indicate the potential of linking high-latitude proxies to low-latitudes ones, but that synchronous phases are time-dependent (Figure A7).

5. Conclusions

The various networks implemented in this study aid in extracting the shared growth signal present in the upper water column of the North Atlantic. We observed a significantly stronger alignment in the context of low extremes between the networks and the strategies employed. Whereas, the interpretation of high growth variability remains ambiguous, as it could be influenced by an inherent bias towards optimal growth conditions (Schöne, 2008) and dynamical ecosystems. We believe that even with additional chronologies to establish larger networks akin those in dendrochronology, it is challenging to mitigate the bias introduced by regional factors. Nevertheless, the inclusion of additional chronologies has the potential to enhance spatial patterns and facilitate regional grouping in future studies. For example, incorporating supplementary chronologies from the western Atlantic region could offer improved insights into the influence of the PNA (Pacific North American) and NAO (North Atlantic Oscillation) relationship on extreme growth.

For the 1764-2000 analysis period, we found that growth reduction in the majority of records used, and relate to warm Atlantic and Pacific surface waters, long-lived cyclonic conditions in the central northern North Atlantic and a negative PNA pattern. In the same analysis period, higher growth is associated with colder waters and blocking conditions over the British Isles. We note that it is difficult to find clear, robust relationships between growth and climate, largely because of the many physical and nonphysical factors that jointly control shell growth, and that there is a high degree of non-stationary. For instance, low growth happens under negative subsurface temperature anomalies correspond-

ing to the Little Ice Ages in the 17^{th} to mid-18^{th} century linked with persistent positive sea level pressure anomalies in the high latitudes.

Although the correlations with various AMO and PDO indexes – which are also reconstructed based on different proxy types and are therefore subject to different uncertainties – are not compelling, their corresponding spatial patterns are evident in the composite maps. Hence, we argue that growth records can detect multidecadal signals from both internal and external sources (see Mann et al., 2021). The concurrent phases of AMO and PDO in the cold period 1800-1880 CE and warm phase 1920-1960 CE explain up to 20 % and 45 %, respectively, of variability in the shared growth signal. Besides these findings, extremes in the shared growth signal have the potential to reveal out-of-phase polarities between AMO and PDO as observed starting with the late 19^{th} century and possible large-scale reorganizations in the coupled air-sea interactions. Moreover, there is a high potential to link high-latitude proxies with tropical ones, at least since the 1800s and late 1800s. Analyzing growth extremes in recent decades holds the potential to uncover unusual patterns in oceanic and atmospheric circulations, including cyclonic and anticyclonic blocking, as well as enhanced warming, all of which impact coastal environments. This information can be valuable in identifying „hotspot“ regions, and addressing future changes in the vulnerable coastal areas of the North Atlantic.

Acknowledgements

We thank Norel Rimbu and Hu Yang for insightful discussions in the early stages of this research. This work was supported by the AWI Strategy Fund Project – PalEX. MI, GL and TB acknowledge further support by the Helmholtz Association via the joint program „Changing Earth – Sustaining our future“ (POF IV) of the Alfred Wegener Institute. MI was supported by the Helmholtz Climate Initiative – REKLIM. We are grateful to all authors and co-authors who made their master shell chronologies public. We acknowledge the use of the following gridded datasets: LMRv2.1 Tardif et al. (2019), ERSSTv.5 Huang et al. (2017), EN4.2.1 (Good et al., 2013) and NOAA's 20^{th} Century Reanalysis V3 (Slivinski et al., 2019). The authors are supported by the Open Access Publication Funds of the Alfred Wegener Institute for Polar and Marine Research.

Data availability

The original shell growth chronologies are publicly available in PANGAEA and NOAA's National Climatic Data Center databases. The climate data used in this study are open-source (see details in section 2.2). The first principle component time series generated for all networks will be made available with the publication.

3

Paper II

The influence of depth-dependent seasonal temperature variability on growth signal in *Arctica islandica* shell growth records

RQ.2	Does *Arctica islandica* exhibit a depth-dependent growth response to seasonal fluctuations in subsurface water temperature and salinity, necessitating consideration in correlation analyses? And if so, is it intertwined with large-scale oceanic circulation patterns?

This chapter features the paper written for the *Frontiers in Marine Science* journal. The published version is found below. The supplementary material for this paper is found in **Appendix B**. As a published version adheres to the journal's style, readers should note that the Supplementary Figures have been renamed (e.g., Figure B1) while retaining their original numbering. Additionally, Supplementary Table 1 is presented as Figure B9 and Figure B10.

Author contributions:
DEC designed the study with support from MI and TB. DEC conducted the analysis, generated the figures and drafted the paper. DA, LB and TB helped with substantial manuscript revision and thoughtful input. GL and MI provided feedback on the manuscript. MI supervised.

Paper II

frontiers in Marine Science

ORIGINAL RESEARCH
published: 29 June 2021
doi: 10.3389/fmars.2021.687318

The Influence of Depth-Dependent Seasonal Temperature Variability on Growth Signal in *Arctica islandica*

Diana E. Caldarescu[1,2], Thomas Brey[2,3,4], Doris Abele[2], Lars Beierlein[2], Gerrit Lohmann[1,5] and Monica Ionita[1]*

[1] Paleo-climate Dynamics Section, Alfred Wegener Institute, Helmholtz Centre for Polar and Marine Research, Bremerhaven, Germany, [2] Functional Ecology Section, Alfred Wegener Institute, Helmholtz Centre for Polar and Marine Research, Bremerhaven, Germany, [3] Helmholtz Institute for Functional Marine Biodiversity (HIFMB), University of Oldenburg, Oldenburg, Germany, [4] Faculty of Biology/Chemistry, University of Bremen, Bremen, Germany, [5] Faculty of Physics and Electrical Engineering, University of Bremen, Bremen, Germany

Bivalve sclerochronological records with annually resolved growth bands are applicable proxies in reconstructing features of the hydro-climate system. Here we evaluate the relationship between growth indices of *A. islandica*, previously collected at approximately 82 m depth in the North Atlantic, and seasonal subsurface temperature at various depths for the 1900–2005 period. Correlations with sea surface temperature at the collection site are not significant during winter and weak for the remaining seasons. The strongest in-phase correlations persist for summer and autumn below 56 m water depth, whereas weaker correlations are lagged by one or two years. We also observe similarities with distant water bodies in the North Atlantic sector, and a corresponding large-scale oceanographic pattern that increases significantly with water depth along the trajectory of the North Atlantic Current. We suggest that by investigating the relationship with the temperature signal at various depths locally and at large-scale increases the reliability and application of bivalve shells as marine archives.

Keywords: *A. islandica*, North Atlantic, seasonality, growth index, temperature variability, sclerochronology

OPEN ACCESS

Edited by:
Philippe Archambault, Laval University, Canada

Reviewed by:
Julien Thebault, Université de Bretagne Occidentale, France
Pierre Poitevin, Department of Fisheries and Oceans (Canada), Canada

****Correspondence:***
Diana E. Caldarescu
diana.caldarescu@awi.de

Specialty section:
This article was submitted to Global Change and the Future Ocean, a section of the journal Frontiers in Marine Science

Received: *29 March 2021*
Accepted: *08 June 2021*
Published: *29 June 2021*

Citation:
Caldarescu DE, Brey T, Abele D, Beierlein L, Lohmann G and Ionita M (2021) The Influence of Depth-Dependent Seasonal Temperature Variability on Growth Signal in Arctica islandica. Front. Mar. Sci. 8:687318. doi: 10.3389/fmars.2021.687318

INTRODUCTION

Past temperature reconstructions are extremely valuable in the context of understanding climate and modes of natural variability. Since the availability of observational data is limited to the last 150 years, marine archives of biogenic carbonate origin have become attractive indicators for temperature reconstructions. For instance, the carbonate shells of bivalves are used for high resolution spatial-temporal records, most commonly derived from sclerochronological and geochemical analyses. To reconstruct ocean temperatures, Weidman et al. (1994) linked the oxygen isotopic composition ($\delta^{18}O_{shell}$) of *Arctica islandica* with annual growth increments, and showed that bottom temperatures are recorded with a precision of ±1.2°C. This study instigated a number of publications exploring the relationship for the North Atlantic sector (e.g., Schöne et al., 2004, 2005a,b; Wanamaker et al., 2008a). The ocean quahog, *A. islandica* became an important climate archive in the North Atlantic sector, which, due to its extreme longevity, allows reconstruction of past environmental signals on multi-centennial time scales

(e.g., Butler et al., 2013; Lohmann and Schöne, 2013; Reynolds et al., 2016). While long-lived *A. islandica* support paleo reconstructions and $\delta^{18}O_{shell}$ variability in shell growth bands proved to be a reliable proxy for oceanic temperature reconstructions, it remains to be determined how well the shell growth index synchronizes with the temperature signal.

Because the atmosphere is in direct exchange with the uppermost surface of the ocean, and an imminent cause of ocean temperature variability (Czaja et al., 2003; Gastineau et al., 2013), temperature reconstructions usually focus on the upper mixed layer. Recent efforts have been made to monitor ocean temperatures at different water depths, but data availability in the North Atlantic is still spatiotemporally limited. Obtaining a significant correlation of the shell archive with temperature is important to assess synchronization of the shell growth index with oceanic conditions and to retrieve signals of the prevailing climate indices. Thus, to validate the temperature effect on shell growth variability, the initial step in the analysis consists in correlations between growth patterns and instrumental or gridded sea surface temperatures (SST). These correlations are often either weak or insignificant, unable to capture high frequency variability (e.g., Butler et al., 2013), leading to inconclusive assumptions regarding the role of temperature in stimulating shell growth.

Bottom water temperature and food availability are pivotal drivers of shell and tissue growth in bivalves, and it is not always easy to confirm the dominance of one over the other (Witbaard et al., 1998; Ballesta-Artero et al., 2018). For instance, Marali and Schöne (2015) found that 43% of annual growth variability of *A. islandica* shells around Iceland is explained by water temperature during the growth season, whereas Schöne et al. (2005a) suggested that 65% of annual growth variability is explained by summer temperature and food supply. However, by analyzing *A. islandica* shells from the Irish Sea, Butler et al. (2010) obtained significant correlations with SST and air temperatures, which were not stable in time and lagged by one year indicating that the delay might come from the physiological response to environmental dynamics. Witbaard et al. (1997) analyzed shell archives of *A. islandica* from Fladen Ground (between Scotland and Norway), which did not correlate significantly with temperature or plankton data, but rather reflected the local hydrology to affect the observed growth variability. Witbaard et al. (1999) suggested that a combination of temperature, primary productivity and vertical depth-dependent coupling between primary productivity and consumer explains 50% of growth variability in shells from the Faroe Islands, Iceland and the White Sea. Interestingly, in their study the shell growth variance increased by a factor of 1.5 for shells from the North Sea, indicating the relationship between the shell archive and the environmental variability to be strongly site-specific.

In this study, we hypothesize that one central starting point in reconstructing past ocean conditions using bivalve proxy records is by location and depth of the collection site. We selected an annually resolved master shell chronology from Butler et al. (2013), comprising a collection of *A. islandica* shells from approximately 82 m water depth on the N. Icelandic shelf, to evaluate whether the temperature forcing on the growth signal is depth-dependent, related to stratification dynamics and, hence, synchronized with atmospheric and oceanic modes of variability. We first examined the correlation with the seasonal temperature signal and assessed the synchronicity with local water temperature during the growth period. In a final step, we explored the strength of correlation with seasonal subsurface water temperature spatially over the common analysis period 1900–2005 and examined the large-scale temperature effects on growth variability of *A. islandica* in the North Atlantic sector. The results of this study explore the potential temperature range and the patterns of thermal shifts that can be reconstructed using the *A. islandica* shell chronology.

MATERIALS AND METHODS

Master Shell Chronology

The master chronology used in this study is based on an assemblage of 29 shells of *A. islandica*, which includes eight individuals with lifespans over 300 years. Shells from this collection had been first mentioned in Wanamaker et al. (2008b) and used later in several other publications (Wanamaker et al., 2012; Butler et al., 2013; Reynolds et al., 2016). The bivalves had been collected during a research cruise in 2006 close to Grimsey Island on the North Icelandic Shelf (NIS) at a water depth of 81–83 m (66.5265°N, −18.19567°W; **Figure 1**). The region of sampling is under the influence of the warm Irminger Current and the cold East Icelandic Current, which makes it interesting to study. The shell series covers the 649 to 2005 time period; however, shell coverage fluctuates at certain timestamps: (1) the period prior to 1175 is covered by two long-lived bivalves which overlap for a short period of 37 years (952–988), (2) during 1175–1937, the sample coverage fluctuates between three to eight shells, (3) the period after 1960 is covered by 15 overlapping shells (see also Figure 3A in Butler et al., 2013). Here we chose the 1900 to 2005 period as a suitable period for analysis with observational data (see section "Environmental data"), because of scarce data and uncertainties before 1900, and generally because of high expressed population strength used in creating the chronology and indicating that the specimens are synchronized (Wigley et al., 1984; see also Figure 3G in Butler et al., 2013). The growth increments were detrended, a necessary practice for chronology construction due to faster growth during juvenile years. Butler et al. (2013) performed two types of detrending techniques, a deterministic detrending using a negative exponential function and an empirical detrending by regional curve standardization (RCS). We chose to apply only the latter method of detrending because it preserves the low-frequency signals (e.g., Esper et al., 2003; Butler et al., 2010; Butler et al., 2013). For further details on shell collection, treatment, sampling and detrending procedures, please refer to Butler et al. (2013). The master shell chronology was obtained from PANGAEA database.[1]

[1]https://doi.pangaea.de/10.1594/PANGAEA.816210

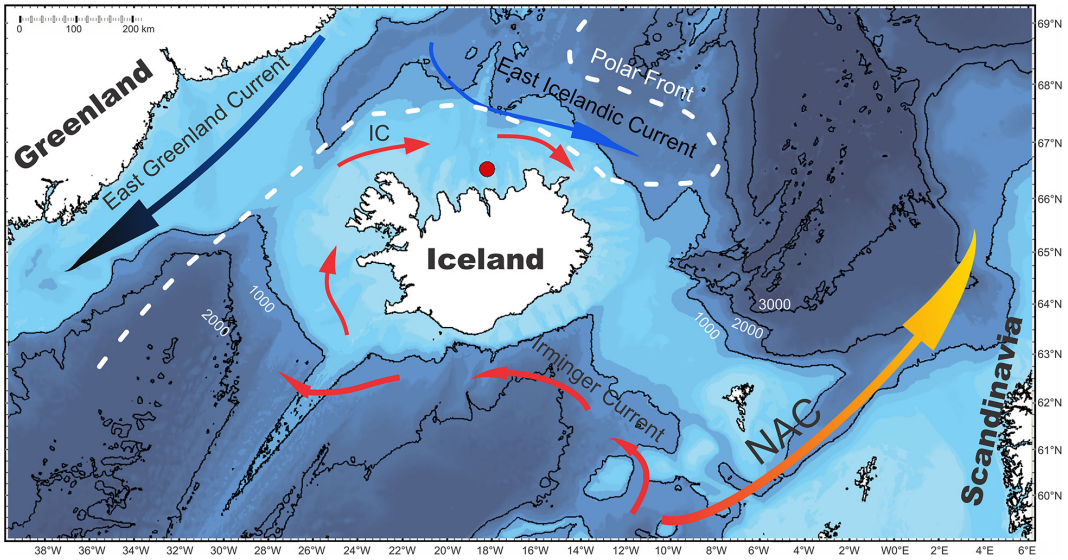

FIGURE 1 | Bathymetric map of the Iceland area. The collection site (red circle) on the North Icelandic Shelf is prone to influences from Irminger Current (IC) and East Icelandic Current (EIC). NAC refers to the North Atlantic Current. Contour lines indicate 1000-m isobaths. The map is adapted after Ran et al. (2011) and Butler et al. (2013).

Environmental Data

For correlations with the master chronology, we used seasonal subsurface seawater temperature and salinity data extracted from the EN.4.2.1 dataset (Good et al., 2013). This dataset consists of monthly-resolved objectively analyzed temperature and salinity values spaced at 1° on the horizontal grid and 42 depth layers. In general, the temporal and spatial data coverage across all depths is adequate for analysis in the North Atlantic sector (see **Supplementary Figure 1**). The temperature uncertainty (one standard deviation) is below 1°C, whereas the salinity uncertainty is in the range of 0.1–0.2 psu in the Iceland area (see **Supplementary Figure 2**). The global ocean temperature and salinity datasets were downloaded from the Met Office website.[2] Additionally, we used the Atlantic Multidecadal Oscillation (AMO) index (van Oldenborgh et al., 2009) to associate different time periods with water temperature anomalies in the North Atlantic sector.[3] We also used the winter (DJF) North Atlantic Oscillation (NAO) index (Hurrell, 1995) for correlations with the growth index.[4] We included in our analysis diatom and copepod abundance data (Batten et al., 2003) from Continuous Plankton Recorder (CPR) for CPR area A6 encompassing the area surrounding Iceland.[5] EN.4.2.1 dataset is available for 1900–present, AMO index between 1850–present, NAO index from 1899–present, however, we selected the common analysis period 1900–2005 across all datasets used. The CPR data are available only since 1958.

[2]https://www.metoffice.gov.uk/hadobs/en4/

[3]https://climexp.knmi.nl/

[4]https://climatedataguide.ucar.edu/climate-data/hurrell-north-atlantic-oscillation-nao-index-pc-based

[5]https://www.cprsurvey.org/

Data Analysis

The shell archive is an annually-resolved master chronology (ARMC). To assess whether the annual shell signal correlates with year-to-year temperature variations at the approximate collection site (66°N, 18°W), we applied standard statistical methods such as the Pearson correlation over a 3-month moving window (i.e., DJF, JFM, FMA, MAM, AMJ, MJJ, JJA, JAS, ASO, SON, OND, and NDJ). To evaluate whether the relationship between shell signal and seasonal water temperature varies with the water depth of the temperature record, the correlations were computed for 10 different depth layers (i.e., 5, 15, 25, 35, 45, 56, 66, 77, 87, and 98 m). To assess which type of variability drives the strength of the correlation between the ARMC and water temperature, we isolated the low and high frequency components. For the low frequency component, we applied a 5-year Savitzky-Golay filter (Savitzky and Golay, 1964) throughout our time series and calculated the Pearson correlation. Thereafter, we isolated the high frequency residual by subtracting the low pass signal from the time series (following e.g., Wanamaker et al., 2008a). We also investigated the spatial extent of this relationship by creating seasonal grid-point correlation maps for the common time period 1900–2005. Gridded temperature data were linearly detrended prior to the analyses. All statistical analyses consider a significance level of 95% ($\alpha = 0.05$) or 99% ($\alpha = 0.01$).

RESULTS

Depth-Dependent Seasonal Variability and Shell Growth

Our results show that the shell growth index time series is significantly and positively correlated with time series of water

temperature during late spring, summer and late autumn, both at surface and with increasing depth (**Figure 2**). The correlation is particularly high at 56–66 m depth throughout the summer and autumn months, and maximal at 56 m depth during SON and OND. In addition, the strongest correlations with water temperature occur during SON along the depth range covered (i.e., 5–98 m depth). Cross-correlation analyses resulted strong and concurrent below 45-meters for summer and autumn (see **Supplementary Figure 3C**).

There is, however, a prominent dissimilarity between surface and bottom water conditions as the correlations above 45 m depth are either not significant or weak (**Figure 2**). For instance, there is no significant correlation ($p < 0.01$) between the ARMC and surface water temperature during winter and spring months, however, some of these correlations are positive at lower significance levels ($p < 0.05$ and $p < 0.1$) (**Supplementary Figures 3A,B**). The strength of the correlation increases below 45-meter depth, but remains generally weaker than observed during summer and autumn months.

Synchronization With Temperature Signal

The strongest correlation between the shell growth index and water temperature for the 1900–2005 period occured during autumn (SON). Additional cross-correlation analyses revealed that such strong correlations are concurrent (**Supplementary Figure 3C**). To evaluate whether the strong correlation with SON water temperature is stable through time, we selected the depth at which the maximal correlation occurred (i.e., 56 m, **Figure 3B**). We observed a decreased synchronization with the temperature time series at 56 m depth during 1962–1976 and after 1980s (**Figure 3A**). It is noteworthy that the decreased growth observed around 1965 matches the decrease in surface water temperature during a cold phase of the Atlantic Multidecadal Oscillation (**Figure 3**). The positive amplitude observed around 1970 in the ARMC signal is not correlated with water temperature at 5 or 56 m depth. Moreover, the positive growth amplitudes between 1980 and 1995 are also out of sync with the surface and bottom (56–77 m) water temperatures, which were colder than usual and relate to

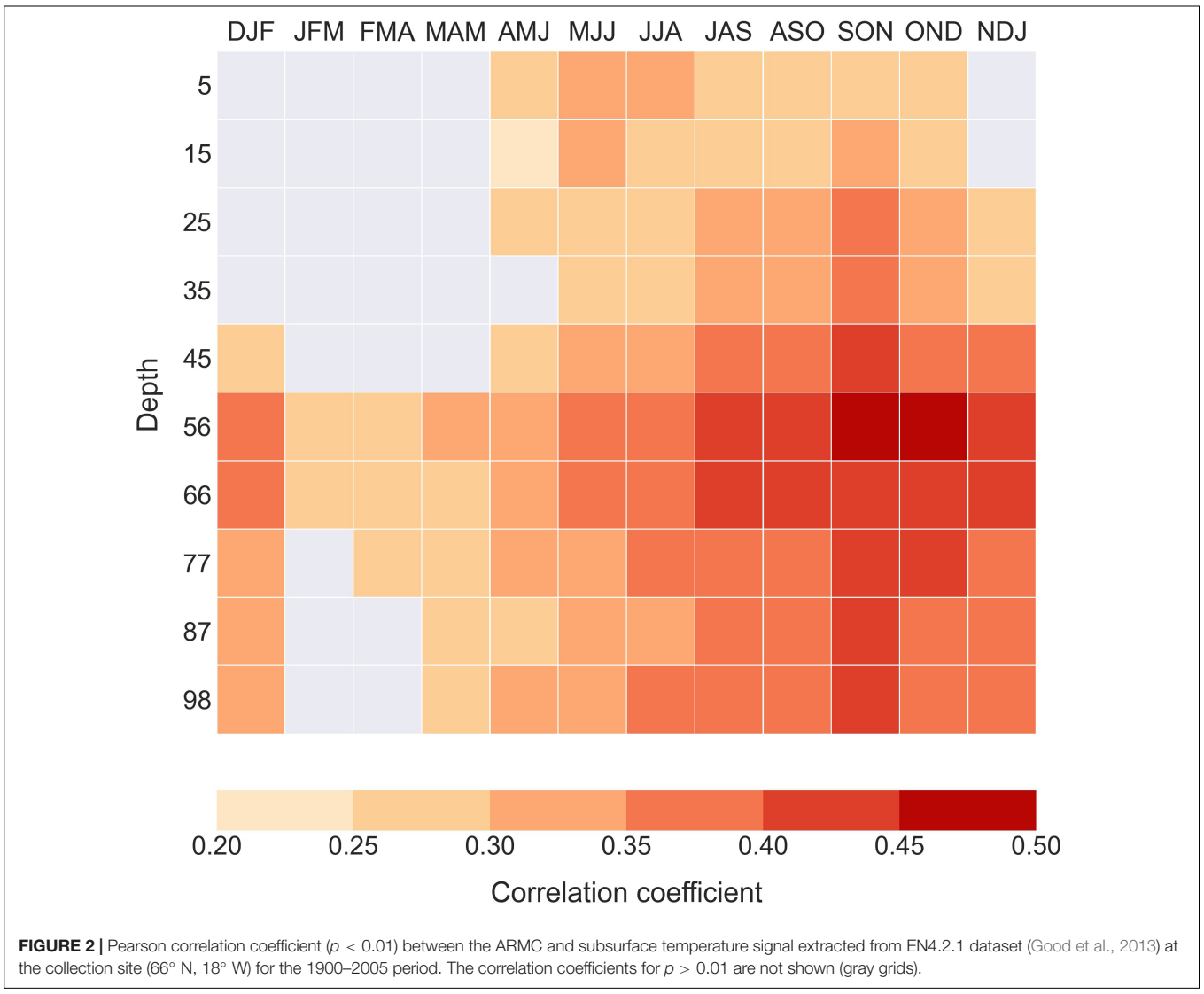

FIGURE 2 | Pearson correlation coefficient ($p < 0.01$) between the ARMC and subsurface temperature signal extracted from EN4.2.1 dataset (Good et al., 2013) at the collection site (66° N, 18° W) for the 1900–2005 period. The correlation coefficients for $p > 0.01$ are not shown (gray grids).

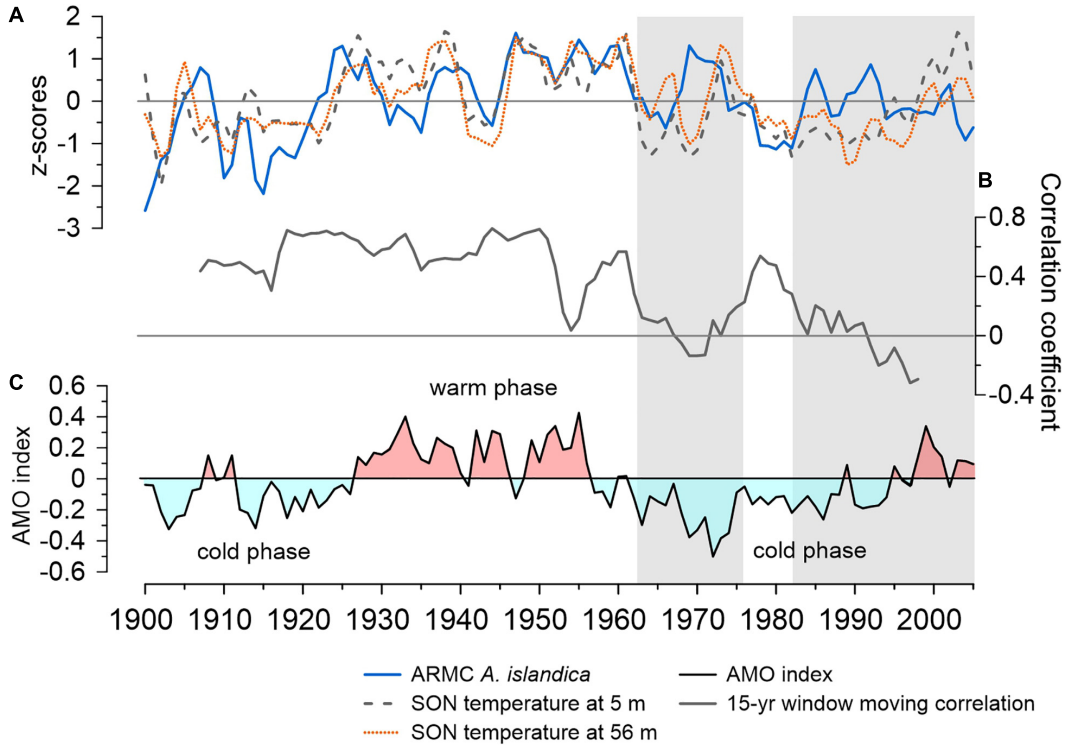

FIGURE 3 | (A) Normalized growth increments of *A. islandica* (blue line) and autumn (SON) water temperature at 5 m (gray dashed line) and 56 m depth (orange dotted line) between 1900 and 2005. A 5-year low-pass filter (i.e., Savitzky-Golay) was applied to the time series. The water temperatures were extracted at the approximate collection site (66° N, 18° W). **(B)** The 15-year running correlation between ARMC and temperature signal at 56 m depth. The gray-shaded sections represent periods in which the shell growth variability does not synchronize with the temperature signal. **(C)** Atlantic Multidecadal Oscillation (AMO) index (van Oldenborgh et al., 2009) showing positive (red shade) and negative (light blue shade) phases in the 1900–2005 period.

the negative temperature anomalies observed in the North Atlantic region.

Since the maximum correlation occurs during SON with the 56 m water depth time series, we analyzed whether the ARMC signal is dominated by high or low frequencies. In this respect, we obtained a stronger correlation when we isolate the low frequency signal ($r = 0.537$; $p < 0.00001$). The correlation between high frequency components of the shell chronology and water temperature is weaker than the low frequency one ($r = 0.336$, $p = 0.000424$).

Depth-Dependent Spatial Variability

To analyze the depth dependence variability, we have computed spatial correlation maps by selecting subsurface water temperatures for winter (DJF), spring (MAM), summer (JJA), and autumn (SON) at three different water depths: the surface (5 m), the water depth at which correlations are maximal (56 m) and near the collection depth (77 m) (**Figure 4**). Positive correlations between the ARMC and water temperatures extend latitudinally from the Labrador Sea to the Arctic Ocean, but also longitudinally from the Baffin Bay to the Barents Sea. The spatial pattern of correlation observed persists at a seasonal level and also becomes stronger at greater depth (i.e., 56–77 m). However, several discrepancies are observed in the correlations with surface and bottom water temperatures. For instance, correlations with surface water temperatures along the NW-Greenland and the Arctic region are substantially weaker than those found at greater depths. Positive correlations with surface water temperatures in the Labrador Sea and the surrounding area are particularly strong only during winter and spring. The strength of the correlation decreases with increasing water depth during DJF, but persists throughout MAM.

Negative correlations between the ARMC and subsurface water temperatures prevail in the tropical North Atlantic Ocean and to some extent in the eastern Pacific Ocean. Such strong correlations are observed during DJF and with increasing water depth in the Caribbean Sea. Negative correlations are also localized in the SE-Greenland in between positive centers resembling a tripole structure. This spatial association is present only during winter at 5 m depth.

DISCUSSION

Site-Specific Growth Conditions

To reconstruct past ocean temperatures and capture ocean variability, as well as variability originating from the atmosphere-ocean coupling, highly resolved bivalve records have been

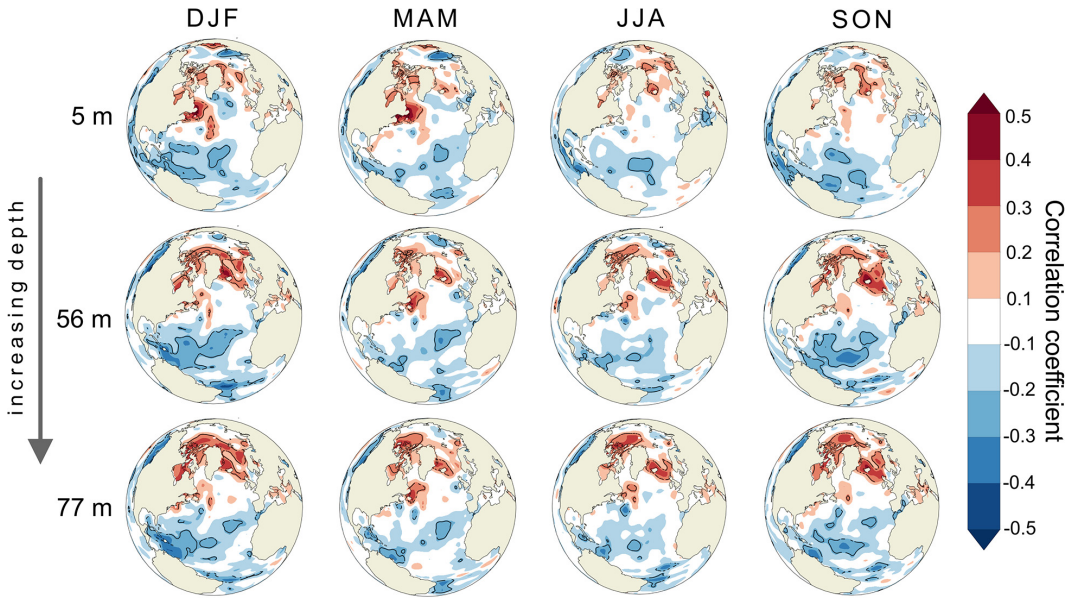

FIGURE 4 | Depth-dependent seasonal variability of growth index time series with water temperature at three different water depths (i.e., 5, 56, and 77 m) for 1900–2005 analysis period. Color shading shows the Pearson correlation coefficient ($p < 0.05$) between ARMC and seasonal water temperature time series at each grid point.

recurrently tested and used (e.g., Lohmann and Schöne, 2013; Marali and Schöne, 2015; Mette et al., 2016; Reynolds et al., 2018; Poitevin et al., 2019). However, when it comes to the influence of temperature signals on bivalve shell growth variability, there is contrasting evidence throughout the North Atlantic region. For instance, in the North Sea area, some studies were unable to find a statistically significant correlation with surface water temperatures (e.g., Witbaard, 1996; Epplé et al., 2006). In the Fladen Ground, the observed shell growth variability has been closely connected to local hydrological dynamics and the advective transport of food to the benthos (Witbaard, 1996; Witbaard et al., 1997). In other locations such as the Gulf of Maine and the coast of Newfoundland, shell growth variability has been associated with seasonal water temperature and stratification conditions (Poitevin et al., 2019; Wanamaker et al., 2019). In the region of Iceland, Lohmann and Schöne (2013) found that their record from the northeast coast of Iceland projects onto blocking situations in the northern North Atlantic with northeasterly flow toward Iceland and weakening in the westerly zonal flow over Europe, potentially affecting food availability controlling the local shell growth. On multi-decadal time scales, the same record shows a pronounced variability linked to North Atlantic temperatures and bears similarity with the AMO pattern (Deser and Blackmon, 1993; Dima and Lohmann, 2007).

Although there is a general consensus that regional conditions affect shell growth variability, more precision is required when establishing relationships with ocean temperatures. Absent or temporally limited instrumental temperature data at shell collection depth is often the culprit of weak or inconclusive correlations with water temperature, leaving studies to rely on gridded or instrumental SST data. Butler et al. (2013) used two long (pre-1900) instrumental and gridded SST time series and one instrumental bottom water temperature record (75 m) to test the relationship with *A. islandica* shell chronology from ∼82 m depth, and found weak correlations with SST data and a statistically insignificant one with the bottom water temperature. The authors furthermore attributed the lack of a strong temperature signal to the possibility that temperature is not the main driver of shell variability, but rather an indirect reflection of phytoplankton productivity in the upper ocean layer. We cannot, at this point, refute the relationship with food availability, however, in our study we found contrasting results upon reanalyzing the shell chronology of Butler et al. (2013). We not only observed weaker strength of correlation with the all-year-round SST signal, but also showed that the temperature signal becomes significantly stronger with increasing water depth layer (**Figure 2**). The observed dichotomy between surface and bottom water bodies (e.g., Schöne et al., 2005b; Wanamaker et al., 2019) brings to attention the need for multi-seasonal ocean depth-layered temperature profiles in performing correlation analyses.

Synchronization With Seasonal Temperature Signal

It is important to consider that bivalve shell growth is maximal during a specific time of the year. Thus, the correlation with water temperature should be optimized for the peak growing season at the specific collection site. For instance, Wanamaker et al. (2019) identified optimal growth conditions for *A. islandica* during the February-May period in the Gulf of Maine by performing

a similar correlation analysis with monthly temperature data. For the Icelandic region in particular, previous research on stable oxygen isotope profiles and annually-resolved shell growth indices of *A. islandica* (Schöne et al., 2005a; Reynolds et al., 2016) showed that the growing season starts early in spring and lasts to mid-late autumn (Feb–March to September–October). Reynolds et al. (2016) further suggested that peak growth occurs between June and October when maximum water temperatures are reached, an observation highly consistent with our own results. The correlation with water temperatures at 56 m depth is slightly better ($r = 0.449$, $p < 0.0001$) for the peak growth period (JJASO) than for the entire growth season ($r = 0.417$–0.438, $p < 0.0001$). The water temperature at the shell collection site ranges from 2.4–3°C in winter to 1.5–2.0°C in spring, 2.4–3.2°C in summer, and 3.2–4.0°C in autumn (**Figure 5**). Witbaard et al. (1998) showed in their experimental study that maximum height growth in *A. islandica* occurs between 3.2 and 6.2°C. Despite the EN4.2.1 temperature uncertainties (**Supplementary Figure 2A**), it is apparent that the ARMC best synchronizes with summer and autumn (JJASO) conditions when water temperatures above 3.2°C prevail, coinciding with depth expansion of the warmer upper ocean mixed layer (**Figures 5C,D**). Hence, we propose that JJASO is the predominant growth season for *A. islandica* collected from NIS, but since maximal correlations are found particularly with the autumn (SON) temperatures, we suggest that these temperatures reflect best the observed ARMC signal.

Failure in identifying the peak growth period reflected by the annually-resolved growth chronology could produce flawed correlations. For instance, Butler et al. (2013) used April–June (AMJ) months for correlations with surface and bottom water temperatures, a period which reflects a strong water column mixing at this location (**Figure 5B**). Using the EN4.2.1 temperature record, we noticed that the correlation with AMJ surface temperature and at the collection site is generally weaker than with the dominant growth season (see **Supplementary Table 1**), indicating unfavorable growing conditions. In addition, our correlations with AMJ surface and bottom temperature data are accompanied by a 2-year lag (**Supplementary Figure 3**). Butler et al. (2010) found similar lags which were attributed to the delayed response of nutrient supply to temperature or possible physiological effects related to reproductive activity. Interestingly, the strongest correlations obtained in this study are centered below the 56 m water depth during summer and autumn and present no time lag (**Supplementary Figure 3**), indicating a similar thermal relationship between the water bodies around the shell's site location (**Figure 5**). In a similar correlations study, Poitevin et al. (2019) found that shallow-water shells from the Newfoundland Shelf correlated significantly with the January and February temperature signal down to 175 m depth and with bottom water temperature (<100 m) for the remaining months (March–December), indicating the distinct impact of seasonal thermal stratification conditions on growth variability.

To better assess the observed thermal stratification pattern and the significance of the 56-m depth boundary layer between the local water bodies, we correlated the year-to-year shell growth variability with the EN4.2.1 salinity record (see **Supplementary Figure 4**). Salinity does not influence shell growth directly (explained variance <1%), but serves here as indicator of the different water bodies and seasonal stratification dynamics. Our results show significant positive correlations only with water layers below 56 m (**Supplementary Figure 4C**). The strongest in-phase correlation is present in late spring-early summer (MJJ), coinciding with the eastward movement of a more saline water body toward the collection site (34.80 isocline; **Supplementary Figure 5**) and with the stratification of the mixed layer throughout the summer and autumn. Strong correlations with seasonal temperature and salinity starting below 56 m depth suggest that the upper mixed layer is above this threshold. In fact, multiple regression analysis showed that 24.3% of the variance is explained by SON water temperature between 56 and 98 m depth, whereas 21.9% of the variance is exclusively explained by the water temperature at 56 m. While this phenomenon may be site-specific, it also reflects the disparity between the upper and lower water bodies, the mixed layer and the water body below the thermocline in their effect on the *Arctica* shell proxy.

Temporal Synchronization With Temperature Signal

In addition to analyzing the seasonal synchronization with local surface and bottom water temperature determinants of the main growth period and reflective of the seasonal stratification, we suggest that it is equally important to evaluate how stable this coupling was during the 106-year analysis period. The 15-year running correlation (**Figure 3B**) yielded a significant correlation ($r > 0.4$) between 1900 and early 1960s, besides a brief decoupling during the early 1950s and for almost a decade between 1970 and 1980. Our analysis showed that the observed growth variability in *A. islandica* responds to a low-frequency signal (section "Synchronization with temperature signal"), most apparent in the strong coupling with AMO phases during the first six decades (**Figure 3**). Despite the weak correlation with AMO index (11-year low-pass filter; $r = 0.250$, $p < 0.05$), the corresponding temperature anomalies in the North Atlantic sector reflect the dominance of Atlantic and Arctic waters on multi-decadal timescales. In turn, these changes modulate shell growth variability resulting in good coupling (cf., Lohmann and Schöne, 2013). The short-term lack of synchronization with SON water temperature at 56 m depth during the early 1950s could be attributed to quasi-decadal ocean variability and a temporal shift in the seasonal pattern. For instance, by computing a 15-year running correlation with JJA water temperature at 56 m depth, we do not observe such brief decoupling (**Supplementary Figure 6**). However, by shifting the season by one month at a time (i.e., JAS, ASO, SON, OND), we observe that the correlation decreases gradually (**Supplementary Figure 6**). Although shell growth variability is best explained by SON temperature during the 1900–2005 period, this finding suggests that short-term changes in the seasonal pattern of coupling can occur and can be tied to shifts in timing of primary productivity patterns, thereby complicating the local hydro-climatic reconstructions. However, the presence of a high frequency ocean component in the growth signal explains why weaker correlations with subsurface water temperature and salinity are often accompanied by a lag (**Supplementary Figures 3**, **4**).

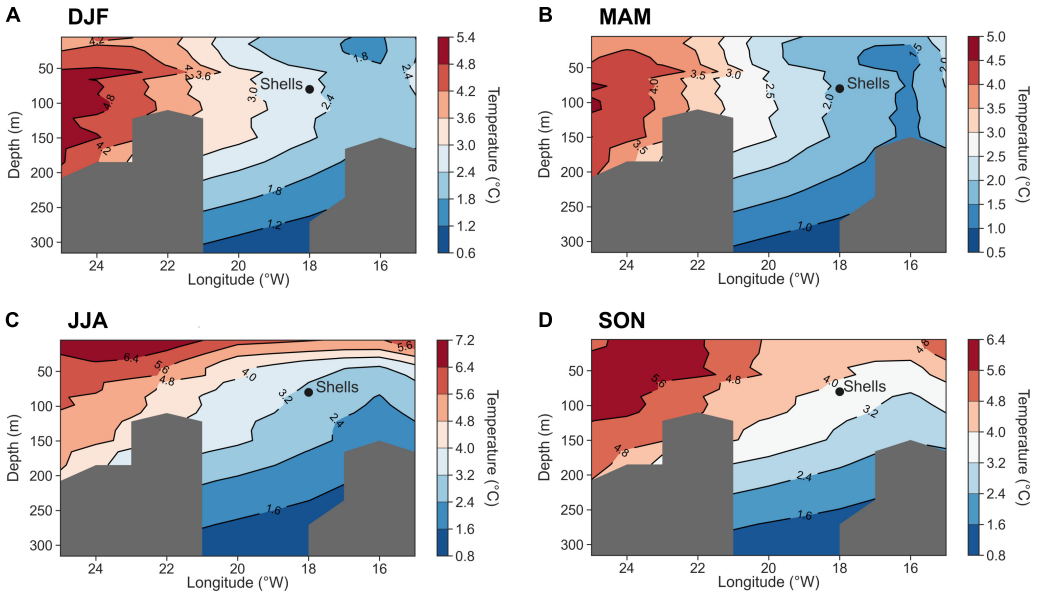

FIGURE 5 | Seasonal temperature-depth profiles along a longitudinal transect (25°W–15°W; 66°N). The EN4.2.1 temperature fields were averaged for **(A)** winter, **(B)** spring, **(C)** summer and **(D)** autumn for the period 1900–2005. The gray-shaded areas represent no available data.

We notice that regardless of the projected season (JJA-SON), the main periods of decreased temporal synchronicity with the water temperature at the collection site remains unchanged (**Figure 3** and **Supplementary Figure 6**). The first decoupled period occurs for almost a decade, between the early 1960s and mid-1970s, coinciding with the occurrence of the Great Salinity Anomaly (GSA) in the Icelandic region (Dickson et al., 1988). The GSA event was an abrupt freshening episode due to extensive sea ice export from the Arctic through the Fram Strait, which affected the entire northern North Atlantic region from mid-1960s to early 1980s (e.g., Ionita et al., 2016). Recognizing such abrupt events in annually-resolved master chronologies is important because it reflects the proxy's ability to record drastic environmental fluctuations. For instance, decreased shell growth during 1965 is also evident in shallow-water shells from NE Iceland (e.g., Lohmann and Schöne, 2013; Marali and Schöne, 2015), reflecting a common response of the *A. islandica* population from North Icelandic shelf to GSA. On the other hand, the positive growth anomaly observed during late 1960s and early 1970s might be related, partially, to a methodological bias as additional shells of low biological age are included in the chronology starting with 1940 (Butler et al., 2013). Butler et al. (2010, 2013) mention that time periods in which the chronology is dominated by series of low biological age might bias the RCS values toward higher values.

The decreased growth from the mid-1970s into the early 1980s synchronizes well with negative SST anomalies being preserved in the upper 200–300 m (Dickson et al., 1988). The second period of decreased synchronization with the temperature signal at the collection site starts in the early 1980s and lasts until the end of the shell chronology. This period is characterized by an overall negative temperature anomaly in the North Atlantic sector and a transition in the 1990s toward more positive anomalies. Although the salinity changes are minimal at this location and depth (±0.2 psu during the 1900–2005 period) and such fluctuations may be prone to some errors given the EN4.2.1 dataset's uncertainty in the North Icelandic shelf area (0.1–0.2 psu; **Supplementary Figure 2B**), we observed that after 1962, the oscillation is more frequent (**Supplementary Figure 7**). Multiple regression analysis indicates that prior to the GSA event, 41% in shell variability was explained by SON temperature and MJJ salinity at 56 m depth. The period post-GSA is hydrologically more variable, with interannual to quasi-decadal alternating influences from IC and EIC leading to changes in shell variability that cannot be explained by either temperature or salinity.

Diatom and copepod monthly abundances from CPR (see section "Materials and Methods") may help to understand the lack of synchronization between temperature and shell growth (**Figure 6**). Diatom blooms indicate high primary production, but access of the benthos to this production depends to a large extent on the presence of zooplankton (Witbaard et al., 2003). Unfortunately, observational data pre-1950s are lacking, so that this analysis was constrained to a shorter time series (1958–2005). Shell growth index correlates marginally with diatom abundance (r = 0.271, p = 0.063), however, the decrease in *A. islandica* growth starting around 1962 coincides with a decline in diatom abundance and a diatom-based SST reconstruction (Ran et al., 2011). The correlation with copepod abundance is not significant (r = 0.187, p = 0.202), however, for the period affected by GSA (1962–1976), 36% of shell growth variability is explained by copepod abundance (p = 0.0551). The growth variability after GSA cannot be explained by a three-parameter model (temperature, diatoms and copepods) besides short temporal observations of an inverse relationship

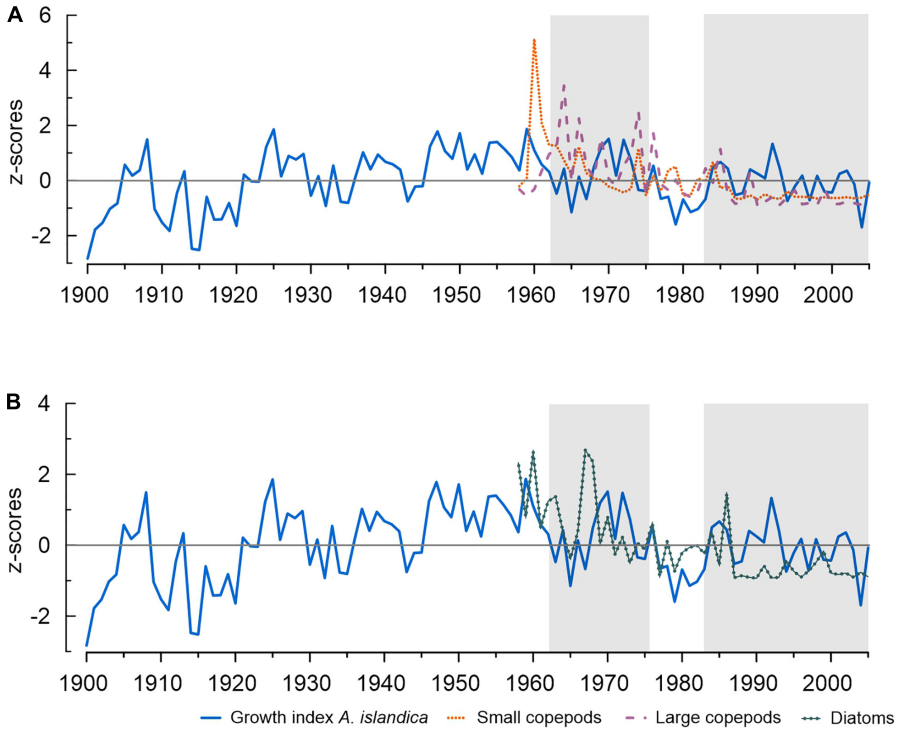

FIGURE 6 | Annual growth variability of *A. islandica* during 1900–2005. **(A)** Copepod and **(B)** Diatom abundances during 1958–2018. Periods of decreased synchronicity with surface (5 m) and water temperature at 56 m depth are shaded (see also **Figure 3**).

with copepod abundance (Witbaard et al., 2003). Lack of synchronization between *A. islandica* growth and environmental parameters in the late 1970s might also be due to a temporal mismatch between primary and secondary producers and a shift in food availability (Olivier et al., 2020). Apparently, our time series are too short and too noisy to enable the detection of correlation patterns and their development over time consistently. We emphasize that the reduced explained variance with temperature post-1960s may also complicate correlations with observational temperature data which are temporally limited and lack monthly to seasonal resolutions. An example is that the instrumental data used by Butler et al. (2013), namely Siglunes Station, is too short (1947–2005) and contains missing data for a statistically robust correlation (e.g., Bonett and Wright, 2000), in particular with JJA-SON bottom water temperature.

Oceanographic Patterns

By expanding our analysis spatially in the North Atlantic sector, we track the positive relationship with water temperature observed locally, and search for similarities with distant water bodies both at surface and with increasing water depth. For northern Norway, Mette et al. (2016) observed that the explained variance between the master-chronology of *A. islandica* and water temperature was higher at large-scale than locally. It is, therefore, interesting to address large-scale ocean variability to explain shell growth variability instead of correlating only with local phenomena.

The positive spatial correlation observed spreads along the Norwegian coast and to the Arctic Ocean, following the path of the North Atlantic Current and also along the western margin of Greenland, speaking for a predominant influence of the Labrador Current. Similarly, Mette et al. (2016) and Poitevin et al. (2019) observed that the spatial correlations are stronger for locations along main current paths, i.e., the Labrador Current and the North Atlantic Current. In this study, the spatial pattern of correlation is stronger at water depths approaching the collection site (56–77 m). This suggests that the mixed ocean layer across the observed locations responds to similar intrinsic modes of variability. Since strong correlations are found only below 56 m depth within a broad oceanographic area (**Figure 4**), we propose that the shell growth variability extracts a common temperature signal in between the mixed layer and the thermocline in the range of the optimal growth temperature. The relatively warm temperature conditions found within this depth range are furthermore suggestive of an intensified North Atlantic Current (NAC) and a predominant influence of Atlantic waters in the Arctic (Spielhagen et al., 2011). The signature of the warm and saline Atlantic water body following the northwards path of the NAC is further observed during spring and summer below 56 m in spatial correlation plots with salinity (**Supplementary Figure 8**). For the period 1900–2005, we remark that a negative phase in Arctic Oscillation (AO) is generally more dominant, with more warm air reaching the Arctic region.

We also observe a strong positive correlation during winter and spring with the surface waters around the coast of

Newfoundland. Poitevin et al. (2019) associated the enhanced shell growth in the area with a negative phase of North Atlantic Oscillation (NAO). The decrease in westerly winds reduces surface ocean heat loss to the atmosphere, thus maintaining a positive ocean temperature anomaly. Such positive anomaly is stronger during spring with increasing water depth, but it is also present during summer and autumn (**Figure 4**), indicating that the surface warming signal trails at greater depths during the next season. Another feature revealing an ocean-atmosphere interaction is the tripole pattern observed during winter (**Figure 4**). The tripole pattern is associated with SST anomalies, similar to the ones generated by NAO variability (Deser et al., 2010; Hurrell and Deser, 2010). The fact that this feature is significantly persistent only during winter, suggests that the signal along the path of Labrador Current is a local response of uppermost layer of the ocean to the variability of NAO. Although correlations with winter NAO index are not significant ($p > 0.05$), we suggest that interactions between NAO and the ocean can be identified interannually during winter, reflecting a winter re-emergence mechanism (Hurrell and Deser, 2010).

The negative temperature association that dominates the tropical Atlantic indicates that the water conditions are inversely related to those experienced by *A. islandica* in the North Atlantic region. The longitudinal extent and the timing of such negative correlations (i.e., autumn and winter) suggest that these are regions affected by a high-pressure and intensified northeasterly trade-winds which typically prevail during winter (Amador et al., 2006). The strongest correlations are centered along the coast of South America below 56 m depth (**Figure 4**) and indicate winter mixing associated with the Southern Caribbean coastal upwelling system (Rueda-Roa and Muller-Karger, 2013). The spatial extent covered by our analysis at various depths indicates that by using growth indices of *A. islandica*, it is possible to track thermal connections between different water bodies.

CONCLUSION

This study explored the depth-dependent relationship of an annually-resolved master chronology of *A. islandica* from the North Icelandic shelf to ocean temperatures. Our findings suggest that positive correlations are exclusively found between the mixed layer and thermocline during summer and autumn corresponding to patterns of thermal expansion of the local water bodies. The spatial extent of the analysis from tropical to extra-tropical regions of the North Atlantic Ocean marks potential source regions responsible for driving shell growth variability affected by interannual to quasi-decadal variability associated with NAO and multi-decadal variability linked to AMO. Such results are important in understanding drivers of variability in *A. islandica* and why correlations with sea surface temperatures can be particularly inconclusive. We, thereby, recommend that for maximizing the use of *A. islandica* as proxy, correlations should be made, as a first step, with water temperature data during the peak growth period, close to the collection site and depth over a long period of time (e.g., several decades and longer).

In the absence of a strong temperature signal, shell growth might synchronize with other environmental conditions (e.g., high diatom abundances) and competition from zooplankton feeding activity. With GSA-like events to be foreseen in the future, abrupt temperature changes do not only impact the growth, but alter the possibility of coupling the shell growth index to environmental parameters. In retrospective, depending on the location, such periods of decadal decoupling might be useful in identifying temperature and climatic anomalies. The use of growth indices in *A. islandica* together with other proxy-based temperature reconstructions (e.g., $\delta^{18}O$ from same chronology) over the past 1000 years or with model simulations for a more robust outlook, could improve our skills in observing large-scale ocean variability at various water depths. Our results enhance the application of *A. islandica* to track thermally linked water bodies across a much broader region and emphasizes the need to look not only at the relationship with the sea surface temperature, but also with the water temperature at different depths.

DATA AVAILABILITY STATEMENT

The sources of all primary data this study is based upon are cited in the paper or the **Supplementary Material**, further inquiries may be directed to the corresponding author.

AUTHOR CONTRIBUTIONS

DC, MI, and TB designed the project. DC analyzed the data, interpreted the results, and wrote the manuscript with contributions from MI, DA, LB, TB, and GL. All authors contributed to the manuscript and approved the submitted version.

FUNDING

MI, GL, DA, TB, and LB were supported by Helmholtz Association through the joint program "Changing Earth - Sustaining our Future" (PoF IV) program of the AWI. Funding by the AWI Strategy Fund Project - PalEX (DC) and by the Helmholtz Climate Initiative - REKLIM (MI) was gratefully acknowledged. We acknowledge support by the Open Access Publication Funds of Alfred-Wegener-Institute for Polar and Marine Research.

ACKNOWLEDGMENTS

We thank Paul Gierz for technical help in creating the spatial correlation maps. We are grateful to Paul G. Butler and others who made available their data for other studies, such as ours, to continue the research. We thank Philippe Archambault for editorial handling and our two reviewers for their expertise and constructive feedback which helped improve our manuscript. We acknowledge the use of gridded temperature

and salinity data (https://www.metoffice.gov.uk/hadobs/en4/), diatom and copepod data (https://www.cprsurvey.org/), AMO index (https://climexp.knmi.nl/), and NAO index (https://climatedataguide.ucar.edu/climate-data/hurrell-north-atlantic-oscillation-nao-index-pc-based).

SUPPLEMENTARY MATERIAL

The Supplementary Material for this article can be found online at: https://www.frontiersin.org/articles/10.3389/fmars.2021.687318/full#supplementary-material

REFERENCES

Amador, J. A., Alfaro, E. J., Lizano, O. G., and Magaña, V. O. (2006). Atmospheric forcing of the eastern tropical Pacific: a review. *Prog. Oceanogr.* 69, 101–142. doi: 10.1016/j.pocean.2006.03.007

Ballesta-Artero, I., Janssen, R., van der Meer, J., and Witbaard, R. (2018). Interactive effects of temperature and food availability on the growth of *Arctica islandica* (*Bivalvia*) juveniles. *Mar. Environ. Res.* 133, 67–77. doi: 10.1016/j.marenvres.2017.12.004

Batten, S. D., Clark, R., Flinkman, J., Hays, G., John, E., John, A. W. G., et al. (2003). CPR sampling: the technical background, materials and methods, consistency and comparability. *Prog. Oceanogr.* 58, 193–215. doi: 10.1016/j.pocean.2003.08.004

Bonett, D. G., and Wright, T. A. (2000). Sample size requirements for estimating pearson, kendall and spearman correlations. *Psychometrika* 65, 23–28. doi: 10.1007/BF02294183

Butler, P. G., Richardson, C. A., Scourse, J. D., Wanamaker, A. D., Shammon, T. M., and Bennell, J. D. (2010). Marine climate in the Irish Sea: analysis of a 489-year marine master chronology derived from growth increments in the shell of the clam *Arctica islandica*. *Quat. Sci. Rev.* 29, 1614–1632. doi: 10.1016/j.quascirev.2009.07.010

Butler, P. G., Wanamaker, A. D., Scourse, J. D., Richardson, C. A., and Reynolds, D. J. (2013). Variability of marine climate on the North Icelandic shelf in a 1357-year proxy archive based on growth increments in the bivalve *Arctica islandica*. *Palaeogeogr. Palaeoclimatol. Palaeoecol.* 373, 141–151. doi: 10.1016/j.palaeo.2012.01.016

Czaja, A., Robertson, A. W., and Huck, T. (2003). "The role of Atlantic Ocean-atmosphere coupling in affecting North Atlantic oscillation variability," in *The North Atlantic Oscillation: Climatic Significance and Environmental Impact*, eds J. W. Hurrell, Y. Kushnir, G. Ottersen, and M. Visbeck (Hoboken: Blackwell Publishing Ltd), 147–172. doi: 10.1029/134GM07

Deser, C., Alexander, M. A., Xie, S.-P., and Phillips, A. S. (2010). Sea surface temperature variability: patterns and mechanisms. *Ann. Rev. Mar. Sci.* 2, 115–143. doi: 10.1146/annurev-marine-120408-151453

Deser, C., and Blackmon, M. L. (1993). Surface climate variations over the North Atlantic Ocean during winter: 1900–1989. *J. Clim.* 6, 1743–1753. doi: 10.1175/1520-04421993006<1743:SCVOTN<2.0.CO;2

Dickson, R. R., Meincke, J., Malmberg, S.-A., and Lee, A. J. (1988). The "Great Salinity Anomaly" in the Northern North Atlantic 1968–1982. *Prog. Oceanogr.* 20, 103–151. doi: 10.1016/0079-6611(88)90049-3

Dima, M., and Lohmann, G. (2007). A hemispheric mechanism for the Atlantic Multidecadal Oscillation. *J. Clim.* 20, 2706–2719. doi: 10.1175/JCLI4174.1

Epplé, V. M., Brey, T., Witbaard, R., Kuhnert, H., and Pätzold, J. (2006). Sclerochronological records of *Arctica islandica* from the inner German Bight. *Holocene* 16, 763–769. doi: 10.1191/0959683606hl970rr

Esper, J., Cook, E., Krusic, P., Peters, K., and Schweingruber, F. (2003). Tests of the RCS method for preserving low-frequency variability in long tree-ring chronologies. *Tree Ring Res.* 59, 81–98.

Gastineau, G., D'Andrea, F., and Frankignoul, C. (2013). Atmospheric response to the North Atlantic Ocean variability on seasonal to decadal time scales. *Clim. Dynamics* 40, 2311–2330. doi: 10.1007/s00382-012-1333-0

Good, S. A., Martin, M. J., and Rayner, N. A. (2013). EN4: quality controlled ocean temperature and salinity profiles and monthly objective analyses with uncertainty estimates. *J. Geophys. Res. Oceans* 118, 6704–6716. doi: 10.1002/2013JC009067

Hurrell, J. W. (1995). Decadal trends in the North Atlantic Oscillation: regional temperatures and precipitation. *Science* 269, 676–679. doi: 10.1126/science.269.5224.676

Hurrell, J. W., and Deser, C. (2010). North Atlantic climate variability: the role of the North Atlantic Oscillation. *J. Mar. Syst.* 79, 231–244. doi: 10.1016/j.jmarsys.2009.11.002

Ionita, M., Scholz, P., Lohmann, G., Dima, M., and Prange, M. (2016). Linkages between atmospheric blocking, sea ice export through Fram Strait and the Atlantic Meridional Overturning Circulation. *Sci. Rep.* 6:32881. doi: 10.1038/srep32881

Lohmann, G., and Schöne, B. R. (2013). Climate signatures on decadal to interdecadal time scales as obtained from mollusk shells (*Arctica islandica*) from Iceland. *Palaeogeogr. Palaeoclimatol. Palaeoecol.* 373, 152–162. doi: 10.1016/j.palaeo.2012.08.006

Marali, S., and Schöne, B. R. (2015). Oceanographic control on shell growth of *Arctica islandica* (*Bivalvia*) in surface waters of Northeast Iceland — Implications for paleoclimate reconstructions. *Palaeogeogr. Palaeoclimatol. Palaeoecol.* 420, 138–149. doi: 10.1016/j.palaeo.2014.12.016

Mette, M. J., Wanamaker, A. D., Carroll, M. L., Ambrose, W. G., and Retelle, M. J. (2016). Linking large-scale climate variability with *Arctica islandica* shell growth and geochemistry in northern Norway. *Limnol. Oceanogr.* 61, 748–764. doi: 10.1002/lno.10252

Olivier, F., Gaillard, B., Thébault, J., Meziane, T., Tremblay, R., Dumont, D., et al. (2020). Shells of the bivalve *Astarte moerchi* give new evidence of a strong pelagic-benthic coupling shift occurring since the late 1970s in the North Water polynya. *Philos. Trans. A Math. Phys. Eng. Sci.* 378:20190353. doi: 10.1098/rsta.2019.0353

Poitevin, P., Thébault, J., Siebert, V., Donnet, S., Archambault, P., Doré, J., et al. (2019). Growth response of *Arctica Islandica* to North Atlantic oceanographic conditions since 1850. *Front. Mar. Sci.* 6:483. doi: 10.3389/fmars.2019.00483

Ran, L., Jiang, H., Knudsen, K. L., and Eiríksson, J. (2011). Diatom-based reconstruction of palaeoceanographic changes on the North Icelandic shelf during the last millennium. *Palaeogeogr. Palaeoclimatol. Palaeoecol.* 302, 109–119. doi: 10.1016/j.palaeo.2010.02.001

Reynolds, D. J., Hall, I. R., Slater, S. M., Mette, M. J., Wanamaker, A. D., Scourse, J. D., et al. (2018). Isolating and reconstructing key components of North Atlantic Ocean variability from a sclerochronological spatial network. *Paleoceanogr. Paleoclimatol.* 33, 1086–1098. doi: 10.1029/2018PA003366

Reynolds, D. J., Scourse, J. D., Halloran, P. R., Nederbragt, A. J., Wanamaker, A. D., Butler, P. G., et al. (2016). Annually resolved North Atlantic marine climate over the last millennium. *Nat. Commun.* 7:13502. doi: 10.1038/ncomms13502

Rueda-Roa, D. T., and Muller-Karger, F. E. (2013). The southern Caribbean upwelling system: sea surface temperature, wind forcing and chlorophyll concentration patterns. *Deep Sea Res. I Oceanogr. Res. Pap.* 78, 102–114. doi: 10.1016/j.dsr.2013.04.008

Savitzky, A., and Golay, M. J. E. (1964). Smoothing and differentiation of data by simplified least squares procedures. *Anal. Chem.* 36, 1627–1639. doi: 10.1021/ac60214a047

Schöne, B. R., Fiebig, J., Pfeiffer, M., Gleβ, R., Hickson, J., Johnson, A. L. A., et al. (2005a). Climate records from a bivalved Methuselah (*Arctica islandica*, Mollusca; Iceland). *Palaeogeogr. Palaeoclimatol. Palaeoecol.* 228, 130–148. doi: 10.1016/j.palaeo.2005.03.049

Schöne, B. R., Pfeiffer, M., Pohlmann, T., and Siegismund, F. (2005b). A seasonally resolved bottom-water temperature record for the period AD 1866-2002 based on shells of *Arctica islandica* (Mollusca, North Sea). *Int. J. Climatol.* 25, 947–962. doi: 10.1002/joc.1174

Schöne, B. R., Freyre Castro, A. D., Fiebig, J., Houk, S. D., Oschmann, W., and Kröncke, I. (2004). Sea surface water temperatures over the period 1884–1983 reconstructed from oxygen isotope ratios of a bivalve mollusk shell (*Arctica islandica*, southern North Sea). *Palaeogeogr. Palaeoclimatol. Palaeoecol.* 212, 215–232. doi: 10.1016/j.palaeo.2004.05.024

Spielhagen, R. F., Werner, K., Sørensen, S. A., Zamelczyk, K., Kandiano, E., Budeus, G., et al. (2011). Enhanced modern heat transfer to the Arctic by warm Atlantic water. *Science* 331, 450–453. doi: 10.1126/science.1197397

van Oldenborgh, G. J., te Raa, L. A., Dijkstra, H. A., and Philip, S. Y. (2009). Frequency- or amplitude-dependent effects of the Atlantic meridional overturning on the tropical Pacific Ocean. *Ocean Sci.* 5, 293–301. doi: 10.5194/os-5-293-2009

Wanamaker, A. D., Butler, P. G., Scourse, J. D., Heinemeier, J., Eiríksson, J., Knudsen, K. L., et al. (2012). Surface changes in the North Atlantic meridional overturning circulation during the last millennium. *Nat. Commun.* 3:899. doi: 10.1038/ncomms1901

Wanamaker, A. D., Griffin, S. M., Ummenhofer, C. C., Whitney, N. M., Black, B., Parfitt, R., et al. (2019). Pacific climate influences on ocean conditions and extreme shell growth events in the Northwestern Atlantic (Gulf of Maine). *Clim. Dynamics* 52, 6339–6356. doi: 10.1007/s00382-018-4513-8

Wanamaker, A. D., Heinemeier, J., Scourse, J. D., Christopher, A. R., Butler, P. G., Eiríksson, J., et al. (2008b). Very long-lived mollusks confirm 17th century AD tephra-based radiocarbon reservoir ages for north Icelandic shelf waters. *Radiocarbon* 50, 399–412.

Wanamaker, A. D., Kreutz, K. J., Schöne, B. R., Pettigrew, N., Borns, H. W., Introne, D. S., et al. (2008a). Coupled North Atlantic slope water forcing on Gulf of Maine temperatures over the past millennium. *Clim. Dynamics* 31, 183–194. doi: 10.1007/s00382-007-0344-8

Weidman, C. R., Jones, G., and Lohmann, K. C. (1994). The long-lived mollusc *Arctica islandica*: a new paleoceanographic tool for the reconstruction of bottom temperatures for the continental shelves of the northern North Atlantic Ocean. *J. Geophys. Res.* 99, 305–318. doi: 10.1029/94JC01882

Wigley, T. M. L., Briffa, K. R., and Jones, P. D. (1984). On the average value of correlated time series, with applications in dendroclimatology and hydrometeorology. *J. Clim. Appl. Meteorol.* 23, 201–213. doi: 10.1175/1520-04501984023<0201:OTAVOC<2.0.CO;2

Witbaard, R. (1996). Growth variations in *Arctica islandica* L. (Mollusca): a reflection of hydrography-related food supply. *ICES J. Mar. Sci.* 53, 981–987. doi: 10.1006/jmsc.1996.0122

Witbaard, R., Duineveld, G. C. A., and De Wilde, P. A. W. J. (1997). A long-term growth record derived from *Arctica Islandica* (Mollusca, *Bivalvia*) from the Fladen Ground (Northern North Sea). *J. Mar. Biol. Assoc. U. K.* 77, 801–816. doi: 10.1017/S0025315400036201

Witbaard, R., Duineveld, G. C. A., and de Wilde, P. A. W. J. (1999). Geographical differences in growth rates of *Arctica islandica* (Mollusca: *Bivalvia*) from the North Sea and adjacent waters. *J. Mar. Biol. Assoc. U. K.* 79, 907–915. doi: 10.1017/S0025315498001076

Witbaard, R., Franken, R., and Visser, B. (1998). Growth of juvenile *Arctica islandica* under experimental conditions. *Helgoländer Meeresuntersuchungen* 51, 417–431. doi: 10.1007/BF02908724

Witbaard, R., Jansma, E., and Sass Klaassen, U. (2003). Copepods link quahog growth to climate. *J. Sea Res.* 50, 77–83. doi: 10.1016/S1385-1101(03)00040-6

Conflict of Interest: The authors declare that the research was conducted in the absence of any commercial or financial relationships that could be construed as a potential conflict of interest.

4

Paper III

Atmospheric blocking signature in *Arctica islandica* growth from Helgoland

RQ.3	Is there a discernible connection between the extreme growth indices observed in *Arctica islandica* and large-scale atmospheric patterns, particularly synoptic atmospheric blocking, in a region prone to such influences as the North Sea?

This chapter showcases the final research paper in the scope of my doctoral degree, which will be shortly submitted to the *Geophysical Research Letters* journal.
The supplementary material corresponding to this manuscript is found in **Appendix C**. The draft version is found below.

Author contributions:
DEC designed the study, conducted the research and wrote the manuscript. TB sourced the master shell chronology. NR calculated and provided the blocking frequency data. GL, NR, TB and KHW contributed meaningful suggestions. MI supervised and gave feedback on the manuscript.

Atmospheric blocking signature in *Arctica islandica* growth from Helgoland

Diana E. Caldarescu[1], Thomas Brey[1,2,3], Norel Rimbu[1], Gerrit Lohmann[1,4], Karen H. Wiltshire[5,6] and Monica Ionita[1,7]

[1]Alfred Wegener Institute, Helmholtz Centre for Polar and Marine Research (AWI), Bremerhaven, Germany [2]Helmholtz Institute for Functional Marine Biodiversity, University of Oldenburg (HIFMB), Oldenburg, Germany [3]Department of Functional Ecology, University of Bremen, Bremen, Germany [4]Department of Environmental Physics, University of Bremen, Bremen, Germany [5]Biological Institute Helgoland, Alfred Wegener Institute for Polar and Marine Research, Helgoland, Germany [6]Wadden Sea Station Sylt, Alfred Wegener Institute for Polar and Marine Research, List, Germany [7]Faculty of Forestry," Stefan cel Mare" University of Suceava, Suceava, Romania

Abstract

Understanding the dynamics and impacts of atmospheric blocking events is essential for improving weather forecasts, assessing climate change impacts, and enhancing resilience to regional extreme weather events. While observational analyses, modeling studies, and statistical approaches provide valuable insights into the complex interactions between blocking and large-scale climate drivers, our focus is on seeking novel perspectives from marine organisms, such as *Arctica islandica* growth records. We evaluate whether growth extremes in an *Arctica islandica* master chronology from Helgoland (southern North Sea) are associated to atmospheric circulation anomalies with the prospect of reconstructing such occurrences in the 1836-2004 period. Our results indicate that years characterized by growth reduction in *Arctica islandica* correspond to positive phase of the North Atlantic Oscillation during the boreal winter, accompanied by spring anticyclonic activity and enhanced blocking frequency centered on the British Isles. Consequently, the wind patterns alter timing, quantity and quality of spring blooms. We conclude that our record from the southern North Sea brings North Atlantic atmospheric blocking into a long-term perspective.

Keywords: *Arctica islandica*; growth extremes; atmospheric blocking, blocking frequency, North Atlantic Oscillation; East Pacific/ North Pacific index; Helgoland.

1. Introduction

In recent years an increase in extreme events (e.g., marine and terrestrial heat waves, droughts, floods) has been observed, which have been caused to a large extent by specific weather patterns, like atmospheric blocking (Chapman et al., 2022; Kautz et al., 2022; Bakke et al., 2023). Atmospheric blocking disrupts the typical eastward progression of mid to upper tropospheric air circulation, acting as a precursor to the development of synoptic extreme weather events. When blocked, the jet stream exhibits meandering patterns over mid- and high-latitudes (Rex, 1951). Depending on their nature—whether cyclonic or anticyclonic—these meandering structures can stall over a region, giving rise to cold-spells (Cai et al., 2024), heavy precipitation leading to flooding (Ionita et al., 2020a), unusual wind patterns (Kautz et al., 2022), and the initiation of both terrestrial and marine heat waves (Perkins et al., 2012; Oliver et al., 2018). Atmospheric blocking is, thereby, a crucial factor in the development of weather extremes (Rimbu et al., 2014; Kautz et al., 2022), which affect both terrestrial ecosystems and marine ecosystems (Smale et al., 2019).

In their statistical analysis of 500 mb geopotential height between 1950 to 1979, Lejenäs and Økland (1983) emphasized that the frequency and duration of atmospheric blocking occurrence is higher in the Atlantic region compared to the Pacific. This observation underscores the pivotal role of atmospheric circulation patterns in shaping regional climate dynamics and the importance of the Euro-Atlantic region (Diao et al., 2006). Seasonal, inter-annual and inter-decadal weather and climate variability over the Euro-Atlantic region is primarily dictated by the North Atlantic Oscillation (NAO) polarity (Hurrell, 1995; Hurrell and Deser, 2010). In its positive phase, a strong dipole in the sea-level pressure develops between Azores and Iceland (Jones et al., 1997), deviating the storm track northwards and bringing warmer and wetter conditions into the high-latitudes (Hurrell, 1995), which contrasts the dry regime of the southern and eastern continental regions. Regardless of its strength, the NAO teleconnection pattern is spatially (e.g., Barnston and Livezey, 1987; Cassou et al., 2004; Hurrell and Deser, 2010) and temporally (Pozo-Vázquez et al., 2001) non-stationary. Recent research efforts have shown that coupling NAO with the second and third leading mode of atmospheric variability—namely, the East Atlantic (EA) and its extended teleconnection, the East Atlantic-West Russian (EA/WR), and the Scandinavian (SCA) pattern—offers a more precise depiction of boreal winter climatology (e.g., Moore and Renfrew, 2012), temperature and precipitation patterns (Comas-Bru and McDermott, 2014; Ionita, 2014; Ionita et al., 2015) and

sea-level changes (Chafik et al., 2017) in the Euro-Atlantic sector.

By employing empirical orthogonal analysis on blocking frequency data, Rimbu et al. (2014) have found that the first three dominant patterns explaining 35 % to 44 % variability on interannual to interdecadal time-scales, respectively, are related to anticyclonic blocking over Greenland, North Sea and Scandinavia. Over the past two decades, frequent blocking over the North Sea has resulted in a significant increase in precipitation deficits over Central Europe (Ionita et al., 2020b). As the North Atlantic Oscillation influences zonal wind patterns, variations and anomalies in the strength of the westerlies redistribute the upper ocean's heat content and density (Bersch, 2002). Additionally, these fluctuations affect the mixed layer depth and the winter recurrence of temperature anomalies (Alexander and Deser, 1995), playing a vital role in supporting primary production and the organisms at dependent trophic levels. In the southern regions of the North Sea, in particular the German Bight, four decades of instrumental recordings from the island of Helgoland reveal a notable change in water conditions: an increase of 1.64 °C and 0.3 PSU (i.e., practical salinity unit) in mean annual temperature and salinity, respectively (Wiltshire et al., 2010). Moreover, the North Sea in general and the German Bight experienced an ecological regime shift after 1987 CE (Reid and Edwards, 2001; Reid et al., 2001; Edwards et al., 2002; Schlüter et al., 2008), aligning with increased marine influences following the occurrence of the shift (Wiltshire et al., 2008).

Considering the interplay between the atmospheric dynamics and a shallow-water environment such as the German Bight, we want to see whether particular atmospheric anomalies, namely atmospheric blocking, can be reconstructed from the growth history of benthic organisms such as *Arctica islandica* (*A. islandica*) bivalve species. Many studies from the North Sea (Schöne et al., 2003a, 2005c,d; Epplé et al., 2006; Holland et al., 2014) have shown that *A. islandica* shell growth signal captures a signature associated with NAO. However, Epplé et al. (2006) have found it challenging to explain growth variability in terms of physical and biological parameters. To overcome such challenges in a dynamic environment, we primarily focus on the extreme growth response of *A. islandica* bivalve species to uncover anomalous atmospheric teleconnection patterns beyond pre-instrumental period.

2. Study area

The island of Helgoland (54° 10′ – 54.6″N, 7° 52′ – 56.6″E) is located 70 km off the coast of Germany, in the German Bight, southern North Sea. In this highly dynamical estuarine sea, water transport alternates between warm and saline Atlantic water entering the northern and southwest North Sea – which has become more dominant in recent decades (Wiltshire et al., 2010) – and less saline and dense coastal waters via the Elbe and Weser rivers (Figure 4.1). The dynamical nature of the area stems from synoptic atmospheric patterns, commonly identified in sea level pressure anomalies, which facilitate or hinder heat and moisture transport from the tropical Atlantic. For instance, Ionita et al. (2008) have shown that anticyclonic conditions over Scandinavia and the German Bight reduce spring moisture and precipitation contributing to low riverine discharge and high salinity anomalies. Later research by Lohmann and Wiltshire (2012) have found that winter blocking conditions over Scandinavia change water conditions (e.g., clear vs. turbid) leading to a delay in the spring diatom bloom, in turn, affecting the performance of dependent members of the food web. Such observations have been enabled by the Helgoland Roads project, which provides high resolution, long-term monitoring of physical, chemical and ecological parameters of this marine protected area since 1962 (Wiltshire and Manly, 2004; Wiltshire et al., 2010, "Helgoländer Felssockel" NSG).

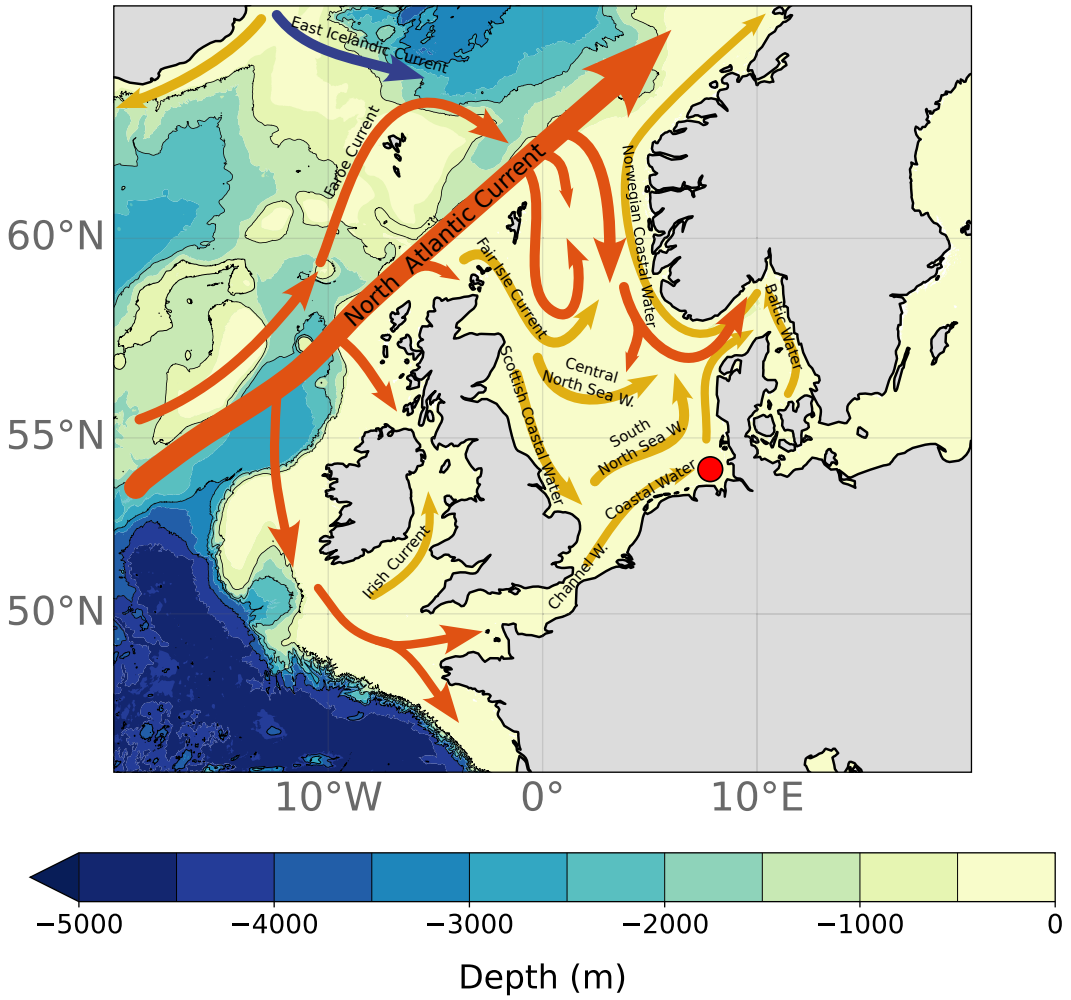

Figure 4.1. Bathymetric map of the Eastern Atlantic region (45°N – 63°N, 30°W – 30°E) showing collection site near the island of Helgoland (red marker), German Bight, North Sea. The red arrows indicate the North Atlantic Current and associated Atlantic waters, the yellow arrows represent coastal waters, and the blue arrows denote Arctic waters. The isolines start from 1000-m depth and link to the depths displayed on the color-bar. Gridded bathymetric data was obtained from The General Bathymetric Chart of the Oceans (GEBCO). After Fig.15 in Turrell et al. (1992) and Fig.5 in Hofmann et al. (2005) and AMAP.

3. Materials and Methods

3.1. Master shell chronology

In this study we used an unpublished master chronology based on growth-increment widths of 25 shells of *A. islandica* from the vicinity of Helgoland (Bauer, 2011). Seventeen *A. islandica* specimens were live-collected at 40-m water depth (54°9′2″N, 7°47′6″E) to (54°9′7″N, 7°49′6″E; see Figure 4.1) in August 2005. The master chronology was supplemented by the following sub-fossil specimens: six shells from the Biologische Anstalt Helgoland (BAH) (coded

HM) and two valves, on loan, from the Zoological Museum of Kiel (courtesy of Bernd Schöne; coded A10L and A11L). The live-collected specimens underwent the standard preparation routine, involving the removal of soft tissue and periostracum. Subsequently, cross-sections were made along the maximum axis of growth, followed by a thorough cleaning, polishing, and etching. The specimens were then stained with Mutvei solution (Schöne et al., 2005b) for visual inspection under stereo-microscope. Cross-dating of live-collected and sub-fossil specimens was achieved visually and with the aid of the dendrochronology software TSAP-Win™. Subsequent increment length corrections were made manually and with the aforementioned software. Further details can be found in Bauer (2011). Increments from the first five years of life were excluded in all individuals, and the ontogenic trend removed by cubic spline function (λ=400) in JMP® software. Thereafter, the growth indices (GI) at year (i) for each chronology was calculated by dividing the measured increment by the predicted increment after the removal of the ontogenic trend (eq. (4.1)).

$$GI_i = \log\left(\frac{\text{Observed incr.}}{\text{Predicted incr.}}\right) \tag{4.1}$$

The relative shell growth per unit time is calculated by standardizing (μ=0; σ=1) the resulting growth indices (eq. (4.2)) in the dimensionless quantity SGI (i.e., Standardized Growth Index).

$$SGI = \frac{\mathrm{GI}_i - \mu}{\sigma} \quad (2) \tag{4.2}$$

In this study, the final SGI measure is calculated by using a dynamic normalization with a moving average of 11 years (eq. (4.3)).

$$\mathrm{SGI}_{11,i} = \frac{\mathrm{SGI}_i - \mathrm{MA}(\mu_{SGI}, 11)}{\mathrm{MA}(\sigma_{SGI}, 11)} \tag{4.3}$$

The resulting SGI covers the 1767-2004 period, although the first four years are covered by only one specimen (A10L) from Zoological Museum of Kiel (see Figure 4.2A).

3.2. Environmental data

We used monthly sea level pressure (SLP) and geopotential height at 500 mb (Z500) at 1° x 1° grid resolution in the period 1836 to 2004 CE as a diagnostic for potential large-scale anomalies in the surface and mid-level atmosphere circulation. Zonal (u-wind) and meridional (v-wind) fields accompany the SLP

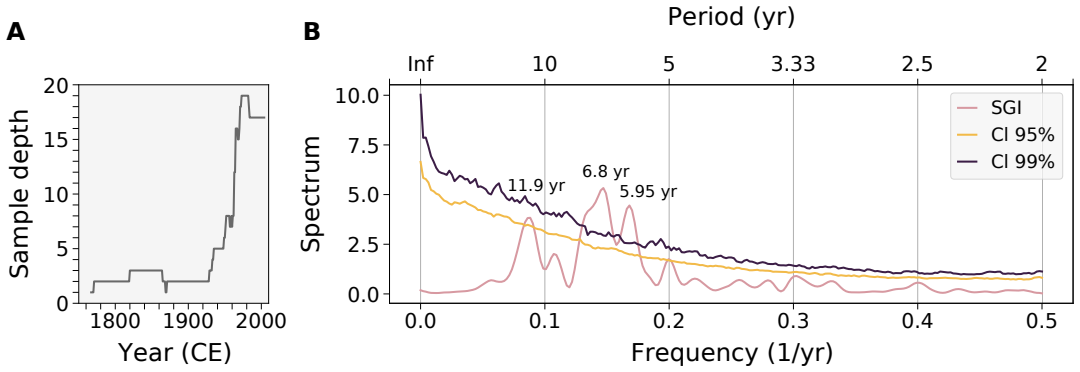

Figure 4.2. **(A)** Life-span of individual shell samples (sample depth) used in the master chronology from Helgoland (Bauer, 2011). **(B)** Spectral analysis of the SGI against AR(1) red noise background at 95 % and 99, %, respectively, confidence limits. Significant peaks are marked on the figure.

and Z500 maps and were extracted at 10 m height and 5500 m height (500mb), respectively. The data were extracted from the 20^{th} Century Reanalysis V3 (Slivinski et al., 2019).

We supplemented our analyses with monthly and seasonally averaged sea-surface temperature (T_{Helgo}) and salinity (S_{Helgo}) from the high-resolution, long-term observational dataset "Helgoland Roads" (54°11.3'N, 7°54.0'E; Wiltshire and Manly, 2004). As a primary productivity marker for local waters and its observed connection to atmospheric blocking (see Lohmann and Wiltshire, 2012), we used diatom data from the Helgoland Roads dataset, and calculated the mean diatom day (MDD) according to Wiltshire and Manly (2004) for the first quarter (January to March) and second quarter (April to June) of the year, respectively.

The first leading mode of atmospheric variability, accounting for one-third of the explained SLP variance and impacting the North Atlantic-European sector on interannual to interdecadal time scales (Hurrell, 1995; Hurrell and Deser, 2010), is represented by NAO. The NAO index is defined as the meridional sea level pressure gradient between Azores islands and Iceland during boreal winter, December to February (DJF). In this study, we primarily used the longest observational index of Jones et al. (1997) starting with 1824 CE. We also compared our master shell chronology to the NAO reconstruction index by Jones and Cox (2001). This index employs instrumental station pressure data and historical archives extending the reconstruction to 1659 CE on a monthly-resolution, and to 1500 CE on a seasonal-resolution.

The second and third leading modes of atmospheric variability represent the

East-Atlantic pattern (EA) and Scandinavian (SCA) pattern, respectively. The EA pattern (Barnston and Livezey, 1987; Cassou et al., 2004) has a positive center of action located central-eastern North Atlantic and North Sea. We also used the extension of the EA pattern, namely the East Atlantic/West Russian (EA/WR), which has a strong positive center over the British Isles and one in Eurasia (Barnston and Livezey, 1987). Compared to the EA, the SCA pattern is displaced over Scandinavia/Russia and subpolar regions (Barnston and Livezey, 1987; Bueh and Nakamura, 2007). We also employed the East Pacific/North Pacific (EP/NP) teleconnection, characterized by a positive center over the North Pacific and Alaska, and a positive but weaker one over the central North Atlantic (Barnston and Livezey, 1987).

The observational teleconnection indices begin with the 1950 CE and are standardized by the 1981-2010 climatology. To mitigate the temporal constraints of the EA and SCA observational indices, Comas-Bru and Hernández (2018) employed an empirical orthogonal function on the NOAA's 20^{th} Century Reanalysis (V2c) SLP data to extract these two modes of variability. Due to data bias, we additionally used the EA and SCA indices starting with 1865 CE.

3.3. Data analysis

In this study, we applied a threshold of lowest 10^{th} percentile and highest 90^{th} percentile to the SGI (e.g, Wanamaker et al., 2019) to define low and high extreme events, respectively. The years obtained with our defined threshold (Table C1) were further used for the composite SLP and Z500 analyses. The statistical significance of the composite maps was determined by a two-sided t-test (confidence level of 90 % and 95 %, respectively).

Additionally, the SGI was correlated via Pearson correlation coefficient (r) analysis with the instrumental T_{Helgo}, S_{Helgo} and MDD data from Helgoland Roads dataset, as well as with the observational and reconstructed teleconnection indices. All correlations take into consideration the presence of lag-1 autocorrelation in the time series. For calculating the effective degrees of freedom (N_{eff}), the greater lag-1 from the time series was selected. The statistical significance of the correlation was set to 90 % and 95 % confidence level, respectively.

We calculated one-dimensional (1D) blocking frequency index and two-dimensional (2D) blocking frequency field by using daily spring (MAM) Z500 data for the climatological period 1836-2004 CE. The southern (GHGS) and northern (GHGN) geopotential height gradients of each point are calculated using eq. (4.4) and eq.

(4.5), respectively (Scherrer et al., 2006). For the 1D blocking index, we calculated gradients using latitudes between 45°N and 65°N, with 55°N serving as our reference latitude. For the 2D field, we used geopotential height data between 20°N to 90°N to effectively cover the 35°N to 75°N region. A grid point is considered blocked only if both the northern geopotential height gradient is above the 0 m/°lat threshold and the southern geopotential height gradient is below the -10 m/°lat threshold, and this configuration persists for five consecutive days or more (Scherrer et al., 2006).

$$GHGS = \frac{Z(\phi_0) - Z(\phi_0 - 15°)}{15°} \tag{4.4}$$

$$GHGN = \frac{Z(\phi_0 + 15°) - Z(\phi_0)}{15°} \tag{4.5}$$

4. Results

The master shell chronology from Helgoland displays regular sub-decadal variability, with an extreme peak occurring at least once per decade, except in the 1900-1920 period (Figure 4.3A; Table C1). Spectral analysis (Figure 4.2B) indicates significant peaks at approximately 6, 7 and 12 years, respectively. We observed a slight change in the frequency regime between 1767 to 1900 and 1900 to 2004, with the first period showing a periodicity of 6.5 years, and the latter of 7.7 years. The wavelet analysis of the SGI validates this subtle shift (Figure C1), and also a lack of variability between 1900 and 1920 (shaded period in Figure C1). At the beginning of the record, for instance, the 1767-1870 CE. time frame corresponds to a periodicity of about 6 years, compared to 8-year period at the end of the record (1956-2004 CE).

4.1. Relationship with instrumental data

Significant correlations with instrumental water temperature at Helgoland (T_{Helgo}) are attained at one-year lag in the boreal winter-spring monthly averages (Table 4.1). Cross-correlation analysis shows that the maximum correlation is observed at lag-5 for JFMA (r= 0.731; N_{eff}=15; p<0.05) and slightly higher for the MA average (r=0.733; N_{eff}=15; p<0.05). In-phase correlations are not significant for the 1962-2004 period. The highest correlation with measured salinity at Helgoland (S_{Helgo}) is observed at lag-1 during early spring and autumn, although – alike the in-phase correlations – these are not statistically significant

(Table 4.1). Multiple regression analyses indicate that the temperature and salinity conditions during early spring (MA) explain 23.2 % (Adj. R^2) of SGI variability one year later. No in-phase or lagged relationships were found with the MDD index of Wiltshire and Manly (2004) for the first two quarters. However, there seems to be a positive, albeit not significant, relationship with winter MDD until 1985, apparent also in cross-wavelet analysis. We observed that coeval low and high extremes occur during 1974-1975, 1984 and 1980, respectively (Table C1).

Table 4.1. Pearson correlation coefficients between SGI of *A. islandica* and instrumental water conditions at Helgoland and observational atmospheric teleconnection indices. The asterisk refers to one-year lag. Statistically not significant correlations are marked by ns. Several correlations improve across multiple analysis periods.

SGI	Season	Pearson's r	N_{eff}	Confidence	Period
T_{Helgo}	JFMA/JFMAM	-0.453*	16	p<0.1	1962-2004
	MA	-0.507*	16	p<0.1	1962-2004
	MAM	-0.489*	16	p<0.1	1962-2004
S_{Helgo}	MA	0.252*	16	ns	1962-2004
	SO	-0.263*	16	ns	1962-2004
MDD	JFM	0.386	9	ns	1968-1985
	AMJ	-0.226	16	ns	1968-2004
NAO	DJF	-0.219*	72	p<0.1	1824-2004
	October	-0.200	72	p<0.1	1824-2004
	Annual	-0.221	72	p<0.1	1824-2004
EA	MAM	-0.228	58	p<0.1	1865-2004
EP/NP	JF	0.427	23	p<0.05	1950-2004
	JF	0.660	13	p<0.05	1970-2004
BF	MAM	-0.437	15	p<0.1	1968-2004
	MAM	-0.677	9	p<0.05	1970-1995

4.2. Relationship with teleconnection indices

In-situ water temperature from winter to early summer at Helgoland shows a significant correlation with NAO_{DJFM} in the period 1962-2004 CE. The most

significant correlation (i.e., r= 0.748; N_{eff}=18; p<0.05) is observed during spring months (MA/MAM). We note analogous findings when comparing the observational winter NAO index (from 1950 onwards) with T_{Helgo}. Furthermore, the winter-spring T_{Helgo} correlates with the winter (DJFM) SCA teleconnection index (e.g., MA: r= -0.438; N_{eff}=18; p<0.1), but not with EA and EA/WR indices. Likewise, the S_{Helgo} is not linked with EA and EA/WR teleconnection indices, but only with SCA during JFM (r= 0.440; N_{eff}=22; p<0.05) and JFMA months (r= 0.370; N_{eff}=23; p<0.1). Analyses with the reconstructed winter (DJF) SCA blocking index of Comas-Bru and Hernández (2018) yielded similar results for the 1962-2004 period. The JFM salinity average correlates also with NAO_{DJFM} in the period 1962-2004 CE (r= -0.390; N_{eff}=22; p<0.1).

Although there is a notable correlation between physical water conditions at Helgoland and some teleconnection indices, no significant relationship was found with the SGI between 1950 and 2004 CE, besides a significant anti-correlation with the longer spring EA reconstruction of Comas-Bru and Hernández (2018) in the period 1865 to 2004 CE (Table 4.1). The relationship with winter NAO_{DJF} is also one-year lagged in the 1824-2004 period, and yet the SGI correlates concurrently with the yearly NAO index and the October month. The master shell chronology did not correlate with the NAO reconstruction of Jones and Cox (2001). Among the teleconnection indices, the January-February EP/NP index demonstrates the strongest correlation with the SGI, which improves significantly after 1970 (Table 4.1). It is intriguing to observe this enhanced correlation, especially considering that the January-February EP/NP index does not significantly correlate with the water conditions at Helgoland.

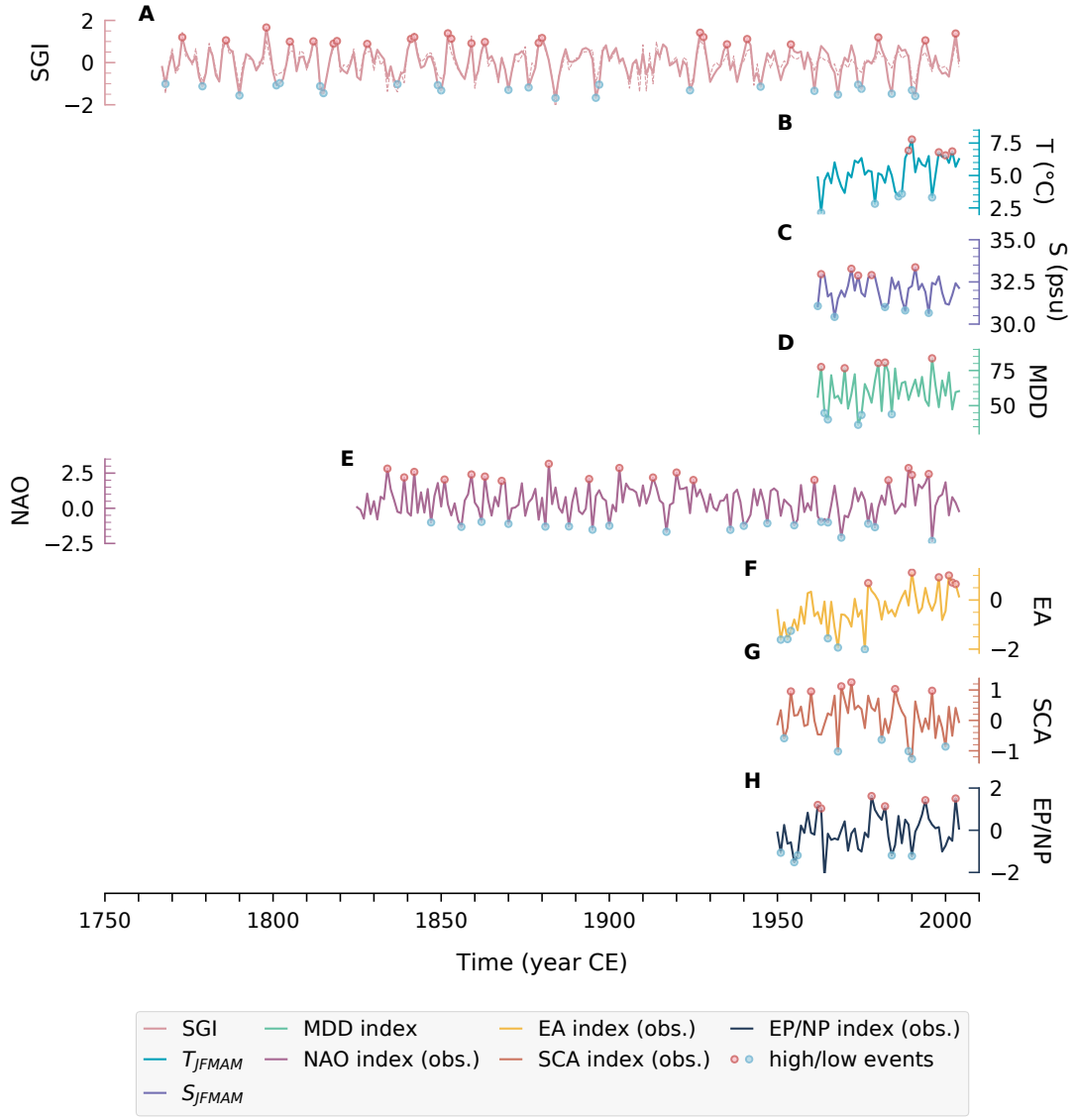

Figure 4.3. **(A)** Annually-resolved standardized growth index (SGI) of *A. islandica* shells from Helgoland showing extreme high (red circles) and low (blue circles) growth values. The threshold for negative and positive extremes is set to 10^{th} and 90^{th} percentile, respectively. Extreme indices for the observational data are also highlighted in panels B to H. The dashed pink line refers to the SGI time series without the 11-year moving average. **(B)** Instrumental sea surface temperature (T_{Helgo}) and **(C)** salinity (S_{Helgo}) data from Helgoland Roads (Wiltshire et al., 2010) during boreal winter-spring months (JFMAM). **(D)** Mean Diatom Day (MDD) for JFM months from Helgoland Roads (Wiltshire et al., 2010). **(E)** North Atlantic Oscillation (NAO) index (Jones et al., 1997) beginning with 1825 CE averaged for DJFM months. **(F)** Observational East Atlantic (EA) index and **(G)** Scandinavian teleconnection index (SCA) averaged for DJFM months. **(H)** January-February averaged East Pacific/ North Pacific observational index.

4.3. Extremes and atmospheric anomalies

Composite analyses indicate that there is a significant relationship between extreme SGI values in the *A. islandica* master chronology from Helgoland and regional spring atmospheric anomalies (Figure 4.4 and Figure C2). The SLP and Z500 patterns corresponding to extreme high SGI display a significant negative, cyclonic, center in the Labrador Sea, close to the Newfoundland coast (Figure C2). Furthermore, the Z500 map (Figure C2.B) indicates positive anomalies over the Greenland and Baffin Bay and central NE Atlantic between 30°N to 40°N. Atmospheric blocking over Greenland is much more prevalent during negative Arctic Oscillation (AO) and NAO years (Rimbu and Lohmann, 2011; Hanna et al., 2016). However, we did not find any correlation between NAO and the Greenland Blocking (GB) index of Hanna et al. (2016) during the period between 1851 and 2004 CE. We find instead that colder spring (MA) T_{Helgo} are associated with winter GB (r= -0.555; N_{eff}=16; p<0.05) and AO (r= 0.637; N_{eff}=18; p<0.05). In this scenario, it is likely that the collection area encounters colder waters that support growth, along with continental north-easterly winds that promote coastal-upwelling.

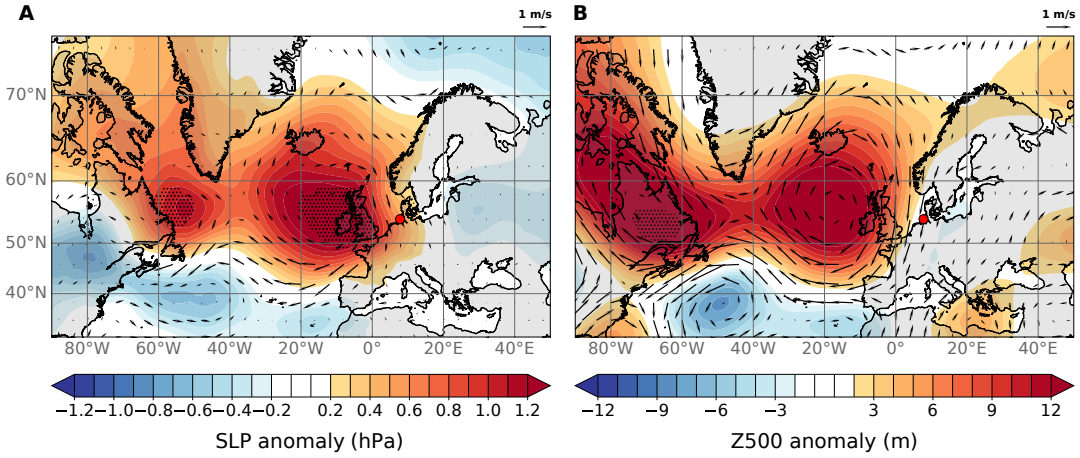

Figure 4.4. Low growth in *A. islandica* from Helgoland (red-filled circle on map) and its association with surface and mid-level atmospheric circulation anomalies during spring months (MAM) for 1836-2004 CE reference period. Composite anomaly maps for **(A)** sea level pressure (SLP) and 10-m wind fields and **(B)** geopotential height at 500 mb (Z500) and zonal and meridional wind vectors at 500 mb extracted from 20^{th} Century Reanalysis V3 dataset (Slivinski et al., 2019). Significant regions at 90 % confidence level are displayed by dotted areas. The arrows indicate the wind vector direction, whereas the length of the arrow refers to the mean anomaly (m/s)

In contrast, during extreme low SGI values, the North Sea is positioned along the eastern pressure gradient formed by a double-connecting anticyclonic structure in the Labrador Sea and the British Isles (Figure 4.4). Significant centers

of action are situated in the NW Atlantic (40°W to 60°W) and NE Atlantic (20°W-0°E), spanning zonally between 50°N to 60°N. As a result, wind anomalies generated along the eastern gradient of the anticyclone (Figure 4.4), enter the North Sea from the northwest, pushing coastal waters in the German Bight and causing higher sea levels.

4.4. Extreme low SGI and spring blocking frequency

Cyclonic-like circulation over the polar regions and a persistent high-pressure system over the British Isles causes a disruption of the zonal flow and leads to an increase in the frequency of atmospheric blocking over the British isle and North Sea (Rimbu et al., 2014). Our analyses show that extreme low SGIs coincide with enhanced blocking frequency in the mid- to high-latitudes (Figure 4.5A). Because a minor shift was noticed in the SGI periodicity pre-1900 CE to post-1900 CE, we looked specifically whether the centers of action also shifted longitudinally in these two time frames (Figure 4.5B). The years associated with extremely low SGI values not only depict the latitudinal mean distribution of spring blocking days, but also show an intensified activity around the centers shown in Figure 4.4A (shaded areas in Figure 4.5B). Our analyses show that, on average, the percentage of spring blocking days increased post-1900 CE. Moreover, we notice that the center identified in the west Atlantic moved westwards, whereas the east Atlantic center broadened. Additionally, a higher percentage of blocking activity is observed in the eastern North Pacific.

Since there is a clear indication between spring blocking activity and suppressed growth in *A. islandica*, we developed a regional blocking index for the 1900-2015 CE period. We selected a region latitudinally bound between 50°N and 65°N, and longitudinally, between 20°W and 10°E as observed to show particularly high blocking in this time frame. The resulting index does not explain year-to-year variability of the SGI, however, we detect that for a higher percentage of blocking days (e.g. >10 %), we could establish a temporally limited correlation (Table 4.1), in particular between 1970 and 1995 CE. High spring T_{Helgo} in the time period 1968-1987 CE are also linked with enhanced spring blocking (r=0.645, N_{eff}= 9, p<0.1). In this time frame, the regional blocking index correlated positively with winter NAO index (r=0.540, N_{eff}= 16, p<0.1). An intriguing observation arising from correlation analyses reveals a connection between regional blocking index in the eastern Atlantic and the EP/NP index during the period 1960-1997 CE (r=-0.424, N_{eff}= 26, p<0.05), thereafter the correlation increases significantly with the SCA index (r=-0.465, N_{eff}= 23, p<0.05; 1997-2015).

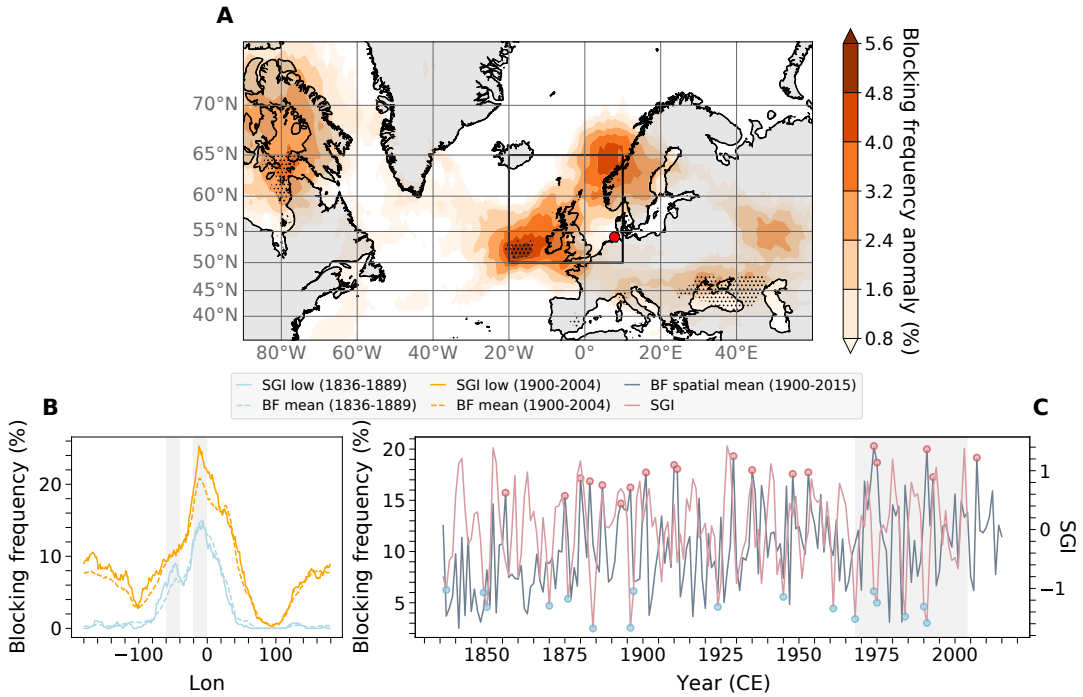

Figure 4.5. **(A)** Spring blocking frequency anomaly (%) for SGI extreme low values in the 1900-2004 CE period. The red marker indicates the site location. The black square shows the area used for the creating the blocking index in panel C. Dotted areas indicate 95 % confidence level. At 90 % confidence level, the Scandinavian center is also highlighted. **(B)** One-dimensional blocking frequency showing longitudinal occurrence of mean blocking days for extreme low SGI values. The shaded longitudinal intervals refer to the anomaly centers in Figure 3A. **(C)** Spatially-averaged spring blocking frequency. The shaded interval represents the 1968-2004 CE time frame, indicating a pronounced anti-correlation. High extremes in the blocking frequency index in panel C are marked by pink circles, whereas low extremes in the SGI are marked by blue circles. The blocking data was calculated from 20^{th} Century Reanalysis V3's Z500 dataset (Slivinski et al., 2019).

5. Discussion

The studied chronology of *Arctica islandica* from Helgoland presents an exceptional case of well-defined growth associated with atmospheric variability. It is therefore interesting to turn our attention to whether analogous climatic signals have been documented in the area. We also have to consider that Marchitto et al. (2000) have found inter-series correlations to decrease with increasing distance (e.g., 50 km), and it is not uncommon for bivalve records to indicate different environmental parameters at short distances (e.g., Witbaard, 1996; Witbaard et al., 1997). However, high-frequency oscillations of 3 to 8 and 12 to 16 years have been reported by Holland et al. (2014) and Butler et al. (2009) across longer distances in the North Sea. Within the German Bight area, Epplé et al.

(2006) have found specific 5- to 7- year periodicity in a master chronology of *A. Islandica* from 15-20 m water depth at Spiekeroog island, located 47 km to the south-west of Helgoland. This particular periodicity encountered in both master-chronologies, and the additional absence of in-phase relationships with physical and biological parameters is thereby specific for the inner German Bight area.

5.1. Lagged response due to atmospheric dynamics

Next, it is important to address the absence of a clear in-phase relationship with instrumental environmental data from Helgoland Roads. Firstly, we agree that 43 years of overlapping data from Helgoland Roads can be statistically insufficient to explain long-term trends and temporal synchronicities. Secondly, the relationship is statistically significant only for the boreal winter-spring months, shedding light on the growth period for *A. islandica* from Helgoland, corroborating Schöne et al. (2005d) findings that *A. islandica* records bottom water temperature starting with February-March, when the water temperature is lowest. Several studies have addressed the one-year lagged response with environmental data. For example, in their analysis of the *Serripes groenlandicus* bivalve species from polar NE Svalbard, Ambrose et al. (2006) have found a similar one-year delayed growth response to environmental conditions which could stem from the bivalve's biological control, involving energy storage and its effective utilization one year later. In the recent study of Mette et al. (2023) using *Arctica islandica* from SW Iceland, the observed one-year lag relationship between growth and temperature was suggested to be indicative of the influence of subpolar gyre dynamics, causing a delay in the availability of food to the benthic community. An alternative explanation for the lagged relationship in both temperature and salinity is that winter-spring water anomalies could be sealed below the surface during summer and autumn due to enhanced water stratification and reemerge the following year as postulated by Alexander and Deser (1995). This may be the case in our study, because NAO modulates the temperature at Helgoland, and the growth – winter NAO relationship is one-year lagged.

Lagged relationships are also common in benthic ecosystems. For instance, Witbaard et al. (2003) noted that spring growth correlated better with autumn phytoplankton color in the previous year rather than with concurrent spring bloom occurrence. In this study, we identify instead a few concurrent years when SGI and MDD extremes align—specifically, in 1974, 1975, and 1984, along with a positive peak in 1980. Thus, when diatom bloom earlier in the year—as suggested by the low MDD, shell growth during that respective year is also

suppressed. An earlier bloom in the first quarter of the year is a consequence of a positive NAO polarity as demonstrated by Lohmann and Wiltshire (2012). To verify this aspect, we generated a winter (DJF) composite pattern for low SGI extremes (Figure C3) and observed a comparable atmospheric pattern as documented in the study of Lohmann and Wiltshire (2012). This positive winter NAO phase triggers milder winter water temperatures, whereas south-westerly winds improve light availability and water conditions for early phytoplankton growth. In warm autumn and winter conditions, surviving zooplankton could rapidly consume the early blooms (Wiltshire et al., 2008), depleting the water column of necessary nutrients of a certain quality for the commencement of bivalve growth in early spring, and suppressing growth. This, however, might not be the case in more open North Sea region, such as Fladen Ground, as highlighted by Witbaard et al. (2003).

It's worth noting that the winter SLP pattern for extreme high MDD as in Lohmann and Wiltshire (2012) and the spring one for extreme high SGI in our study (Figure C2), respectively, exhibit atmospheric patterns indicating continental prevailing easterly winds over the southern North Sea. It is, therefore, likely that an extreme delay in diatom bloom could overlap with the start of growing season in *A. islandica* leading to better opportunities for shell growth. In the numerical experiments of Schrum (1997), it is found that thermohaline stratification tends to occur in certain locations of the German Bight under prevailing westerly and easterly winds. Note that the bivalve collection site is in the proximity of Helgoland, albeit at deeper waters than 8-m as in the analysis of Lohmann and Wiltshire (2012), therefore it is possible that the easterly winds push coastal waters offshore where stratification could develop. This may also explain the delay in diatom bloom under light limitations, whereas colder and saline bottom waters could be preserved from the previous year. At this point, we cannot fully pinpoint the mesoscale wind pattern at the collection site and exact timing or existence of thermohaline stratification. We have yet good reasons to believe mixing in spring; temperature profiles at 35- and 45-m below surface from EN4.2.1 dataset (Good et al., 2013) match well with the T_{Helgo}. Achieving a comprehensive understanding of growth extremes in relation to the lateral and vertical advection of surface waters requires future regional numerical studies complementing composite analyses.

5.2. Atmospheric blocking and teleconnections

Although the SGI of *Arctica islandica* does not correlate well with the teleconnection indexes, the water temperature at Helgoland shows strongest relationship

with NAO and SCA indexes. According to Chafik et al. (2017) study, the combination of positive NAO and negative SCA pattern during boreal winter leads to a sea level rise over the German Bight region. These results are consistent with the north-western wind pattern entering the German Bight from open North Sea obtained in our study (Figure 4.4A) and the second dominating water transport at the German Bight explaining 17 % of the variability identified by Wiltshire et al. (2010). The SLP pattern obtained in this study is fairly similar to the second mode of blocking frequency obtained by Rimbu et al. (2014) and the blocking pattern of Häkkinen et al. (2011). The blocking centers we identified are slightly south-westward displaced (Figure 4.4A) and less centered on the North Sea in the 1836-2004 period. However, enhanced blocking activity across 80°W to 20°E (Figure 4.5B) is coherent with Rimbu et al. (2014) findings. In addition, we find that extreme low SGI are associated with climatology mean of blocking frequency (Figure 4.5B) and also an eastward band of enhanced activity between 0°E-20°E in the 1900-2004 period.

Hilmer and Jung (2000) documented that SLP anomalies associated with NAO are displaced eastward in the 1978-1997 period compared to the previous two decades, resulting in enhanced sea ice export. Davini et al. (2012) also discusses that the eastward NAO shift relates to decreased Greenland blocking in that time frame. Through the analysis of two distinct periods of summer sea-ice decline in the polar Atlantic, Deser et al. (2000) have found that negative sea-ice anomalies tend to occur when spring SLP anomalies—modulated by winter anomalies—are positive in the eastern North Atlantic, although the associated patterns differ to some degree. Aiming at comprehending the dynamics of sea-ice-free ecosystems and species growth patterns, this finding, coupled with our study results, highlights the potential to integrate sea-ice decline observations and proxy-based reconstructions such as coralline algae (Halfar et al., 2013) with *Arctica islandica*'s potential for detecting atmospheric anomalies. By projecting these onto our results, we can indicate that spring blocking over the eastern Atlantic and summer ice decline result in reduced bivalve growth, it could align with Carroll et al. (2014) observations of higher growth in cold, sea-ice dominating environments. In the arctic North Pacific, the picture might be different, as Reynolds et al. (2022) have found bivalve growth rate to be higher in warmer, sea-ice free environments.

In future studies, it is worthwhile to explore several links. Rimbu et al. (2014) suggest an upper tropospheric mechanism for a Rossby wave train extending from the central Atlantic to Eurasia, providing insight into why their blocking

pattern mirrors the EA/WR pattern. At this point, without further investigation, we cannot fully explain the association behind the SGI and regional blocking index, respectively, with the January-February EP/NP index, however we observe a wave train generated in the North Pacific in the spring Z500 composite anomaly map (Figure C4). This observation could also relate to the enhanced blocking both in North Atlantic and Pacific (Figure 4.5B). The time frame of the significant relationships is intriguing and pinpoints at atmospheric changes between late 1960s and 1970s as well as 1997, a period of predominantly positive NAO polarity. By analyzing the oxygen isotopic composition of a coral from Red Sea, Rimbu et al. (2003) find proxy evidence of an atmospheric shift in the 1970s associated with a change in the ENSO teleconnections (e.g., PNA) over the Atlantic/Eurasia. Several studies suggest that the atmospheric shift could relate to a change of periodicity in: (1) NAO from a weakly decadal global mode between 1930-1960 CE to a decadal regional mode limited to the Atlantic region post-1970 (Walter and Graf, 2002), and (2) ENSO periodicity and amplitude from 3 years between 1961-1975 to 4-5 years during 1981-1995 and more intense episodes (Wang and An, 2001). Interestingly, the spring regional blocking index we generate – besides its link to suppressed bivalve growth between 1960 to early 2000s (Figure 4.5C) – is inversely correlated with the January-February EP/NP index and spring Niño 3.4 index. This result corroborates other studies which indicate the influence of a cold tropical ocean and negative AMO state on blocking frequency. We also find that from 1998 onwards, the regional blocking index is linked to SCA instead of EP/NP, which might relate to the switch between the global and regional NAO modes. Moreover, Wang and An (2001) identified an eastward expansion of equatorial trade winds between 1981-1995 CE in their model study, whereas Yeh et al. (2018) suggest that there is an eastward shift in North Pacific Oscillation mid-1990s.

Through investigating shell growth extremes, we not only identify an atmospheric fingerprint associated with increased blocking frequency in western Europe, but also unveil connections between blocking occurrences and teleconnection indices, warranting a deeper comprehension of the underlying mechanisms and the non-stationary aspect of the Pacific-Atlantic teleconnections. We also highlight that the East Pacific/North Pacific teleconnection pattern might be more important than previously sought. We note that when studying biological organisms, the atmospheric processes can be delayed and display intermittent connections (see also Rimbu et al., 2003). Anomalous atmospheric patterns that are enforced by oceanic conditions and persist for decades have an impact on the ecosystem. Some shifts might not even be identified. For instance, the

1987/1988 phytoplankton regime shift identified in central North Sea (Reid and Edwards, 2001; Reid et al., 2001; Edwards et al., 2002) and also German Bight (Schlüter et al., 2008; Wiltshire et al., 2008) is not apparent in the growth variability of *A. islandica*. Wiltshire et al. (2008) remark that despite the ongoing changes of the past decades, phytoplankton bloom dynamics is yet resilient, a resilience that can be observed in *Arctica islandica*.

6. Conclusion

Our study represents one of the first attempts to establish a relationship between extreme growth indices of *Arctica islandica* and coherent atmospheric patterns. Standard correlation analyses with atmospheric teleconnection indices prove inadequate in elucidating growth variability. However, certain lagged relationships, such as those with the NAO index, when supplemented by Helgoland Roads data suffice to explain the underlying dynamical processes modulating temperature and spring bloom timing, aligning with previous research studies. Through a narrowed focus on extreme low growth events in *A. islandica*, we demonstrate a synchronous relationship with positive polarity of winter NAO and enhanced spring blocking activity over the British Isles. *Arctica islandica* from Helgoland also exhibits correlations with the EP/NP teleconnection index and blocking frequency, contributing to our understanding of broader atmospheric shifts occurring during the 1960-1970 time frame in the Northern Hemisphere. The shifts may be connected to the variability of ENSO and NAO modes, and necessitate further investigation into the mechanistic aspect. Our study based on extreme low growth in *A. islandica* help uncover information beyond the instrumental record, which may not be readily apparent otherwise, and warrant further exploration with additional datasets sourced from marine and terrestrial climate archives.

Acknowledgements

This study was supported by the Alfred Wegener Institute (AWI) Strategy Fund Project (PalEX). MI, GL, NR and TB acknowledge support by the Helmholtz Association via the joint program „Changing Earth – Sustaining our future“ (POF IV) of the AWI. MI was additionally supported by the Helmholtz Climate Initiative – REKLIM. We acknowledge the use of gridded atmospheric data retrieved from NOAA's 20^{th} Century Reanalysis V3 (Slivinski et al., 2019) and the teleconnection indices mentioned in section 3.2. The authors are supported by the Open Access Publication Funds of the Alfred Wegener Institute for Polar

and Marine Research.

Data availability

The shell growth chronology of *Arctica islandica* from Helgoland will be made available upon publication.

5

Conclusion

This doctoral research demonstrates the importance of extreme shell growth events in *Arctica islandica* records as indicators of large-scale climatic patterns, and contribute to the groundwork laid by Wanamaker et al. (2019) in the NW Atlantic and Lohmann and Schöne (2013) in the NE Iceland. We can confidently confirm the questions of whether extreme shell growth events correspond to sea-surface temperature and sea-level pressure anomalies (see **Answers to Research Questions** section). Extreme low indices identified in the shared growth signal of bivalve-based networks highlight potential climatic stressors. These include warm-water pools in the extratropical and polar regions of the North Atlantic sector prevalent under positive AMO polarity (e.g., the 1920-1950 CE period), which link with Atlantic tropical cyclones (e.g., Wang et al., 2008). Extreme low indices showcase the possibility of cyclonic conditions in the central North Atlantic, corroborating Wang et al. (2008), and coupled with the weakening of the Aleutian Low in the North Pacific adhere to a typical negative PNA pattern. High indices likely reflect optimal growth conditions in the North Atlantic, characterized by cold water pools. Interestingly, this scenario is accompanied by positive PNA pattern and a prominent anticyclone center in the central North Atlantic. A similar anticyclonic center of action, albeit associated with extreme low indices, is indicated by the growth record of *A. islandica* from Helgoland. The research findings consolidate not only that low growth events have a greater potential for unveiling climatic anomalies, but that we can also unify the large-scale patterns observed, despite regional hydrography related responses to the same climatic stressors (see example of contrasting NAO influence in Schöne et al., 2003a,b).

Extreme events provide valuable insights that are not easily discernible solely through the study of shell growth variability. For example, the extreme low growth events in *A. islandica* from Helgoland in Paper III are synchronously

associated with positive winter NAO and spring blocking in the central-eastern North Atlantic. In contrast, correlations with the atmospheric teleconnections and environmental parameters do not depict the same picture; the correlations do not attain robust significance levels, and are present only within specific time periods (e.g., Figure 4.5C; Table 4.1). A similar observation was made in Paper II, where the relationship with winter NAO is not significant, but the large-scale spatial correlation map (i.e., Figure 4) reveals how the NAO impacts the winter mixing layer through the presence of the tripole SST pattern (Deser et al., 2010). It's worth noting that although extremes were not the focus of Paper II, the Pearson correlation used in correlation maps and other analyses is sensitive to extreme values (Schober et al., 2018). In another example, the growth extremes within the common signal of the bivalve-based network align with patterns of natural oscillatory modes like the AMO in the Atlantic region and the PDO in the North Pacific (Figure 2.6; Figure 2.7). Once again, the relationship with AMO and PDO indices failed to provide compelling evidence of a potential causal relationship highly sought for reconstruction purposes (Figure 2.5).

When correlation analyses yield lagged or non-significant results (e.g., lagged response with surface temperature and salinity in Figure B3 and Figure B4, respectively), it does not mark the conclusion of the analysis, as explicitly pointed out in Paper II. Instead, one should view the identified shifts as potential climate transitions (e.g., GSA and negative AMO shift in Figure 3 and Figure 6; BF index in Figure 4.5C; EP/NP index in Table 4.1), prompting further investigation through alternative analyses. The alternative analyses used in this thesis, namely composite maps on extremes, correlation maps and PCA analysis – frequently used in meteorology – prove to be valuable tools applicable to growth records of *Arctica islandica*.

Key findings from Paper I and Paper III suggest that *Arctica islandica* growth proxy from the North Atlantic region captures signals from the North Pacific, opening up opportunities for future studies to establish connections between these basins using equally advantageous climate archives (see also **Appendix D: Future studies**). Moreover, extremes in *A. islandica* growth bands indicate an interesting switch in the PDO patterns occurring in the mid-late 19^{th} century (Minobe, 1997). A curious connection with the North Pacific is identified in the relationship between the EP/NP teleconnection index and spring blocking frequency in the eastern Atlantic. These connections warrant further validation through the integration of marine and terrestrial proxy data, making the field of sclerochonology an exciting contributor to climate sciences.

5.1 Research limitations

Relying solely on observational and reanalysis data to understand growth patterns in *Arctica islandica* bivalve species, or any other species for that matter, poses a series of limitations, particularly when inferring past climate conditions. Observational and reanalysis products are valuable for present-day climate conditions, but these may not represent historical climate accurately. Observational data is often temporally and spatially limited and can vary due to methodology and data sources. Reanalysis products which assimilate observational data with numerical models, introduce additional uncertainties related to the assimilation process, model parameterizations and grid resolution. One clear example in this case is the regional differences between composite maps generated with the Last Millenium Reanalysis compared to those from ERSSTv.5 or EN4.2.1 (compare Figure 2.6 and Figure A2 with Figure 2.7 and Figure A3 and Figure A4), although some discrepancies were also seen between the latter two. In another example, the wind field vectors depicted in Figure 4.4A indicate the direction from which the westerlies enter the North Sea and hint at possible large-scale effects. However, discerning the exact processes at local scale remains challenging due to grid resolution of reanalysis data, and requires an in-depth analysis using a highly-resolved regional model. Another example is the interpolation of subsurface water temperature data, both horizontally and vertically, which may distort actual conditions at specific sites and generate values that are not characteristic of the study site. Therefore, whenever possible, I attempted to validate the findings with available instrumental data, although biases in the reconstructed proxy in relation to observations/reconstructions were, so far, negligible.

While assumptions are integral to driving research forward, it remains unclear whether bivalve growth-climate relationships observed in the recent past withstand the test of time. Firstly, the relationship between growth and climate is inherently complex, influenced not only by multiple environmental factors (water temperature and salinity, hydrographic dynamics, nutrient availability, timing of spring blooms, to name a few), but also by metabolic processes within the organism. These metabolic processes can sometimes produce deviations from expected growth responses, complicating the interpretation of growth data in relation to climate conditions. To address this complexity and compensate for unclear relationships, it is essential to incorporate abiotic proxy data for additional information. Oftentimes, coral- and tree-derived proxy data seem more appropriate to reconstruct particular environmental factors such as air temperature, sea-surface temperatures and precipitation in tropical and terrestrial

regions, which can be used to compare and augment data acquired from mollusks.

Secondly, growth-climate relationships may be changing over time due to natural variability and non-linear and non stationary relationships within climate system itself. This combination can present challenges when extrapolating growth-climate relationships inferred from observational data to past or future periods. To address this issue, machine learning algorithms are valuable tools for maintaining temporal variability in growth-climate relationships. However, implementing such statistical approaches required an extensive number of samples to train the model, in the range of thousands, which may not be readily available. Well-defined intrannual growth increments in long-lived individuals could potentially increase these sample requirements. Furthermore, the validity of the growth-climate relationships relies on the degree of similarity between the paleo-environment and the present-day conditions, particularly in terms of mean temperature and seasonal amplitude. The non-stationary nature of growth-climate relationships can also be seen advantageous by providing insights into the dynamic and evolving aspects of the climate that may not be readily apparent otherwise. Such threads of information should not be discarded, but rather explored further with other biotic and abiotic proxy data and through multi-proxy networks.

Thirdly, a main caveat in interpreting growth variability within the climate context arises from the statistical removal of age-related growth in such growth-based chronologies. As a result, multidecadal periodicites are often removed adding complexity to the interpretation (see also section 4.2 of the Discussion in Chapter 2/ Paper I). While I cannot dismiss the possibility that detrending the Helgoland chronology has preserved only high-frequency variability, it is equally plausible that this represents the environmental signal rather than merely an artifact of detrending.

Additional research limitations which are not discussed here may be found in each individual study.

5.2 Answers to Research Questions

In this section, I return to my original research questions posed at the beginning of the thesis, and address them in detail. These answers are intended to provide a concise summary of the key findings and enhance the overall understanding of each study.

RQ.1	Which large-scale climatic phenomena are associated with the common growth signal of a bivalve-based network from the northern North Atlantic? Which large-scale phenomena particularly stand out when analyzing extreme growth indices?

To extract the common growth signal in *Arctica islandica* from the North Atlantic basin, I gathered published growth records and applied principle component analysis. I followed the nested PCA approach as outlined by Reynolds et al. (2018), marking the first application of this method to growth records, whereas Reynolds et al. (2018) originally applied it to the oxygen isotopic composition of bivalve shells. The main network, N_{1764}, spanning from 1764 to 2001 and comprising six chronologies, exhibits a signal with a decadal to multidecadal trend. This trend correlates with the observational and reconstruction indices of the AMO and PDO indices, respectively. Although such correlations were significant but low, in the range of -0.2 to -0.3, I demonstrate that coupling PCA with composite maps on extreme growth provides an excellent method for identifying large-scale climatic phenomena. I also find that supplementing the network with additional chronologies does not alter the trend. However, some chronologies may potentially express a stronger regional climatic signal, which could stem from pre-processing techniques. The large-scale climate phenomena associated with the extremes of the common growth signal correspond to the sea surface temperature patterns of the AMO in the North Atlantic and the PDO, in the North Pacific. I am keen to mention that the eastern side of the PDO can resemble the NE Pacific pattern described by Johnstone and Mantua (2014). In terms of atmospheric patterns, the PNA pattern and the NAO are dominant, acting as atmospheric bridges that connect regional climate systems (e.g., Alexander et al., 2002). These patterns stand out when analyzing growth extremes of the common signal from a bivalve network.

Significance and contribution of the study:

- Principle component analysis is a statistical tool applicable to growth records of *Arctica islandica* across the North Atlantic basin for extracting the shared growth signal. It is particularly useful when inter-series

correlations are weak, providing insights into the large-scale variability of the common growth.

- Composite analysis of extreme growth events is a valuable method for identifying large-scale climate patterns and anomalies.
- Low growth extremes exhibit greater coherence across different time periods and networks utilized. The low growth events indicate common climatic stressors, which are valuable for understanding both past climate conditions and future scenarios.
- High growth coincides with the negative phases of the AMO and PDO during the cold period from 1800-1850 CE, while low growth aligns with the positive phases during the warm period from 1920-1960 CE.
- Composite maps of extremes across different reference periods may reveal out-of-phase polarities between AMO and PDO.
- The large-scale patters in SST and SLP across the Northern Hemisphere are key to identifying „hotspot“ locations relevant in a warming climate.

RQ.2	Does *Arctica islandica* exhibit a depth-dependent growth response to seasonal fluctuations in subsurface water temperature and salinity, necessitating consideration in correlation analyses? And if so, is it intertwined with large-scale oceanic circulation patterns?

To address this particular question, I explore the growth signal from the master shell chronology at 82 m depth from Butler et al. (2013). I selected this depth because it is deeper compared to the collection sites of other chronologies, and the chronology itself is one of the longer ones available, offering an excellent opportunity to investigate the matter more thoroughly. I primarily used three-month averages of temperature and salinity data from EN4.2.1 dataset (Good et al., 2013), extracted at the collection site for the observational period 1900-2004. I successfully demonstrated that the growth signal originates not from sea surface temperatures but from subsurface temperatures starting at 56 m depth during boreal summer and autumn. This finding explains why correlations with sea surface temperatures are often not convincing, and suggests a lagged response to conditions in the uppermost layer of the ocean. By plotting correlation maps at several water depths, I highlight that it is possible to traced thermally linked water bodies across the North Atlantic. These water bodies are linked to AMO phases and NAO influence on the SSTs (e.g., winter tripole pattern explained in Deser et al. (2010)). During periods of decreased correlation with subsurface

temperature, the growth signal may be associated with phytoplankton variability and zooplankton activity.

Significance and contribution of the study:

- It is one of the first studies to utilize heatmaps of correlation with 3-month average subsurface temperature, similar to Poitevin et al. (2019), and additionally incorporates salinity data to link growth variability in *A. islandica* with environmental factors at different water depths.
- The most significant result is that I demonstrate correlations with the SST are lagged by 1 to 2 years, and that stronger correlation coefficients are observed starting from 56 m depth and extending towards the 82 m depth of the collection site during summer and autumn.
- The use of correlation maps to track water bodies with similar temperature and salinity in the North Atlantic and establish connections between distant regions is a highly effective approach.
- This study underscores that achieving meaningful correlations with environmental parameters requires analyzing a long time period and sub-annual data. Performing these correlations helps to identify the growth period accurately.

RQ.3	Is there a discernible connection between the extreme growth indices observed in *Arctica islandica* and large-scale atmospheric patterns, particularly synoptic atmospheric blocking, in a region prone to such influences as the North Sea?

The NAO, along with associated EA and SCA blocking patterns, influences weather patterns by modifying the westerlies over Europe and the North Sea, thereby altering moisture transport, heat fluxes, wind shear, storm tracks, and temperature gradients in these regions. Previous studies investigating growth variability in *Arctica islandica* from the North Sea have demonstrated periodicities of 5-7 years, which align with atmospheric modes of variability. My study is the first of its kind to indicate that extreme growth in *Arctica islandica* from the Helgoland region in the southern North Sea corresponds to large-scale atmospheric patterns. The extreme low events identified using the 10^{th} lowest percentile, as in Paper I of this thesis, indicate significant blocking anticyclones over the central eastern part of the North Atlantic during boreal spring. This corresponds to an increase in blocking frequency over the region compared to the reference periods. An intriguing link is found with the EP/NP teleconnection

index, suggesting that the potential atmospheric mechanism involves a Rossby wave originating in the North Pacific.

Significance and contribution of the study:

- This study represents one of the first attempts made to connect extreme growth in *Arctica islandica* with large-scale atmospheric circulation and blocking.
- Low growth indices correspond to positive winter NAO conditions in the Euro-Atlantic sector and spring blocking activity over the British Isles.
- The high-pressure system identified during spring in conjunction with a positive winter NAO polarity, alters wind patterns over the North Sea. These altered wind patterns, in turn, influence nutrient mixing and light availability, ultimately affecting the timing and quality of spring blooms necessary for growth. These results support the findings by Lohmann and Wiltshire (2012).
- A particularly strong correlation between the EP/NP teleconnection index and the regional blocking index emerges after the 1970s, suggesting a potential shift in atmospheric dynamics during that time-frame.
- Composite map analysis can complement and enhance correlation analysis between teleconnection indices and growth variability, particularly for studying extreme events.

Appendix A: Supplementary material for Paper I

Figure A1. Power spectrum of $PC1_{S2}$ time series (black line) in the period 1764-2001 C.E. using N_{1764} network. Significance is shown at two confidence levels (90 % and 95 %) based on red-noise AR (1) model (red lines). The analysis was performed using the "dplR" package developed for dendrochronology analyses in R.

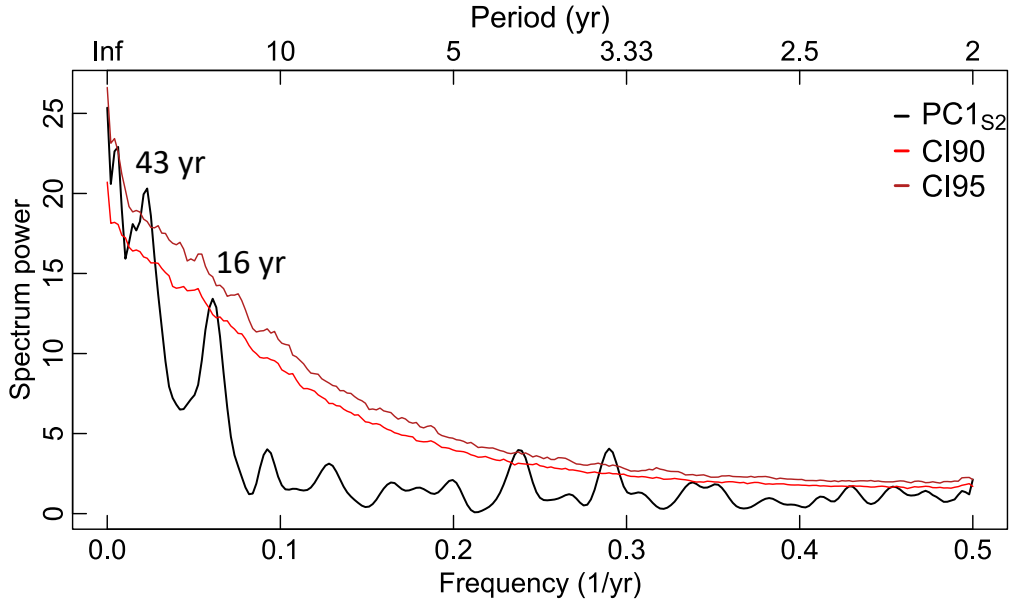

Table A1. List of extreme high and low PC1 indices obtained from main networks: long N_{1764} and shorter N_{1900}. The 90^{th} percentile and 10^{th} percentile threshold was used for high and low extremes, respectively.

Network	*Low indices*						*High indices*					
	$PC1_{S1}$		$PC1_{S2}$		$PC1_{S3}$		$PC1_{S1}$		$PC1_{S2}$		$PC1_{S3}$	
$\mathbf{N}_{1764}$	1768	1785	1768	1772	1768	1800	1811	1817	1811	1815	1765	1766
	1786	1787	1785	1786	1802	1807	1823	1824	1817	1818	1773	1777
	1788	1802	1787	1788	1809	1837	1826	1827	1823	1826	1782	1794
	1840	1841	1792	1800	1838	1839	1828	1829	1828	1845	1810	1815
	1892	1896	1802	1809	1840	1841	1845	1847	1849	1852	1818	1828
	1908	1925	1839	1841	1851	1896	1849	1852	1855	1856	1829	1845
	1929	1931	1896	1908	1902	1906	1853	1855	1859	1883	1849	1859
	1939	1941	1925	1929	1908	1925	1856	1859	1898	1900	1865	1883
	1947	1948	1947	1948	1929	1947	1860	1866	1901	1914	1914	1915
	1950	1952	1950	1952	1950	1952	1869	1883	1915	1944	1935	1944
	1955	1956	1955	1956	1955	1956	1915	1977	1977	1978	1963	1976
	1959	1973	1959	1973	1959	1987	1978	1983	1979	1983	1991	1992
$\mathbf{N}_{1900}$	1908	1925	1908	1925	1908	1925	1900	1901	1900	1903	1900	1915
	1929	1947	1929	1939	1929	1931	1903	1914	1914	1915	1918	1922
	1948	1950	1947	1948	1939	1947	1915	1918	1918	1974	1932	1935
	1952	1954	1950	1952	1950	1952	1932	1944	1977	1978	1938	1944
	1955	1959	1954	1955	1955	1959	1977	1997	1983	1997	1964	1974
	1987		1959		1987		1999		1999		1977	

Figure A2. Annually-resolved sea-surface temperature and sea-level pressure data from Tardif et al. (2019) indicating anomalies when **(A)** $PC1_{S1}$ and **(B)** $PC1_{S3}$ indices are above the 90^{th} percentile (high) and below the 10^{th} percentile (low) threshold, respectively. The capital letters "H" (i.e., positive anomalies) and "L" (i.e., negative anomalies) show high- and low-pressure centers, respectively. The analysis covers the period from 1764 to 2000 C.E. using the N_{1764} network of this study.

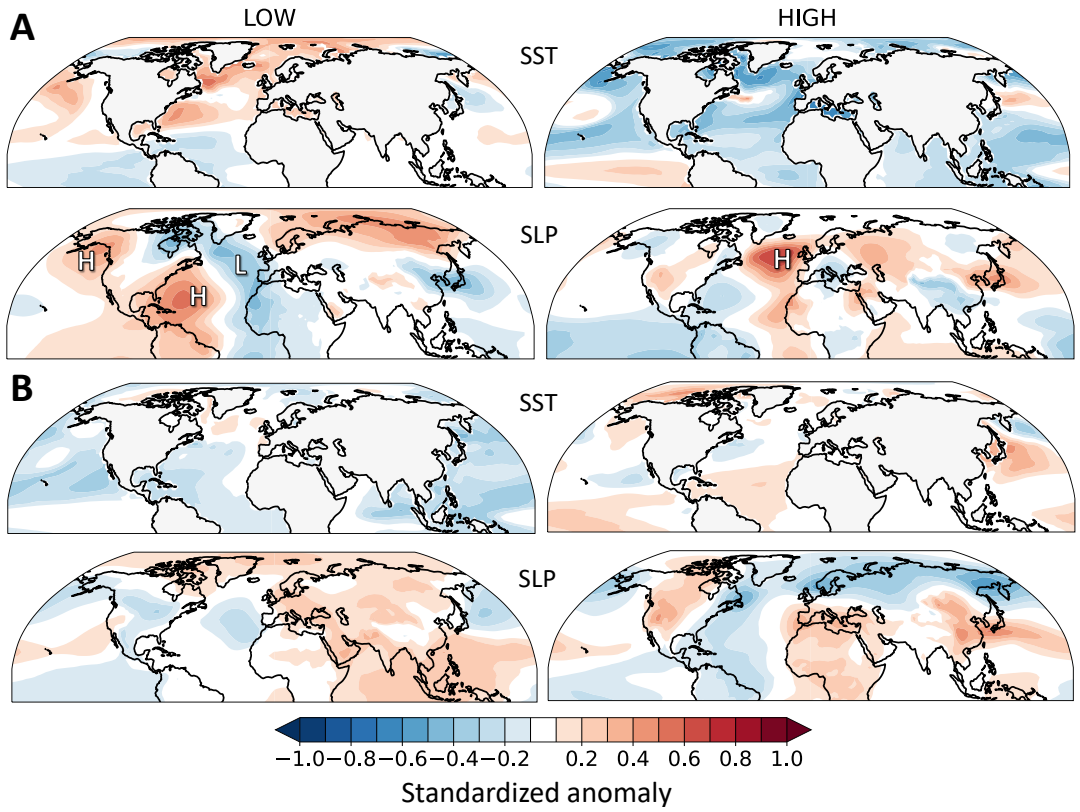

Figure A3. Annually-resolved sea-surface temperature from ERSSTv.5 dataset (Huang et al., 2017) and boreal spring (MAM) sea level pressure data from 20^{th} Century Reanalysis V3 (Slivinski et al., 2019) indicating anomalies when **(A)** $PC1_{S1}$ and **(B)** $PC1_{S3}$ indices are above the 90^{th} percentile (high) and below the 10^{th} percentile (low) threshold, respectively. The capital letters "H" (i.e., positive anomalies) and "L" (i.e., negative anomalies) indicate high- and low-pressure centers, respectively. The analysis covers the period from 1900 to 2001 C.E. using the N_{1900} network of this study.

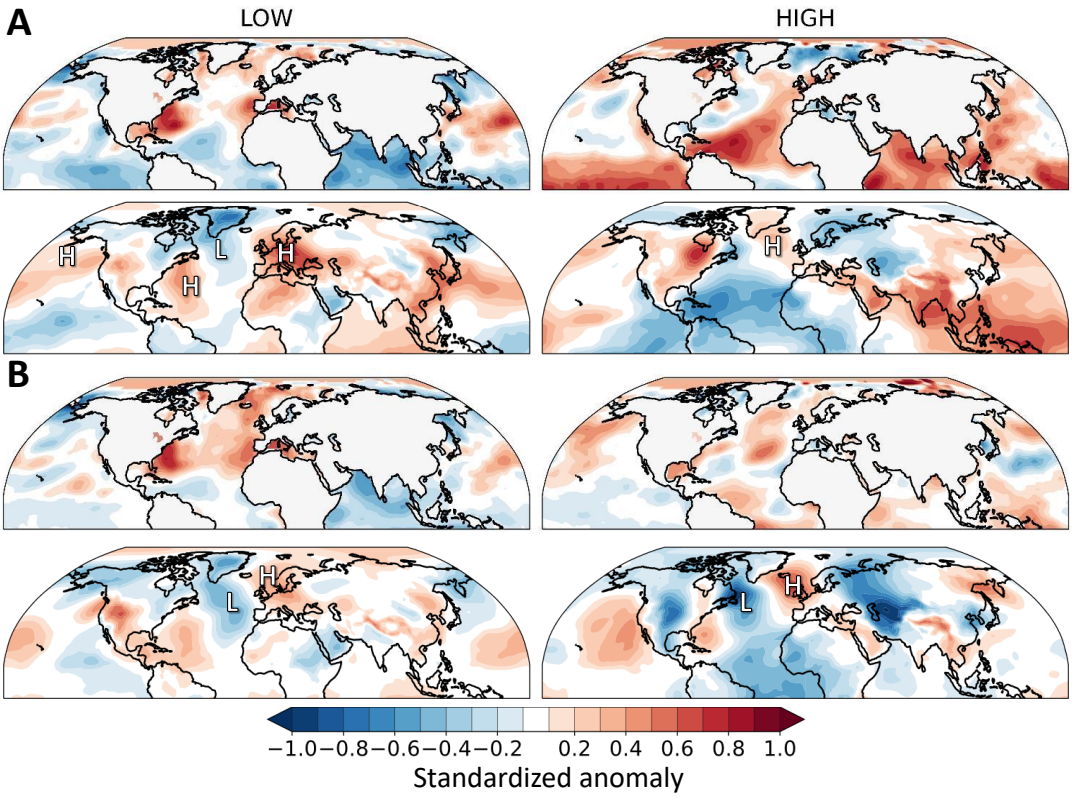

Figure A4. Composite map of subsurface temperature anomalies using EN4.2.1 dataset (Good et al., 2013) at **(A)** 5-m depth (annual average) and **(B)** 45-m depth (spring (MAM) average). The analysis was made using $PC1_{S2}$ of N_{1900} network in the 1900-2000 C.E. analysis period.

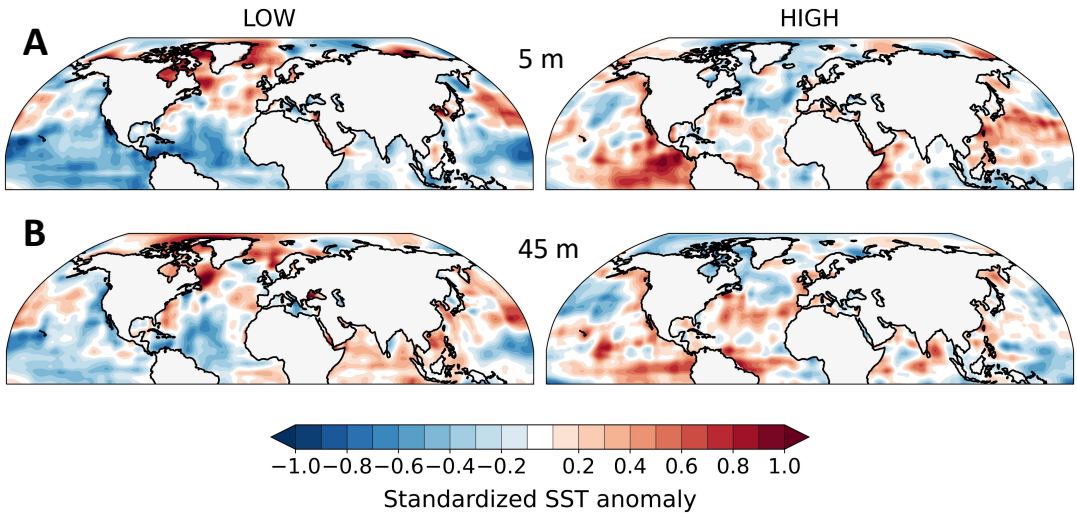

Figure A5. Composite map of SST using LMRv2.1 (Tardif et al., 2019) for extreme indices in $PC1_{S2}$ of N_{1764} between 1764-1899 C.E. period.

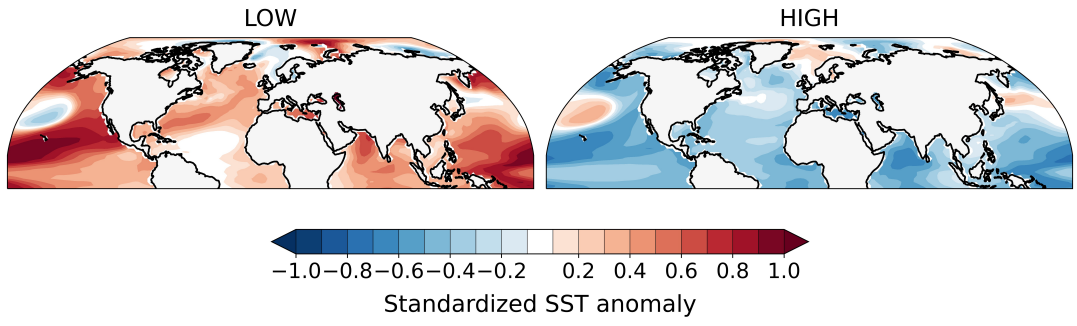

Figure A6. Comparison of PC1 time series for the three strategies with a reference period adjusted to 1764-1800 C.E.

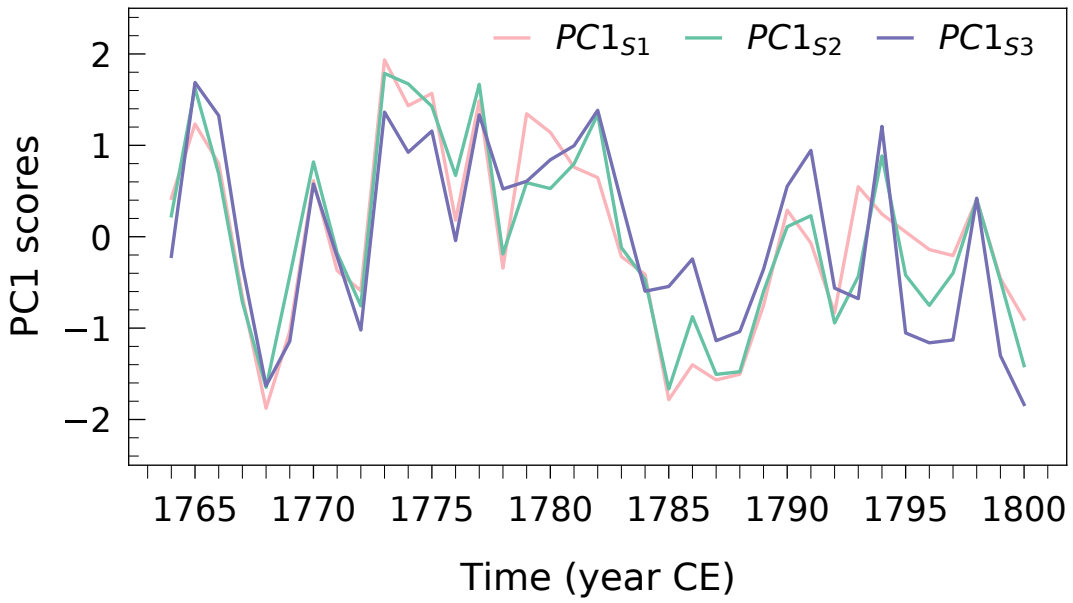

Figure A7. Comparison between $PC1_{S1}$ of extended networks N_{1516} (grey line) and N_{1545} (dashed grey line) with N_{1764} (pink line) and **(A)** Tierney et al. (2015) reconstructed SSTs from western tropical Atlantic Ocean and **(B)** Tierney et al. (2015) reconstructed SSTs from equatorial eastern Pacific. The period of higher frequency variability (1516-1650 C.E) as compared to the 1650-2000 C.E. period is highlighted in light blue.

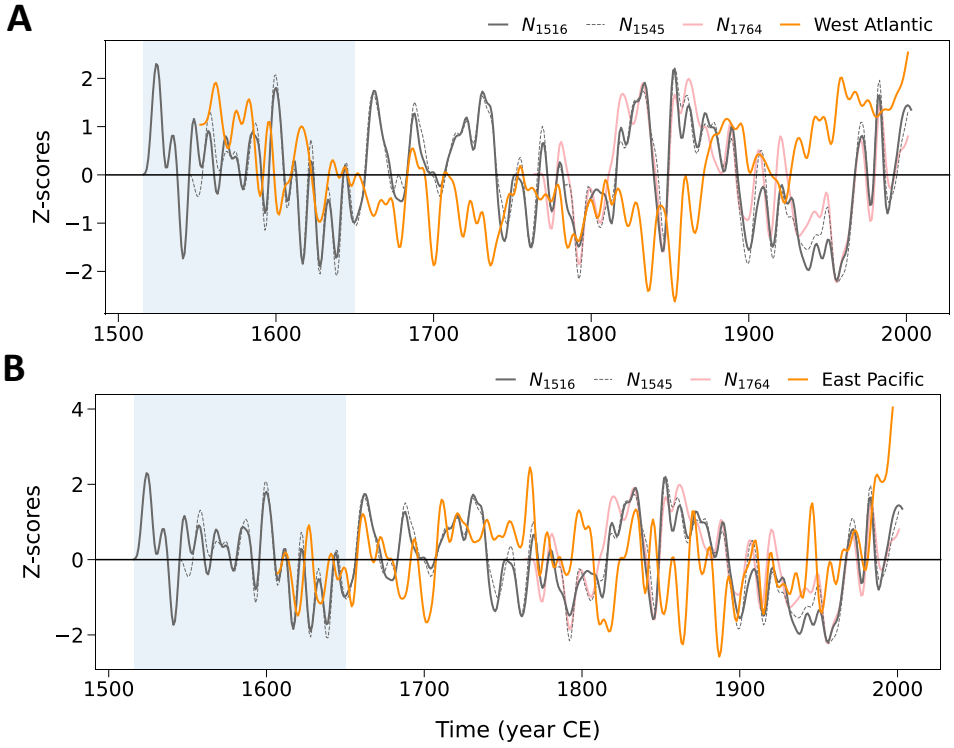

Figure A8. Composite map for sea-surface temperature and sea level pressure extracted from LMRv2.1 (Tardif et al., 2019) using the extremes indices of $PC1_{S1}$ (N_{1516} network) in the 1516-1763 C.E. period: **(A)** SST in reference to the 1900-2000 C.E. period, **(B)** SST in reference to the entire 1516-2000 C.E. period **(C)** SLP in reference to the 1900-2000 C.E. period.

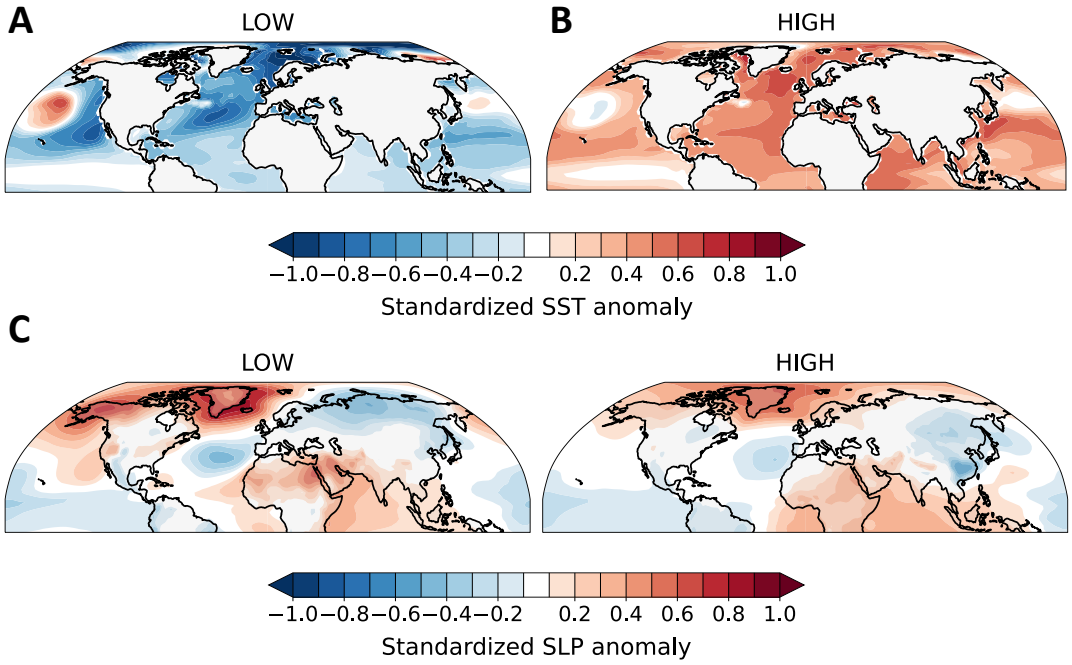

Appendix B: Supplementary material for Paper II

Figure B1. Global distribution of seasonal **(A)** temperature and **(B)** salinity observation weights extracted from EN4.2.1 dataset (Good et al., 2013) at 5-m and 56-m depth, respectively.

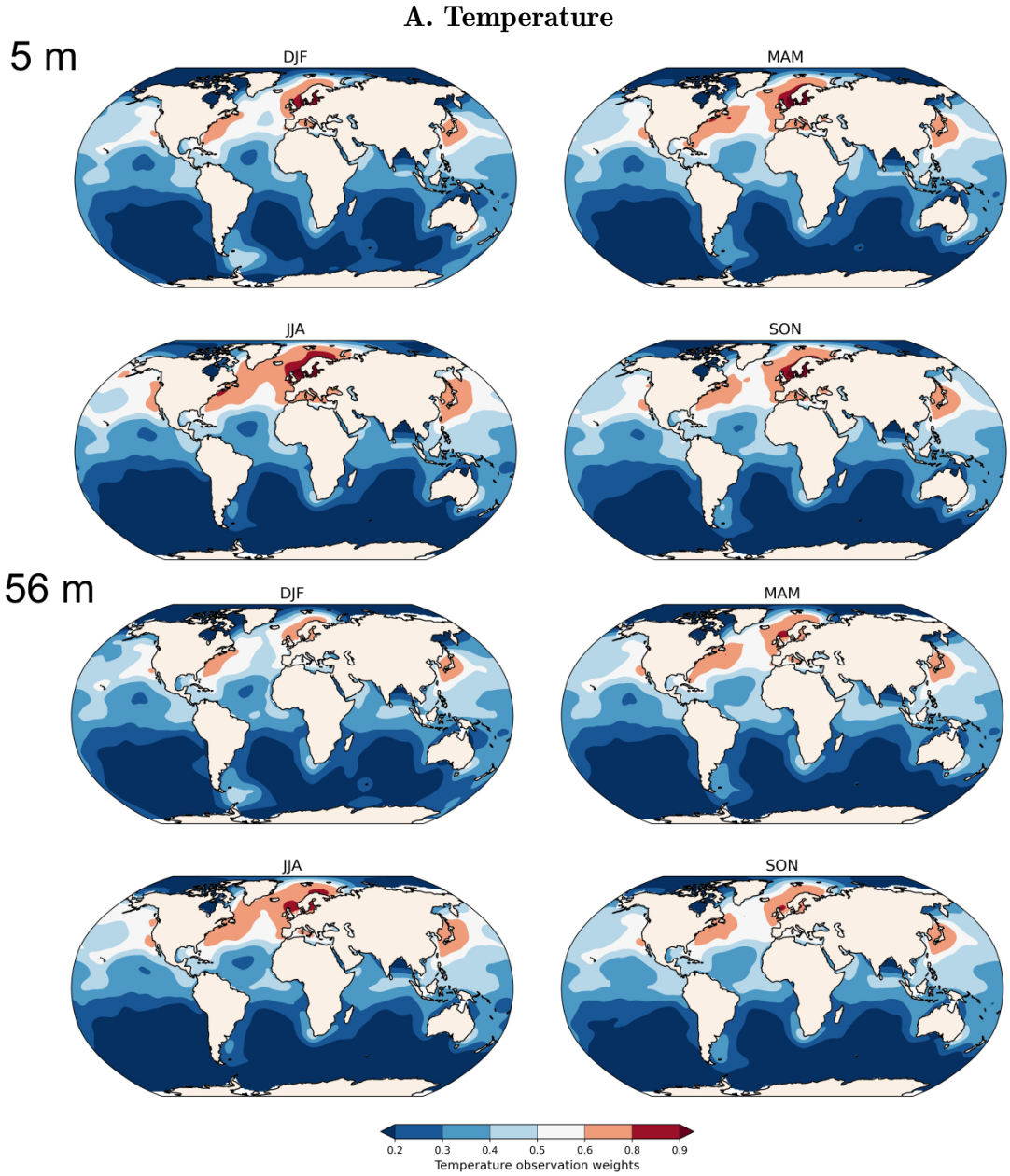

B. Salinity

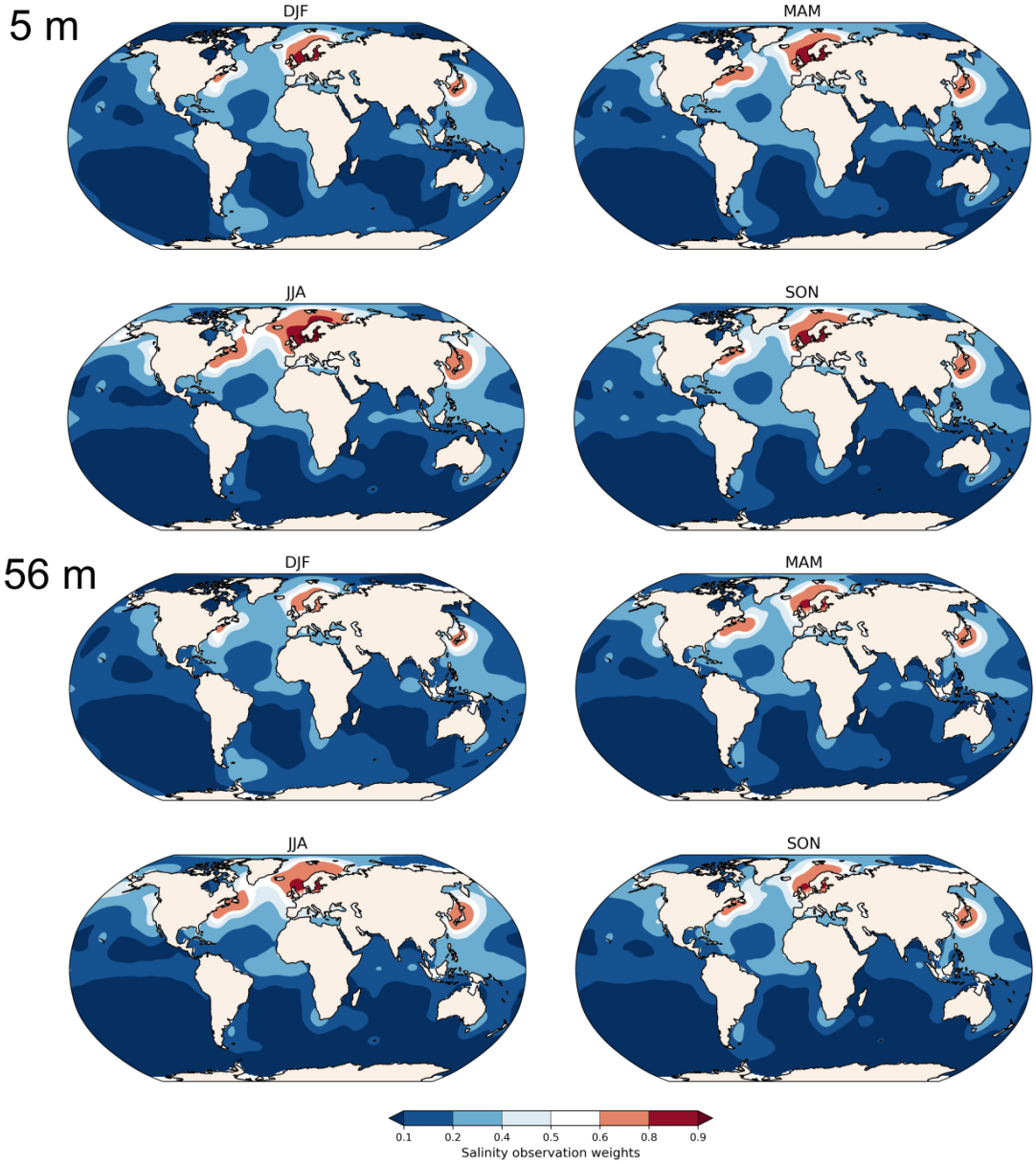
5 m
DJF
MAM
JJA
SON
56 m
DJF
MAM
JJA
SON
0.1
0.2
0.4
0.5
0.6
0.8
0.9
Salinity observation weights

Figure B2. Global distribution of seasonal **(A)** temperature and **(B)** salinity uncertainties (standard deviation) extracted from EN4.2.1 dataset (Good et al., 2013) at 5-m and 56-m depth, respectively.

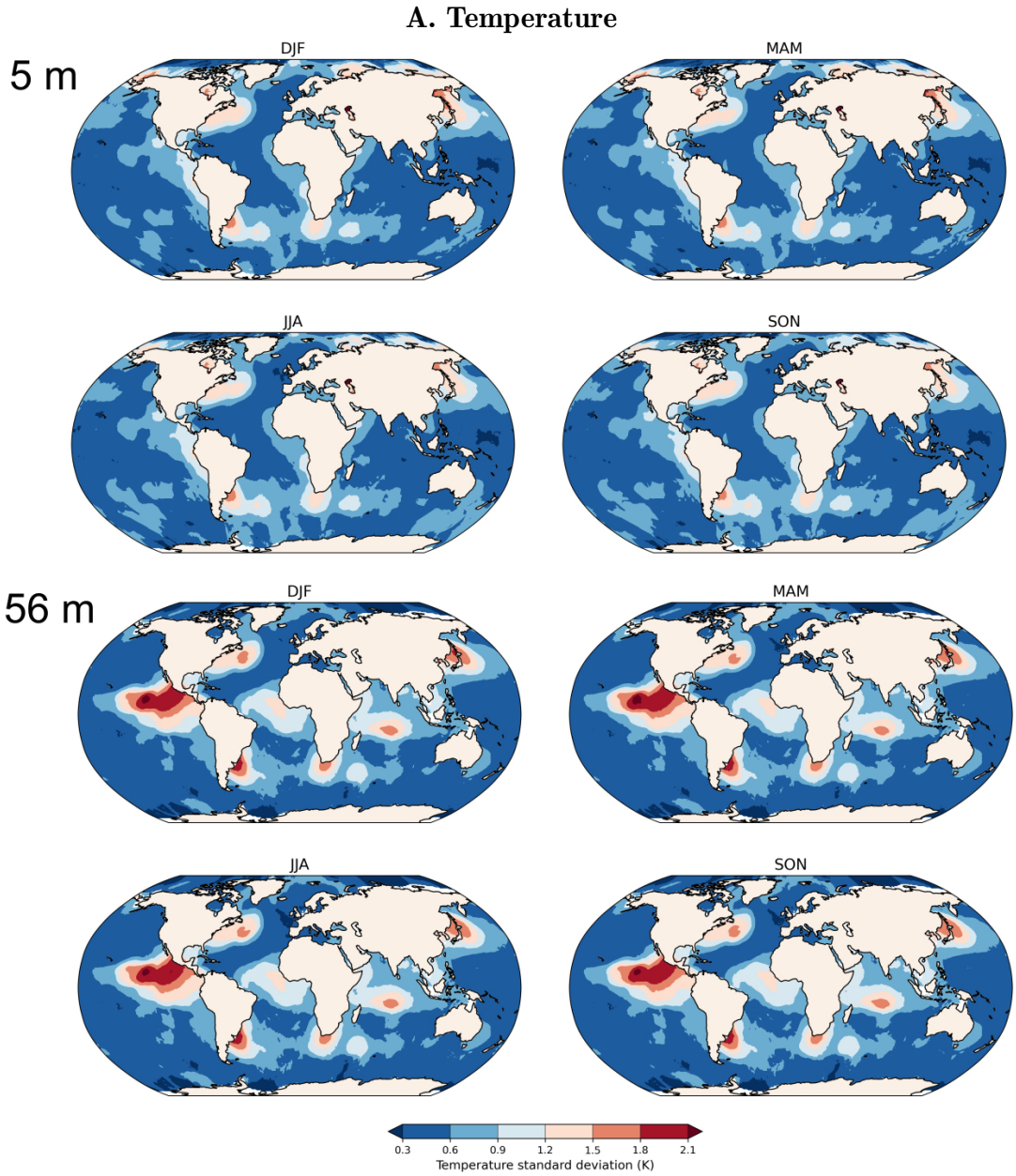

B. Salinity

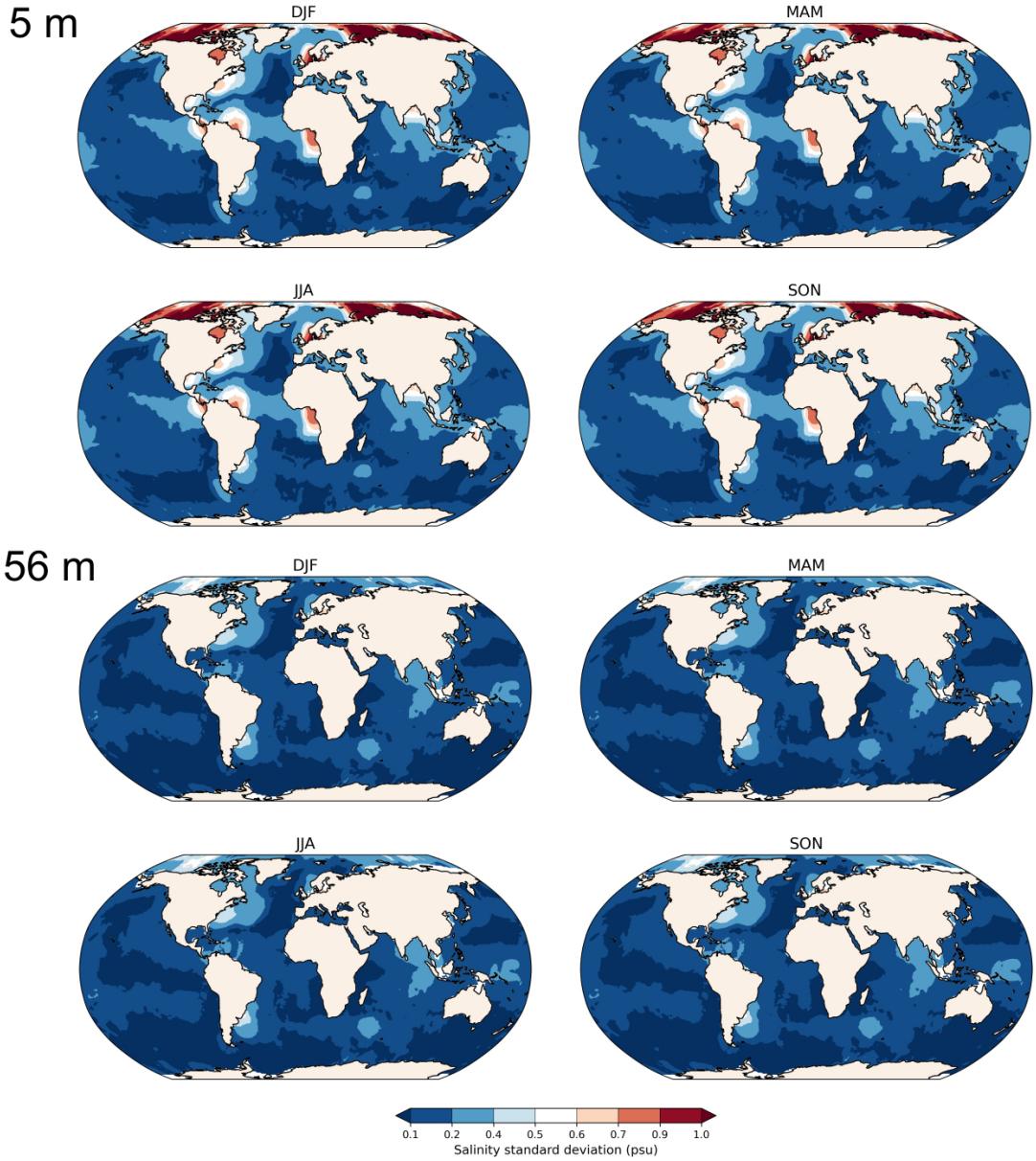
5 m
DJF
MAM
JJA
SON
56 m
DJF
MAM
JJA
SON
0.1
0.2
0.4
0.5
0.6
0.7
0.9
1.0
Salinity standard deviation (psu)

Figure B3. Multi-seasonal Pearson correlation analysis between the shell growth signal and subsurface water temperature at the approximate collection site (66°N, 18°W) for the 1900-2005 C.E. period at different significance levels: **(A)** 90 %, **(B)** 95 % and **(C)** 99 %. The correlation coefficients above the significance threshold are not shown (grey grids). The numbers represent the lag (yr) at which the maximum correlation occurs.

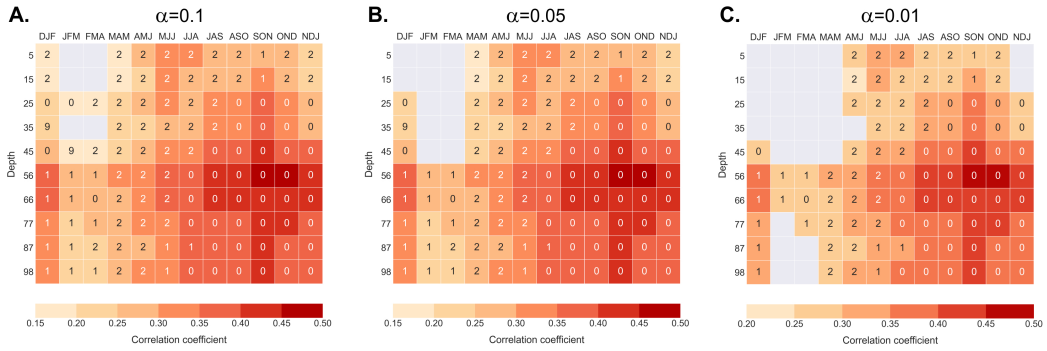

Figure B4. Multi-seasonal Pearson correlation analysis between the shell growth signal and subsurface salinity at the approximate collection site (66°N, 18°W) for the 1900-2005 C.E. period. The correlation results are presented for different significance levels: **(A)** 90 %, **(B)** 95 % and **(C)** 99 %. The correlation coefficients above the significance threshold are not shown (grey grids). The numbers represent the lag (yr) at which the maximum correlation occurs.

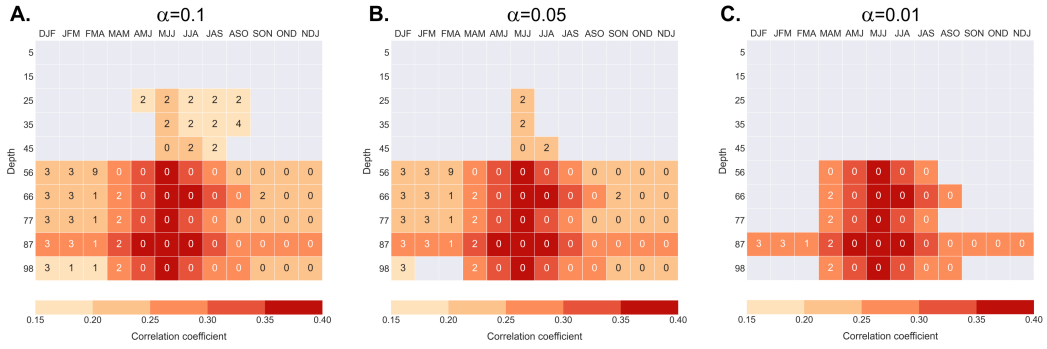

Figure B5. Seasonal salinity-depth profiles along a longitudinal transect (25°W – 15°W; 66°N). The transect is close to the shell collection site (black filled circle). The grey-shaded areas represent no available data.

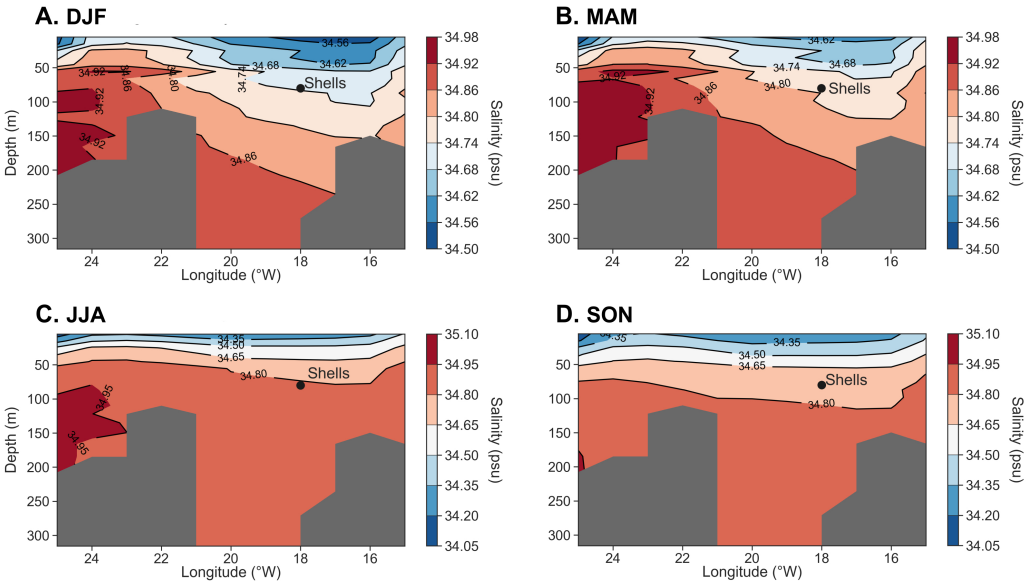

Figure B6. A 15-yr running correlation between the annually resolved master shell chronology and the water temperature at 56-m depth during boreal summer and autumn 3-month averages. Periods of decreased synchronization are shaded in grey.

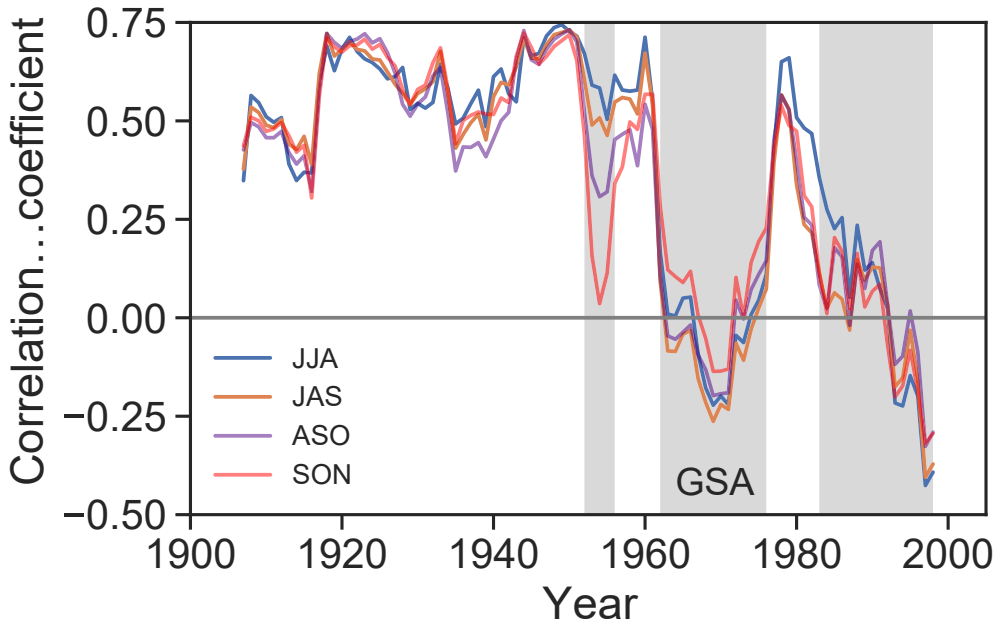

Figure B7. Salinity variation at 56-m depth during May-July (MJJ) for the 1900-2005 C.E analysis period (grey line). Salinity values above 0 signify a pronounced influence of Atlantic waters, while values below 0 indicate Arctic influences. The salinity time series, obtained from EN4.2.1 dataset (Good et al., 2013) at the shell collection site (66°N, 18°W), underwent detrending and standardization. A 5-yr Savitsky-Golay (low-pass) filter (Savitzky and Golay, 1964) was applied to the time series (blue line). The shaded area denotes a period of diminished synchrony with water temperature.

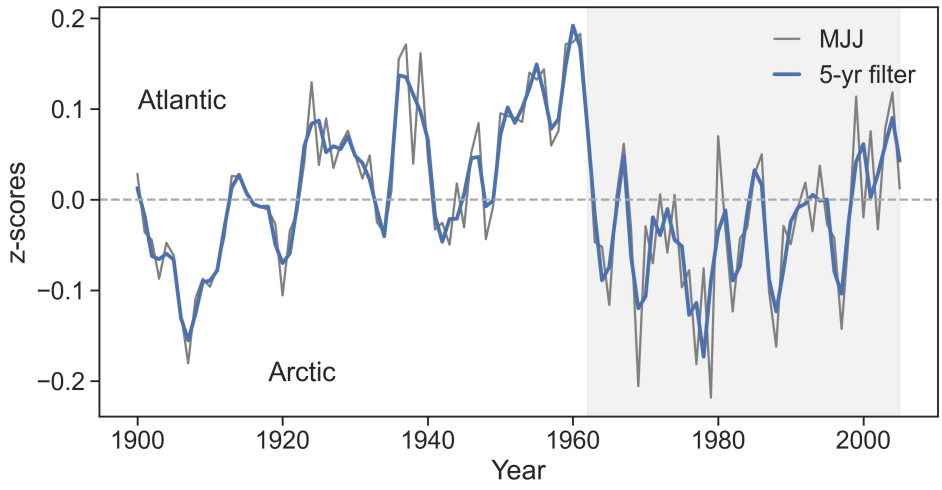

Figure B8. Depth-dependent seasonal variability of growth index time series at four different water depths (i.e., 5-, 56-, 66- and 77-m) for the 1900-2005 C.E. analysis period. Color shading shows the Pearson correlation coefficient ($p<0.05$) between ARMC and seasonal salinity time series at each grid point.

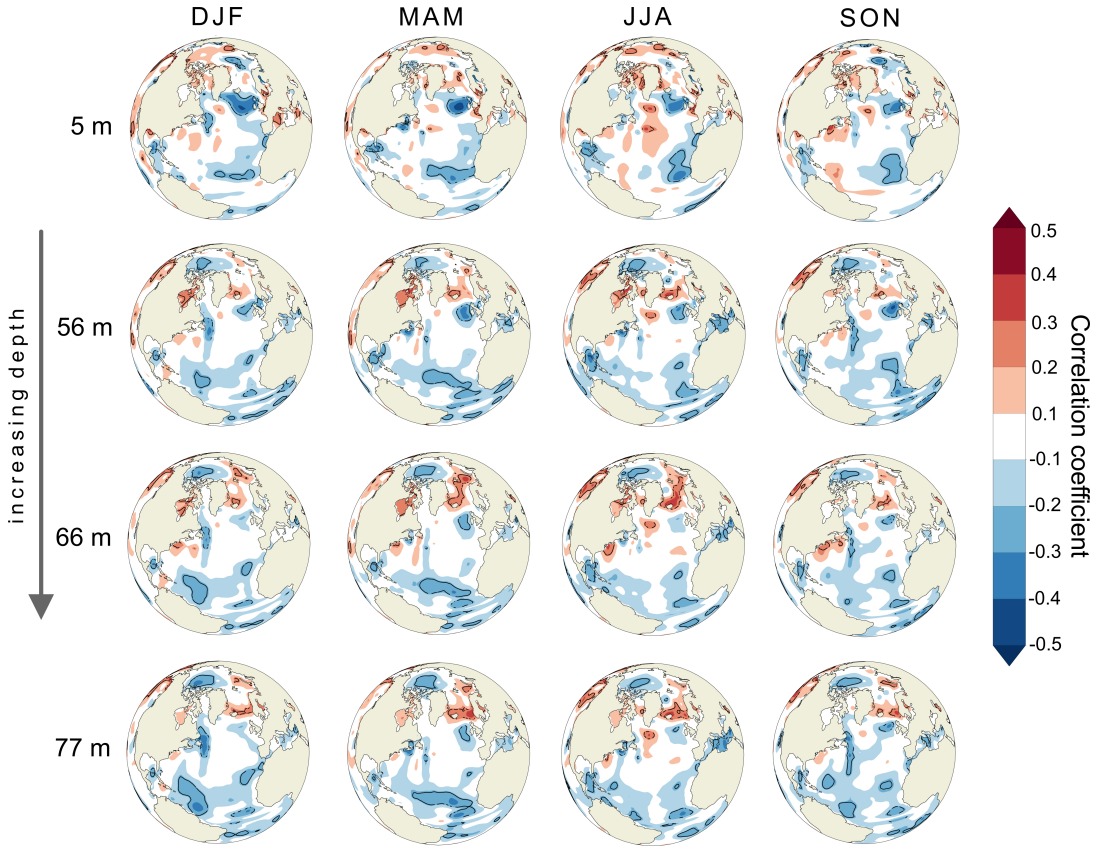

Figure B9. Pearson correlation coefficients between growth indices of *A. islandica* collected at approx. 82-m depth (Butler et al., 2013) and seasonal water temperature at various depths (5 to 98 m) for the common analysis period 1900-2005 C.E. The temperature time series were extracted from EN4.2.1 dataset (Good et al., 2013) close to the bivalve collection site (66°N, 18°W).

Depth	DJF	JFM	FMA	MAM	AMJ	MJJ	JJA	JAS	ASO	SON	OND	NDJ
5	0.188	0.138	0.125	0.197	0.275	0.335	0.311	0.296	0.283	0.297	0.265	0.247
15	0.176	0.134	0.124	0.194	0.249	0.309	0.295	0.298	0.296	0.317	0.278	0.244
25	0.220	0.173	0.169	0.227	0.267	0.300	0.288	0.306	0.328	0.356	0.320	0.283
35	0.213	0.143	0.144	0.203	0.248	0.289	0.284	0.315	0.340	0.366	0.330	0.279
45	0.282	0.173	0.174	0.219	0.257	0.311	0.329	0.365	0.386	0.412	0.394	0.355
56	0.391	0.272	0.282	0.305	0.334	0.378	0.399	0.423	0.438	0.468	0.466	0.443
66	0.367	0.263	0.277	0.299	0.336	0.374	0.388	0.404	0.405	0.430	0.424	0.405
77	0.328	0.232	0.252	0.276	0.310	0.348	0.367	0.388	0.388	0.415	0.403	0.373
87	0.310	0.221	0.239	0.263	0.297	0.332	0.350	0.374	0.379	0.404	0.388	0.354
98	0.315	0.211	0.230	0.257	0.303	0.343	0.362	0.383	0.386	0.409	0.397	0.363

Figure B10. Significance levels of the Pearson correlation coefficients in **Figure B9**.

Depth	DJF	JFM	FMA	MAM	AMJ	MJJ	JJA	JAS	ASO	SON	OND	NDJ
5	*	ns	ns	**	***	***	***	***	***	***	***	**
15	*	ns	ns	**	***	***	***	***	***	***	***	**
25	**	*	*	**	***	***	***	***	***	***	***	***
35	**	ns	ns	**	**	***	***	***	***	***	***	***
45	***	*	*	**	***	***	***	***	***	***	***	***
56	***	***	***	***	***	***	***	***	***	***	***	***
66	***	***	***	***	***	***	***	***	***	***	***	***
77	***	**	***	***	***	***	***	***	***	***	***	***
87	***	**	**	***	***	***	***	***	***	***	***	***
98	***	**	**	***	***	***	***	***	***	***	***	***

ns = not significant
* significant at 90%
** significant at 95%
*** significant at 99%

Appendix C: Supplementary material for Paper III

Figure C1. Spectral analysis of the standardized growth index (SGI) of *Arctica islandica*: **(A)** Wavelet transform (Morlet wavelet) and **(B)** Global wavelet power spectra. The black contour in panel A and dashed line in panel B indicate 95 % significance level using a red-noise background spectrum. The wavelet analysis was computed in Python using the Torrence and Compo (1998) algorithm.

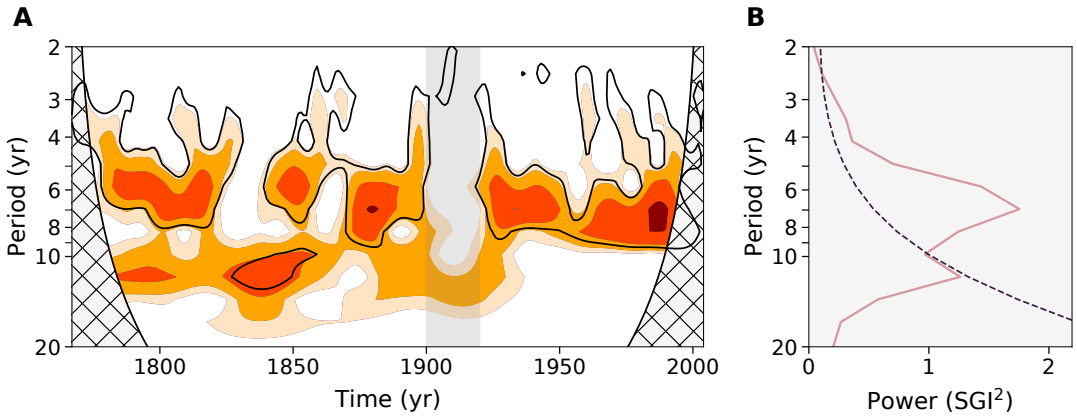

Table C1. Years corresponding to growth extremes in the SGI of *A. islandica* from Helgoland. The threshold used to define extremes is set at the lowest 10^{th} percentile and the upper 90^{th} percentile, respectively.

Low extremes	High extreme
1768, 1779, 1790, 1801, 1802, 1814, 1815, 1837, 1849, 1850, 1870, 1876, 1884, 1896, 1897, 1924, 1945, 1961, 1968, 1974, 1975, 1984, 1990, 1991	1773, 1786, 1798, 1805, 1812, 1818, 1819, 1828, 1841, 1842, 1852, 1853, 1859, 1863, 1879, 1880, 1927, 1928, 1935, 1941, 1954, 1980, 1994, 2003

Figure C2. Composite maps for extreme high SGI values in *Arctica islandica* from Helgoland (red marker on map) associated with boreal spring (MAM) atmospheric anomalies represented by **(A)** sea level pressure (SLP) and **(B)** geopotential height at 500 mb (Z500) and their zonal and meridional wind vectors at 10 m and 5500 m, respectively. The arrows indicate the wind vector direction, whereas the length of the arrow refers to the mean anomaly (m/s). Regions indicating statistical significance at 90 % level are displayed by dotted areas. The data were extracted from 20^{th} Century Reanalysis V3 dataset (Slivinski et al., 2019).

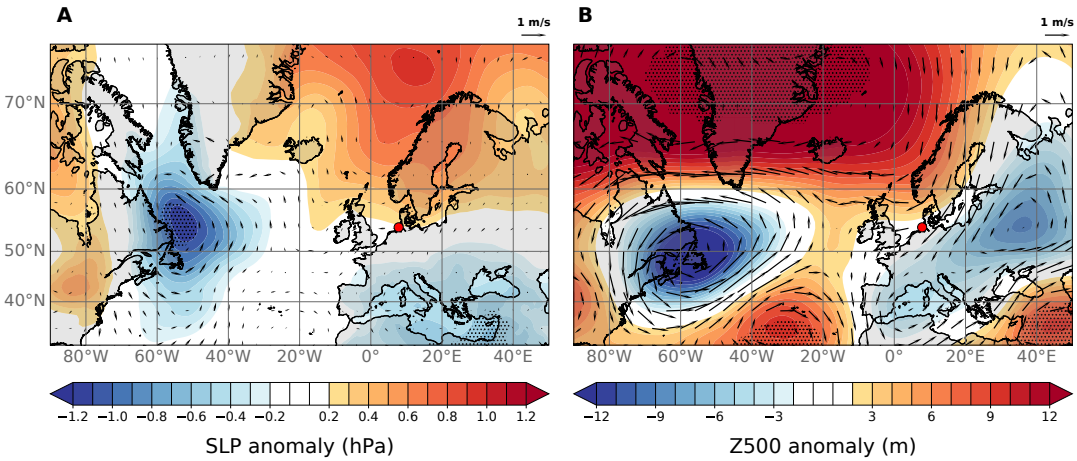

Figure C3. Composite maps for extreme low SGI values in *Arctica islandica* from Helgoland (red marker on map) associated with boreal winter (DJF) atmospheric anomalies represented by **(A)** sea level pressure (SLP) and **(B)** geopotential height at 500 mb (Z500) and their zonal and meridional wind vectors at 10 m and 5500 m, respectively. The arrows indicate the wind vector direction, whereas the length of the arrow refers to the mean anomaly (m/s). Regions indicating statistical significance at 90 % level are displayed by dotted areas. The data were extracted from 20^{th} Century Reanalysis V3 dataset (Slivinski et al., 2019).

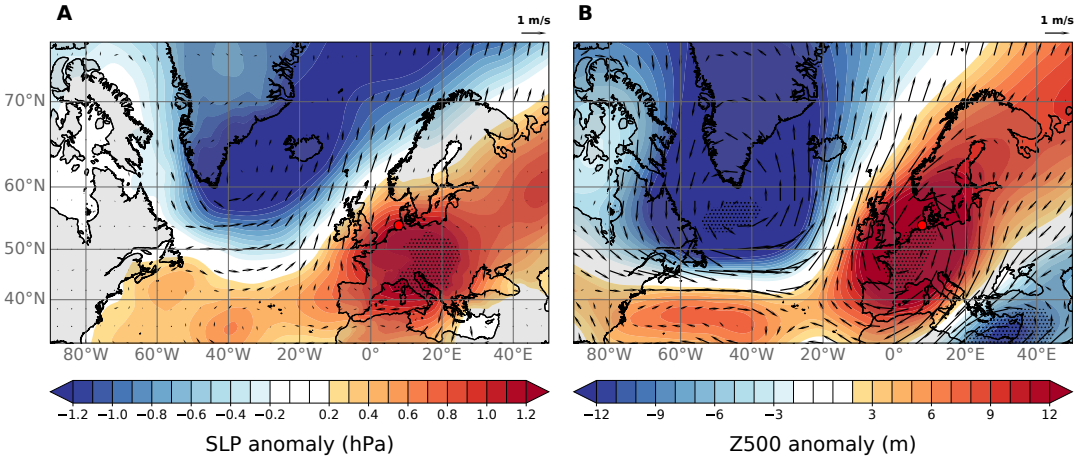

Figure C4. Boreal spring (MAM) upper tropospheric anomalies (Z500) associated with extreme low values in **(A)** January-February EP/NP index and **(B)** SGI of *Arctica islandica* from Helgoland (red marker on map). The extreme low values were selected for the 1950-2004 and 1900-2004 time periods for the EP/NP and SGI indices, respectively. Significant regions at 90 % confidence level against the climatological mean are displayed by dotted areas. Geopotential height data was extracted from 20^{th} Century Reanalysis V3 dataset (Slivinski et al., 2019).

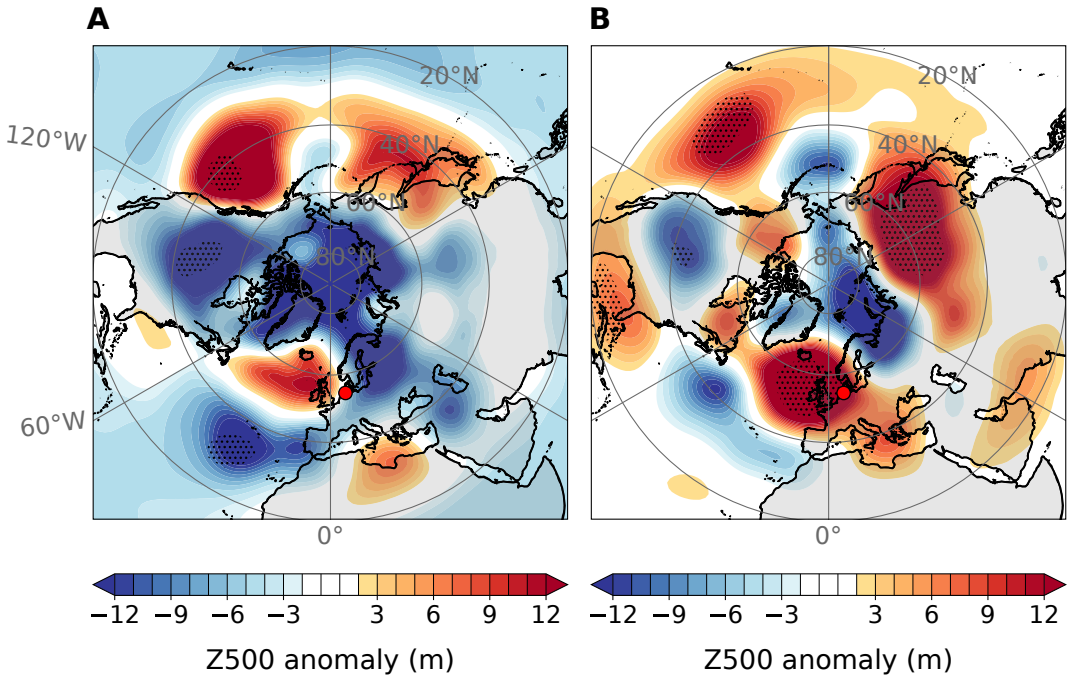

Appendix D: Future studies

Below, I present a compilation of interesting threads that I have either found or thought of during my research. These are intended to serve as inspiration for future studies.

- Intra-annual (e.g., daily, seasonal) growth increments have been observed in *A. islandica* from North Sea (Schöne et al., 2005c). However, to establish robust correlations with synoptic atmospheric circulation patterns, a level of temporal resolution exceeding that of traditional annual-based increments is required. This high-resolution sampling in bivalve shells could potentially increase the sample size for advanced statistical methods (e.g., machine learning).

- Schöne et al. (2005) have found that 58 % in daily growth variation is linked with temperature and food availability. Increasing the annual sampling resolution or employing physiological assessments and growth models could enhance the predictability of growth, a crucial aspect for ecological assessments in a changing climate. Moreover, this information holds practical value for aquaculture practices, enabling the optimization of cultivation conditions and maximizing yield. Information about environmental conditions affecting bivalve growth can aid in forecasting and managing harvests, contributing to sustainable seafood production. Additionally, deriving environmental predictors from numerical model output, reanalysis data, and other proxy sources can enhance paleo-reconstructions.

- In Figure 4.4, dual centers of action are evident in the atmospheric configuration requiring further analyses. Chronologies from the western-side of the Atlantic could supplement and clarify this finding. One could also look into the Baffin Bay-West Atlantic index and its associated pattern as it holds significant potential for identifying blocking occurrences in the North Atlantic (e.g., Wazneh et al., 2021). Such investigation may also offer valuable insights into the mechanisms driving extreme growth occurrences on both sides of the Atlantic Ocean.

- Developing bivalve networks by integrating master shell chronologies which capture the dynamics above and below the thermocline. My hypothesis is that composite chronologies from the upper 20 meters would be better at recording atmospheric shifts and anomalies, while those near or below the thermocline ($\sim$ 80-100 meters deep depending on the region, could be more effective at capturing long-term climate signals (e.g., AMO). Unfortunately, there are not sufficient composite chronologies that 1) span centuries and 2) the bivalves are collected from the same water depth layer. A

higher percentage of composite chronologies are based on bivalves mixed from different water depths (e.g., Figure 2.2). The development of future chronologies could make this possible. Alternatively, instead of focusing on a network, one could concentrate on surface vs. bottom ocean dynamics and extreme growth processes by using just two chronologies: one from the below the thermocline and one from above. It could provide insights into the depth-dependent vertical processes and potential lagged responses (e.g., Schöne et al., 2005d). Here, seasonally-resolved δ^{18}O records combined with growth records (e.g., Mette et al., 2016) are more appropriate for paleoclimate applications.

- Inter-basin comparison with the Pacific from a bivalve perspective could be insightful (e.g., Hetzinger et al., 2012). Bivalve chronologies produced for local reconstructions in the eastern and central North Pacific could be combined with *Arctica islandica* chronologies from the North Atlantic or compared in terms of extremes to identify potential teleconnections. Cross-validation on extremes is definitely a strength, however one could run into synchronization issues. The composite and correlation maps derived from the findings of all three papers can aid in identifying „hotspot“ locations and could thereby optimize the synchrony of chronologies.

- Case studies on bivalve extreme growth and corresponding regional and large-scale weather patterns. By examining in detail each individual extreme year and analyzing which specific weather configuration is linked to extreme indices, it is likely to uncover critical thresholds or triggers for extreme growth events in bivalves. For instance, Figure 4.4 depicts the average atmospheric pattern; however this configuration is not specific to some extreme years.

- To explore extremes derived from a multiproxy network, I did some preliminary findings. However, instead of combining proxy data from trees, corals and bivalves and running a principle component analysis for extracting the common signal, I performed PCA on each group of climate archives. I selected 10 tree cellulose-based δ^{18}O records from ISONET which were located in proximity to the eastern margin of the North Atlantic basin, two δ^{18}O coral records from tropical Atlantic (Goodkin et al., 2008; Hetzinger et al., 2010) and one from the Red Sea (Felis et al., 2000) in addition to the bivalve-based network from Chapter 2. I also looked into a couple bivalve chronologies from the German Bight. Next, I used the 10^{th}-90^{th} percentile thresholds for defining extremes for each leading time

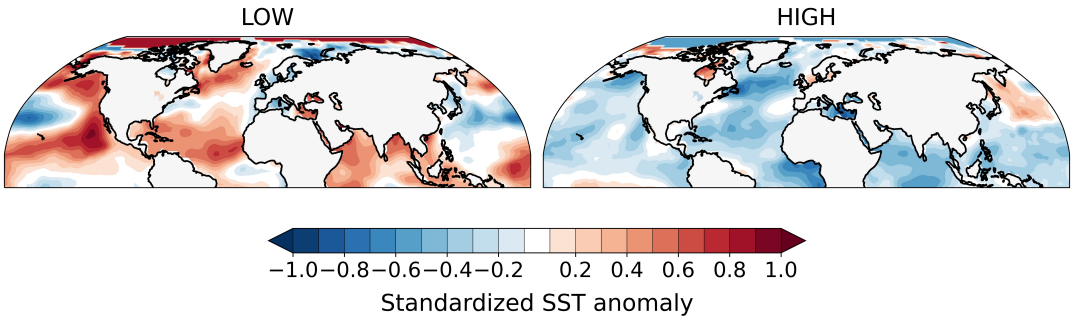

Figure D1. Composite spring SST map using the PCA-derived δ^{18}O signal from a collection of tropical Atlantic corals. The SST data was extracted from the ERSSTv.5 dataset (Huang et al., 2017). The 10^{th} and 90^{th} percentile threshold was used for identifying extreme low and high growth indices, respectively. Reference period: 1896-1995 CE.

series and generated composite SST maps for boreal spring, which were subsequently compared. Some preliminary results showed better coherence among tree- and coral-based proxy records. This could be the choice of δ^{18}O proxy for trees and corals as compared to growth bands in bivalves or simply a lagged response in bivalve growth which required further investigation. However, the most intriguing result is shown below in Figure D1 and Figure D2. It appears that low indices in the common δ^{18}O signal in both tree cellulose and corals correspond to the same spring SST pattern: positive PDO pattern in the Pacific and anomalously warm water-bodies in the tropical and high-latitudes of the Atlantic. The patterns for high growth also share some similarities, i.e., in the western side of the subpolar North Atlantic. Because δ^{18}O in tree cellulose is a good marker for hydroclimate, the high indices are likely indicating drought conditions over western Europe and positive sea-surface temperatures along the eastern margin of the Atlantic Ocean.

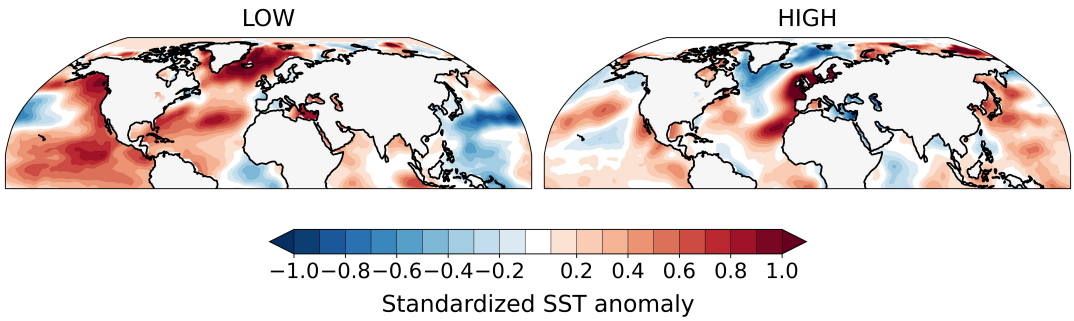

Figure D2. Composite spring SST map using the PCA-derived signal from 10 tree-based δ^{18}O chronologies of ISONET. The SST data was extracted from the ERSSTv.5 dataset (Huang et al., 2017). The 10^{th} and 90^{th} percentile threshold was used for identifying extreme low and high growth indices, respectively. Reference period: 1896-1995 CE.

List of acronyms

AO → Arctic Oscillation
AMO/AMV → Atlantic Multidecadal Oscillation/ Variability
AMOC → Atlantic Meridional Overturning Circulation
ARMC → Annually-resolved master chronology
BF → Blocking frequency index defined in Paper III
BP → Before Present (i.e., 1950)
CE → Common Era
EA → East-Atlantic pattern
EA/WR → East-Atlantic/ West-Russian pattern
EGC → East Greenland current
EIC → East Icelandic current
ENSO → El Niño-Southern Oscillation
EOF → Empirical orthogonal function
EP/NP → East Pacific/ North Pacific pattern
GB → Greenland blocking pattern
GSA → Great Salinity Anomaly (1968-1982 CE)
IC → Irminger current
LIA → Little Ice Age ($\sim$ 1300-1850 CE)
MDD → Mean Diatom Day index
NAC → North Atlantic current
NAO → North Atlantic Oscillation
NIS → North Icelandic shelf
PCA → Principle component analysis
PC1 → The 1^{st} principle component time series
PNA → Pacific-North American pattern
PDO → Pacific Decadal Oscillation
RCS → Regional Curve Standardization
SCA → Scandinavian blocking pattern
SGI → Standardized Growth Index
SST → Sea-surface temperature

Bibliography

Abele, D. (2002). Toxic oxygen: The radical life-giver. *Nature*, *420*(6911), 27–27, https://doi.org/10.1038/420027a https://www.nature.com/articles/420027a.

Alexander, M. A., Bladé, I., Newman, M., Lanzante, J. R., Lau, N.-C., & Scott, J. D. (2002). The Atmospheric Bridge: The Influence of ENSO Teleconnections on Air–Sea Interaction over the Global Oceans. *Journal of Climate*, *15*(16), 2205–2231, https://doi.org/10.1175/1520-0442(2002)015<2205:TABTIO>2.0.CO;2.

Alexander, M. A. & Deser, C. (1995). A Mechanism for the Recurrence of Wintertime Midlatitude SST Anomalies. *Journal of Physical Oceanography*, *25*(1), 122–137, https://doi.org/10.1175/1520-0485(1995)025<0122:AMFTRO>2.0.CO;2 http://journals.ametsoc.org/doi/10.1175/1520-0485(1995)025{%}3C0122:AMFTRO{%}3E2.0.CO;2.

Ambrose, W. G., Carroll, M. L., Greenacre, M., Thorrold, S. R., & McMahon, K. W. (2006). Variation in Serripes groenlandicus (Bivalvia) growth in a Norwegian high-Arctic fjord: evidence for local- and large-scale climatic forcing. *Global Change Biology*, *12*(9), 1595–1607, https://doi.org/10.1111/j.1365-2486.2006.01181.x https://onlinelibrary.wiley.com/doi/10.1111/j.1365-2486.2006.01181.x.

Andersen, K. K., et al. (2004). High-resolution record of Northern Hemisphere climate extending into the last interglacial period. *Nature*, *431*(7005), 147–151, https://doi.org/10.1038/nature02805 https://www.nature.com/articles/nature02805.

Andersson, C., Pausata, F. S. R., Jansen, E., Risebrobakken, B., & Telford, R. J. (2010). Holocene trends in the foraminifer record from the Norwegian Sea and the North Atlantic Ocean. *Climate of the Past*, *6*(2), 179–193, https://doi.org/10.5194/cp-6-179-2010 https://cp.copernicus.org/articles/6/179/2010/.

Baker, A., C. Hellstrom, J., Kelly, B. F. J., Mariethoz, G., & Trouet, V. (2015). A composite annual-resolution stalagmite record of North Atlantic climate over the last three millennia. *Scientific Reports*, *5*(1), 10307, https://doi.org/10.1038/srep10307 https://www.nature.com/articles/srep10307.

Bakke, S. J., Ionita, M., & Tallaksen, L. M. (2023). Recent European drying and its link to prevailing large-scale atmospheric patterns. *Scientific Reports*, *13*(1), 21921, https://doi.org/10.1038/s41598-023-48861-4 https://www.nature.com/articles/s41598-023-48861-4.

Ballesta-Artero, I., Janssen, R., van der Meer, J., & Witbaard, R. (2018). Interactive effects of temperature and food availability on the growth of Arctica islandica (Bivalvia) juveniles. *Marine Environmental Research*, *133*, 67–77, https://doi.org/10.1016/j.marenvres.2017.12.004 https://linkinghub.elsevier.com/retrieve/pii/S0141113617305858.

Balting, D. F., et al. (2021). Large-scale climate signals of a European oxygen isotope network from tree rings. *Climate of the Past*, *17*(3), 1005–1023, https://doi.org/10.5194/cp-17-1005-2021 https://cp.copernicus.org/articles/17/1005/2021/.

Bar-Matthews, M., Ayalon, A., & Kaufman, A. (2000). Timing and hydrological conditions of Sapropel events in the Eastern Mediterranean, as evident from speleothems, Soreq cave, Israel. *Chemical Geology*, *169*(1-2), 145–156, https://doi.org/10.1016/S0009-2541(99)00232-6 https://linkinghub.elsevier.com/retrieve/pii/S0009254199002326.

Barker, S., et al. (2011). 800,000 Years of Abrupt Climate Variability. *Science*, *334*(6054), 347–351, https://doi.org/10.1126/science.1203580 https://www.science.org/doi/10.1126/science.1203580.

Barnston, A. G. & Livezey, R. E. (1987). Classification, Seasonality and Persistence of Low-Frequency Atmospheric Circulation Patterns. *Monthly Weather Review*, *115*(6), 1083–1126, https://doi.org/10.1175/1520-0493(1987)115<1083:CSAPOL>2.0.CO;2 http://journals.ametsoc.org/doi/10.1175/1520-0493(1987)115{%}3C1083:CSAPOL{%}3E2.0.CO;2.

Basova, L., Begum, S., Strahl, J., Sukhotin, A., Brey, T., Philipp, E., & Abele, D. (2012). Age-dependent patterns of antioxidants in Arctica islandica from six regionally separate populations with different lifespans. *Aquatic Biology*, *14*(2), 141–152, https://doi.org/10.3354/ab00387 https://www.int-res.com/abstracts/ab/v14/n2/p141-152/.

Basova, L., Strahl, J., Philipp, E. E. R., Brey, T., Sukhotin, A., & Abele, D. (2017). Lipofuscin accumulation in tissues of Arctica islandica indicates faster ageing in populations from brackish environments. *Marine Biology*, *164*(4), 72, https://doi.org/10.1007/s00227-017-3110-4 https://link.springer.com/article/10.1007/s00227-017-3110-4.

Bauer, F. (2011). *Eine Masterchronologie von Arctica islandica bei Helgoland*. Bachelor thesis, University of Bremen https://epic.awi.de/id/eprint/34811/.

Begum, S., Basova, L., Heilmayer, O., Philipp, E. E. R., Abele, D., & Brey, T. (2010). Growth and Energy Budget Models of the Bivalve Arctica islandica at Six Different Sites in the Northeast Atlantic Realm. *Journal of Shellfish Research*, *29*(1), 107–115, https://doi.org/10.2983/035.029.0103 https://bioone.org/journals/journal-of-shellfish-research/volume-29/issue-1/035.029.0103/Growth-and-Energy-Budget-Models-of-the-Bivalve-Arctica-islandica/10.2983/035.029.0103.full.

Begum, S., et al. (2009). A Metabolic Model for the Ocean Quahog Arctica islandica —Effects of Animal Mass and Age, Temperature, Salinity, and Geography on Respiration Rate. *Journal of Shellfish Research*, *28*(3), 533–539, https://doi.org/10.2983/035.028.0315 https://bioone.org/journals/journal-of-shellfish-research/volume-28/issue-3/035.028.0315/A-Metabolic-Model-for-the-Ocean-Quahog-Arctica-islandicaEffects-of/10.2983/035.028.0315.full.

Beierlein, L., Salvigsen, O., Schöne, B. R., Mackensen, A., & Brey, T. (2015). The seasonal water temperature cycle in the Arctic Dicksonfjord (Svalbard) during the Holocene Climate Optimum derived from subfossil Arctica islandica shells. *The Holocene*, *25*(8), 1197–1207, https://doi.org/10.1177/0959683615580861 http://journals.sagepub.com/doi/10.1177/0959683615580861.

Berkelmans, R. & Oliver, J. K. (1999). Large-scale bleaching of corals on the Great Barrier Reef. *Coral Reefs*, *18*(1), 55–60, https://doi.org/10.1007/s003380050154 http://link.springer.com/10.1007/s003380050154.

Bersch, M. (2002). North Atlantic Oscillation–induced changes of the upper layer circulation in the northern North Atlantic Ocean. *Journal of Geophysical Research: Oceans*, *107*(C10), 20–1, https://doi.org/10.1029/2001JC000901 https://agupubs.onlinelibrary.wiley.com/doi/10.1029/2001JC000901.

Biondi, F., Gershunov, A., & Cayan, D. R. (2001). North Pacific Decadal Climate Variability since 1661. *Journal of Climate*, *14*(1), 5–10, https://doi.org/10.1175/1520-0442(2001)014<0005:NPDCVS>2.0.CO;2.

Black, B. A. (2009). Climate-driven synchrony across tree, bivalve, and rockfish growth-increment chronologies of the northeast Pacific. *Marine Ecology Progress Series*, *378*, 37–46, https://doi.org/10.3354/meps07854 http://www.int-res.com/abstracts/meps/v378/p37-46/.

Black, B. A., et al. (2019). The revolution of crossdating in marine palaeoecology and palaeoclimatology https://royalsocietypublishing.org/doi/10.1098/rsbl.2018.0665.

Black, B. A., Copenheaver, C. A., Frank, D. C., Stuckey, M. J., & Kormanyos, R. E. (2009). Multi-proxy reconstructions of northeastern Pacific sea surface temperature data from trees and Pacific geoduck. *Palaeogeography, Palaeoclimatology, Palaeoecology*, *278*(1-4), 40–47, https://doi.org/10.1016/j.palaeo.2009.04.010 https://linkinghub.elsevier.com/retrieve/pii/S0031018209001412.

Black, B. A., Gillespie, D. C., MacLellan, S. E., & Hand, C. M. (2008). Establishing highly accurate production-age data using the tree-ring technique of crossdating: a case study for Pacific geoduck (Panopea abrupta). *Canadian Journal of Fisheries and Aquatic Sciences*, *65*(12), 2572–2578, https://doi.org/10.1139/F08-158 http://www.nrcresearchpress.com/doi/10.1139/F08-158.

Black, B. A., et al. (2016). The value of crossdating to retain high-frequency variability, climate signals, and extreme events in environmental proxies. *Global Change Biology*, *22*(7), 2582–2595, https://doi.org/10.1111/gcb.13256 https://onlinelibrary.wiley.com/doi/10.1111/gcb.13256.

Black, B. A., et al. (2014). Six centuries of variability and extremes in a coupled marine-terrestrial ecosystem. *Science*, *345*(6203), 1498–1502, https://doi.org/10.1126/science.1253209 https://www.science.org/doi/10.1126/science.1253209.

Black, D. E., Peterson, L. C., Overpeck, J. T., Kaplan, A., Evans, M. N., & Kashgarian, M. (1999). Eight Centuries of North Atlantic Ocean Atmosphere Variability. *Science*, *286*(5445), 1709–1713, https://doi.org/10.1126/science.286.5445.1709 https://www.science.org/doi/10.1126/science.286.5445.1709.

Bond, N. A., Cronin, M. F., Freeland, H., & Mantua, N. (2015). Causes and impacts of the 2014 warm anomaly in the NE Pacific. *Geophysical Research Letters*, *42*(9), 3414–3420, https://doi.org/10.1002/2015GL063306 https://agupubs.onlinelibrary.wiley.com/doi/10.1002/2015GL063306.

Bonitz, F. G. W., Andersson, C., Trofimova, T., & Hátún, H. (2018). Links between phytoplankton dynamics and shell growth of Arctica islandica on the Faroe Shelf. *Journal of Marine Systems*, *179*, 72–87, https://doi.org/10.1016/j.jmarsys.2017.11.005 https://linkinghub.elsevier.com/retrieve/pii/S092479631730252X.

Bretherton, C. S., Widmann, M., Dymnikov, V. P., Wallace, J. M., & Bladé, I. (1999). The effective number of spatial degrees of freedom of a time-varying field. *Journal of Climate*, *12*(7), 1990–2009, https://doi.org/10.1175/1520-0442(1999)012<1990:TENOSD>2.0.CO;2.

Brey, T., Arntz, W., Pauly, D., & Rumohr, H. (1990). Arctica (Cyprina) islandica in Kiel Bay (Western Baltic): growth, production and ecological significance. *Journal of Experimental Marine Biology and Ecology*, *136*(3), 217–235, https://doi.org/10.1016/0022-0981(90)90162-6 https://linkinghub.elsevier.com/retrieve/pii/0022098190901626.

Brocas, W., Reynolds, D., Butler, P., Richardson, C., Scourse, J., Ridgway, I., & Ramsay, K. (2013). The dog cockle, Glycymeris glycymeris (L.), a new annually-resolved sclerochronological archive for the Irish Sea. *Palaeogeography, Palaeoclimatology, Palaeoecology*, *373*, 133–140, https://doi.org/10.1016/j.palaeo.2012.03.030 https://linkinghub.elsevier.com/retrieve/pii/S0031018212001794.

Brocas, W. M., et al. (2016). Last interglacial temperature seasonality reconstructed from tropical Atlantic corals. *Earth and Planetary Science Letters*, *449*, 418–429, https://doi.org/10.1016/j.epsl.2016.06.005 https://linkinghub.elsevier.com/retrieve/pii/S0012821X16302928.

Brown, B. E. (1997). Coral bleaching: causes and consequences. *Coral Reefs*, *16*(SUPPL. 1), S129–S138, https://doi.org/10.1007/s003380050249 http://link.springer.com/10.1007/s003380050249.

Bueh, C. & Nakamura, H. (2007). Scandinavian pattern and its climatic impact. *Quarterly Journal of the Royal Meteorological Society*, *133*(629), 2117–2131, https://doi.org/10.1002/qj.173 https://rmets.onlinelibrary.wiley.com/doi/10.1002/qj.173.

Busecke, J. J. & Abernathey, R. P. (2019). Ocean mesoscale mixing linked to climate variability. *Science Advances*, *5*(1), https://doi.org/10.1126/sciadv.aav5014 https://www.science.orghttps://www.science.org/doi/10.1126/sciadv.aav5014.

Butler, P. G., et al. (2009). Accurate increment identification and the spatial extent of the common signal in five Arctica islandica chronologies from the Fladen Ground, northern North Sea. *Paleoceanography*, *24*(2), https://doi.org/10.1029/2008PA001715 https://agupubs.onlinelibrary.wiley.com/doi/10.1029/2008PA001715.

Butler, P. G., Wanamaker, A. D., Scourse, J. D., Richardson, C. A., & Reynolds, D. J. (2013). Variability of marine climate on the North Icelandic Shelf in a 1357-year proxy archive based on growth increments in the bivalve Arctica islandica. *Palaeogeography, Palaeoclimatology, Palaeoecology*, *373*, 141–151, https://doi.org/10.1016/j.palaeo.2012.01.016 https://linkinghub.elsevier.com/retrieve/pii/S0031018212000302.

Cai, D., Lohmann, G., Chen, X., & Ionita, M. (2024). The linkage between autumn Barents-Kara sea ice and European cold winter extremes. *Frontiers in Climate*, *6*, https://doi.org/10.3389/fclim.2024.1345763 https://www.frontiersin.org/articles/10.3389/fclim.2024.1345763/full.

Caldarescu, D. E., Brey, T., Abele, D., Beierlein, L., Lohmann, G., & Ionita, M. (2021). The Influence of Depth-Dependent Seasonal Temperature Variability on Growth Signal in Arctica islandica. *Frontiers in Marine Science*, *8*, 823, https://doi.org/10.3389/fmars.2021.687318 https://www.frontiersin.org/articles/10.3389/fmars.2021.687318/full.

Cargnelli, L., Griesbach, S., Packer, D., & Weissberger, E. (1999). Essential fish habitat source document: Ocean quahog, Arctica islandica, life history and habitat characteristics. *NOAA Technical Memorandum NMFS-NE Series*, *148*, 1–88 https://repository.library.noaa.gov/view/noaa/3153.

Carroll, M. L., Ambrose, W. G., Locke V, W. L., Ryan, S. K., & Johnson, B. J. (2014). Bivalve growth rate and isotopic variability across the Barents Sea Polar Front. *Journal of Marine Systems*, *130*, 167–180, https://doi.org/10.1016/j.jmarsys.2013.10.006 https://linkinghub.elsevier.com/retrieve/pii/S0924796313002121.

Casella, L. A., et al. (2017). Experimental diagenesis: insights into aragonite to calcite transformation of <i>Arctica islandica</i> shells by hydrothermal treatment. *Biogeosciences*, *14*(6), 1461–1492, https://doi.org/

10.5194/bg-14-1461-2017 https://bg.copernicus.org/articles/14/1461/2017/.

Cassou, C., Terray, L., Hurrell, J. W., & Deser, C. (2004). North Atlantic winter climate regimes: Spatial asymmetry, stationarity with time, and oceanic forcing. *Journal of Climate*, *17*(5), 1055–1068, https://doi.org/10.1175/1520-0442(2004)017<1055:NAWCRS>2.0.CO;2.

Cavole, L., et al. (2016). Biological Impacts of the 2013–2015 Warm-Water Anomaly in the Northeast Pacific: Winners, Losers, and the Future. *Oceanography*, *29*(2), 273–285, https://doi.org/10.5670/oceanog.2016.32 https://tos.org/oceanography/article/biological-impacts-of-the-20132015-warm-water-anomaly-in-the-northeast-paci.

Chafik, L., Nilsen, J. E. Ø., & Dangendorf, S. (2017). Impact of North Atlantic teleconnection patterns on northern European sea level. *Journal of Marine Science and Engineering*, *5*(3), 1–23, https://doi.org/10.3390/jmse5030043.

Chan, P., et al. (2017). Multicentennial record of Labrador Sea primary productivity and sea-ice variability archived in coralline algal barium. *Nature Communications*, *8*(1), 15543, https://doi.org/10.1038/ncomms15543 https://www.nature.com/articles/ncomms15543.

Chapman, C. C., Monselesan, D. P., Risbey, J. S., Feng, M., & Sloyan, B. M. (2022). A large-scale view of marine heatwaves revealed by archetype analysis. *Nature Communications*, *13*(1), 7843, https://doi.org/10.1038/s41467-022-35493-x https://www.nature.com/articles/s41467-022-35493-x.

Charles, C. D., Cobb, K., Moore, M. D., & Fairbanks, R. G. (2003). Monsoon–tropical ocean interaction in a network of coral records spanning the 20th century. *Marine Geology*, *201*(1-3), 207–222, https://doi.org/10.1016/S0025-3227(03)00217-2 https://linkinghub.elsevier.com/retrieve/pii/S0025322703002172.

Cobb, K. M., Charles, C. D., & Hunter, D. E. (2001). A central tropical Pacific coral demonstrates Pacific, Indian, and Atlantic decadal climate connections. *Geophysical Research Letters*, *28*(11), 2209–2212, https://doi.org/10.1029/2001GL012919 https://agupubs.onlinelibrary.wiley.com/doi/10.1029/2001GL012919.

Cobb, K. M., et al. (2013). Highly Variable El Niño–Southern Oscillation Throughout the Holocene. *Science*, *339*(6115), 67–70, https:

//doi.org/10.1126/science.1228246 https://www.science.org/doi/10.1126/science.1228246.

Comas-Bru, L. & Hernández, A. (2018). Reconciling North Atlantic climate modes: revised monthly indices for the East Atlantic and the Scandinavian patterns beyond the 20th century. *Earth System Science Data*, *10*(4), 2329–2344, https://doi.org/10.5194/essd-10-2329-2018 https://essd.copernicus.org/articles/10/2329/2018/.

Comas-Bru, L. & McDermott, F. (2014). Impacts of the EA and SCA patterns on the European twentieth century NAO–winter climate relationship. *Quarterly Journal of the Royal Meteorological Society*, *140*(679), 354–363, https://doi.org/10.1002/qj.2158 https://rmets.onlinelibrary.wiley.com/doi/10.1002/qj.2158.

Cook, E. R., Briffa, K. R., Meko, D. M., Graybill, D. A., & Funkhouser, G. (1995). Chronology Development for Palaeoclimatic Studies. *The Holocene*, *5*(2), 229–237.

Cook, E. R., D'Arrigo, R. D., & Briffa, K. R. (1998). A reconstruction of the North Atlantic Oscillation using tree-ring chronologies from North America and Europe. *The Holocene*, *8*(1), 9–17, https://doi.org/10.1191/095968398677793725 http://journals.sagepub.com/doi/10.1191/095968398677793725.

Cook, E. R., D'Arrigo, R. D., & Mann, M. E. (2002). A Well-Verified, Multiproxy Reconstruction of the Winter North Atlantic Oscillation Index since <scp>a.d.</scp> 1400*. *Journal of Climate*, *15*(13), 1754–1764, https://doi.org/10.1175/1520-0442(2002)015<1754:AWVMRO>2.0.CO;2 http://journals.ametsoc.org/doi/10.1175/1520-0442(2002)015{%}3C1754:AWVMRO{%}3E2.0.CO;2.

Crippa, G. & Raineri, G. (2015). The genera Glycymeris, Aequipecten and Arctica, and associated mollusk fauna of the lower Pleistocene Arda river section (Northern Italy). *Rivista Italiana di Paleontologia e Stratigrafia*, *121*(1), 61–101, https://doi.org/10.13130/2039-4942/6401 https://riviste.unimi.it/index.php/RIPS/article/view/6401.

Dahlgren, T. G., Weinberg, J. R., & Halanych, K. M. (2000). Phylogeography of the ocean quahog (Arctica islandica): influences of paleoclimate on genetic diversity and species range. *Marine Biology*, *137*(3), 487–495, https://doi.org/10.1007/s002270000342 http://link.springer.com/10.1007/s002270000342.

Dansgaard, W., et al. (1993). Evidence for general instability of past climate from a 250-kyr ice-core record. *Nature*, *364*(6434), 218–220, https://doi.org/10.1038/364218a0 https://www.nature.com/articles/364218a0.

D'Arrigo, R., Villalba, R., & Wiles, G. (2001). Tree-ring estimates of Pacific decadal climate variability. *Climate Dynamics*, *18*(3-4), 219–224, https://doi.org/10.1007/s003820100177 http://link.springer.com/10.1007/s003820100177.

D'Arrigo, R., Wiles, G., Jacoby, G., & Villalba, R. (1999). North Pacific sea surface temperatures: Past variations inferred from tree rings. *Geophysical Research Letters*, *26*(17), 2757–2760, https://doi.org/10.1029/1999GL900504 https://agupubs.onlinelibrary.wiley.com/doi/10.1029/1999GL900504.

Davini, P., Cagnazzo, C., Neale, R., & Tribbia, J. (2012). Coupling between Greenland blocking and the North Atlantic Oscillation pattern. *Geophysical Research Letters*, *39*(14), https://doi.org/10.1029/2012GL052315 https://agupubs.onlinelibrary.wiley.com/doi/10.1029/2012GL052315.

Delworth, T. L. & Mann, M. E. (2000). Observed and simulated multidecadal variability in the Northern Hemisphere. *Climate Dynamics*, *16*(9), 661–676, https://doi.org/10.1007/s003820000075 http://link.springer.com/10.1007/s003820000075.

Demarchi, B., Williams, M. G., Milner, N., Russell, N., Bailey, G., & Penkman, K. (2011). Amino acid racemization dating of marine shells: A mound of possibilities. *Quaternary International*, *239*(1-2), 114–124, https://doi.org/10.1016/j.quaint.2010.05.029 https://linkinghub.elsevier.com/retrieve/pii/S1040618210002260.

Deser, C., Alexander, M. A., Xie, S.-P., & Phillips, A. S. (2010). Sea Surface Temperature Variability: Patterns and Mechanisms. *Annual Review of Marine Science*, *2*(1), 115–143, https://doi.org/10.1146/annurev-marine-120408-151453 http://www.annualreviews.org/doi/10.1146/annurev-marine-120408-151453.

Deser, C. & Phillips, A. S. (2006). Simulation of the 1976/77 climate transition over the North Pacific: Sensitivity to tropical forcing. *Journal of Climate*, *19*(23), 6170–6180, https://doi.org/10.1175/JCLI3963.1 http://journals.ametsoc.org/doi/10.1175/JCLI3963.1.

Deser, C., Walsh, J. E., & Timlin, M. S. (2000). Arctic Sea Ice Variability in the Context of Recent Atmospheric Circulation Trends. *Jour-*

nal of Climate, *13*(3), 617–633, https://doi.org/10.1175/1520-0442(2000)013<0617:ASIVIT>2.0.CO;2 http://journals.ametsoc.org/doi/10.1175/1520-0442(2000)013{%}3C0617:ASIVIT{%}3E2.0.CO;2.

Di Lorenzo, E. & Mantua, N. (2016). Multi-year persistence of the 2014/15 North Pacific marine heatwave. *Nature Climate Change*, *6*(11), 1042–1047, https://doi.org/10.1038/nclimate3082 https://www.nature.com/articles/nclimate3082.

Diao, Y., Li, J., & Luo, D. (2006). A New Blocking Index and Its Application: Blocking Action in the Northern Hemisphere. *Journal of Climate*, *19*(19), 4819–4839, https://doi.org/10.1175/JCLI3886.1 http://journals.ametsoc.org/doi/10.1175/JCLI3886.1.

Diaz, R. J. & Rosenberg, R. (2008). Spreading Dead Zones and Consequences for Marine Ecosystems. *Science*, *321*(5891), 926–929, https://doi.org/10.1126/science.1156401 https://www.science.org/doi/10.1126/science.1156401.

Dima, M., Felis, T., Lohmann, G., & Rimbu, N. (2005). Distinct modes of bidecadal and multidecadal variability in a climate reconstruction of the last centuries from a South Pacific coral. *Climate Dynamics*, *25*(2-3), 329–336, https://doi.org/10.1007/s00382-005-0043-2.

Dima, M. & Lohmann, G. (2007). A Hemispheric Mechanism for the Atlantic Multidecadal Oscillation. *Journal of Climate*, *20*(11), 2706–2719, https://doi.org/10.1175/JCLI4174.1 http://journals.ametsoc.org/doi/10.1175/JCLI4174.1.

Dima, M. & Lohmann, G. (2010). Evidence for two distinct modes of large-scale ocean circulation changes over the last century. *Journal of Climate*, *23*(1), 5–16, https://doi.org/10.1175/2009JCLI2867.1 https://journals.ametsoc.org/view/journals/clim/23/1/2009jcli2867.1.xml.

Dima, M., Lohmann, G., Ionita, M., Knorr, G., & Scholz, P. (2022). AMOC modes linked with distinct North Atlantic deep water formation sites. *Climate Dynamics*, *59*(3-4), 837–849, https://doi.org/10.1007/s00382-022-06156-w https://link.springer.com/article/10.1007/s00382-022-06156-w.

Dima, M., Nichita, D. R., Lohmann, G., Ionita, M., & Voiculescu, M. (2021). Early-onset of Atlantic Meridional Overturning Circulation weakening in response to atmospheric CO2 concentration. *npj Climate and Atmospheric*

Science, *4*(1), 27, https://doi.org/10.1038/s41612-021-00182-x http://www.nature.com/articles/s41612-021-00182-x.

Doney, S. C. (2010). The Growing Human Footprint on Coastal and Open-Ocean Biogeochemistry. *Science*, *328*(5985), 1512–1516, https://doi.org/10.1126/science.1185198 https://www.science.org/doi/10.1126/science.1185198.

Doney, S. C., Fabry, V. J., Feely, R. A., & Kleypas, J. A. (2009). Ocean Acidification: The Other CO2 Problem. *Annual Review of Marine Science*, *1*(1), 169–192, https://doi.org/10.1146/annurev.marine.010908.163834 https://www.annualreviews.org/doi/10.1146/annurev.marine.010908.163834.

Dowsett, H. J., Chandler, M. A., Cronin, T. M., & Dwyer, G. S. (2005). Middle Pliocene sea surface temperature variability. *Paleoceanography*, *20*(2), 1–8, https://doi.org/10.1029/2005PA001133 https://agupubs.onlinelibrary.wiley.com/doi/pdf/10.1029/2005PA001133.

Edwards, M., Beaugrand, G., Reid, P. C., Rowden, A. A., & Jones, M. B. (2002). Ocean climate anomalies and the ecology of the North Sea. *Marine Ecology Progress Series*, *239*, 1–10, https://doi.org/10.3354/meps239001.

Emile-Geay, J., et al. (2017). A global multiproxy database for temperature reconstructions of the Common Era. *Scientific Data*, *4*(1), 170088, https://doi.org/10.1038/sdata.2017.88 https://www.nature.com/articles/sdata201788.

Epplé, V. M., Brey, T., Witbaard, R., Kuhnert, H., & Pätzold, J. (2006). Sclerochronological records of Arctica islandica from the inner German Bight. *The Holocene*, *16*(5), 763–769, https://doi.org/10.1191/0959683606hl970rr http://journals.sagepub.com/doi/10.1191/0959683606hl970rr.

Esper, J., Cook, E. R., Krusic, P. J., Peters, K., & Schweingruber, F. H. (2003). Tests of the RCS method for preserving low-frequency variability in long tree-ring chronologies. *Tree-Ring Research*, *59*(2), 81–98 http://hdl.handle.net/10150/262573.

Estrella-Martínez, J., Schöne, B. R., Thurstan, R. H., Capuzzo, E., Scourse, J. D., & Butler, P. G. (2019). Reconstruction of Atlantic herring (Clupea harengus) recruitment in the North Sea for the past 455 years based on the δ 13 C from annual shell increments of the ocean quahog (Arctica islandica). *Fish and Fisheries*, *20*(3), 537–551, https://doi.org/10.1111/faf.12362 https://onlinelibrary.wiley.com/doi/10.1111/faf.12362.

Felis, T., Pätzold, J., Loya, Y., Fine, M., Nawar, A. H., & Wefer, G. (2000). A coral oxygen isotope record from the northern Red Sea documenting NAO, ENSO, and North Pacific teleconnections on Middle East climate variability since the year 1750. *Paleoceanography*, *15*(6), 679–694, https://doi.org/10.1029/1999PA000477 https://agupubs.onlinelibrary.wiley.com/doi/10.1029/1999PA000477.

Felis, T., Suzuki, A., Kuhnert, H., Dima, M., Lohmann, G., & Kawahata, H. (2009). Subtropical coral reveals abrupt early-twentieth-century freshening in the western North Pacific Ocean. *Geology*, *37*(6), 527–530, https://doi.org/10.1130/G25581A.1 http://pubs.geoscienceworld.org/geology/article/37/6/527/29975/Subtropical-coral-reveals-abrupt.

Felis, T., Suzuki, A., Kuhnert, H., Rimbu, N., & Kawahata, H. (2010). Pacific Decadal Oscillation documented in a coral record of North Pacific winter temperature since 1873. *Geophysical Research Letters*, *37*(14), n/a–n/a, https://doi.org/10.1029/2010GL043572 https://agupubs.onlinelibrary.wiley.com/doi/10.1029/2010GL043572.

Frank, D. & Esper, J. (2005). Characterization and climate response patterns of a high-elevation, multi-species tree-ring network in the European Alps. *Dendrochronologia*, *22*(2), 107–121, https://doi.org/10.1016/j.dendro.2005.02.004 https://linkinghub.elsevier.com/retrieve/pii/S1125786505000032.

Frieler, K., Meinshausen, M., Golly, A., Mengel, M., Lebek, K., Donner, S. D., & Hoegh-Guldberg, O. (2013). Limiting global warming to 2 °C is unlikely to save most coral reefs. *Nature Climate Change*, *3*(2), 165–170, https://doi.org/10.1038/nclimate1674 https://www.nature.com/articles/nclimate1674.

Frölicher, T. L., Fischer, E. M., & Gruber, N. (2018). Marine heatwaves under global warming. *Nature*, *560*(7718), 360–364, https://doi.org/10.1038/s41586-018-0383-9 https://www.nature.com/articles/s41586-018-0383-9.

Funder, S. & Weidick, A. (1991). Holocene boreal molluscs in Greenland - palaeoceanographic implications. *Palaeogeography, Palaeoclimatology, Palaeoecology*, *85*(1-2), 123–135, https://doi.org/10.1016/0031-0182(91)90029-Q.

Gazeau, F., et al. (2013). Impacts of ocean acidification on marine shelled molluscs. *Marine Biology*, *160*(8), 2207–2245, https://doi.org/10.1007/

s00227-013-2219-3 https://link.springer.com/article/10.1007/s00227-013-2219-3.

Gilbert, D., Rabalais, N. N., Díaz, R. J., & Zhang, J. (2010). Evidence for greater oxygen decline rates in the coastal ocean than in the open ocean. *Biogeosciences*, *7*(7), 2283–2296, https://doi.org/10.5194/bg-7-2283-2010 https://bg.copernicus.org/articles/7/2283/2010/.

Good, S. A., Martin, M. J., & Rayner, N. A. (2013). EN4: Quality controlled ocean temperature and salinity profiles and monthly objective analyses with uncertainty estimates. *Journal of Geophysical Research: Oceans*, *118*(12), 6704–6716, https://doi.org/10.1002/2013JC009067 https://agupubs.onlinelibrary.wiley.com/doi/10.1002/2013JC009067.

Goodkin, N. F., Hughen, K. A., Curry, W. B., Doney, S. C., & Ostermann, D. R. (2008). Sea surface temperature and salinity variability at Bermuda during the end of the Little Ice Age. *Paleoceanography*, *23*(3), n/a–n/a, https://doi.org/10.1029/2007PA001532 https://agupubs.onlinelibrary.wiley.com/doi/10.1029/2007PA001532.

Gove, J. M., et al. (2023). Coral reefs benefit from reduced land–sea impacts under ocean warming. *Nature*, *621*(7979), 536–542, https://doi.org/10.1038/s41586-023-06394-w https://www.nature.com/articles/s41586-023-06394-w.

Gray, S. T., Graumlich, L. J., Betancourt, J. L., & Pederson, G. T. (2004). A tree-ring based reconstruction of the Atlantic Multidecadal Oscillation since 1567 A.D. *Geophysical Research Letters*, *31*(12), https://doi.org/10.1029/2004GL019932 https://agupubs.onlinelibrary.wiley.com/doi/10.1029/2004GL019932.

Grissino-Mayer, H. (2001). Evaluating crossdating accuracy: A Manual and Tutotial for the computer program COFECHA. *Tree-Ring Research*, *57*(2), 205–221 https://repository.arizona.edu/handle/10150/251654.

Gruber, N. (2011). Warming up, turning sour, losing breath: ocean biogeochemistry under global change. *Philosophical Transactions of the Royal Society A: Mathematical, Physical and Engineering Sciences*, *369*(1943), 1980–1996, https://doi.org/10.1098/rsta.2011.0003 https://royalsocietypublishing.org/doi/10.1098/rsta.2011.0003.

Häkkinen, S., Rhines, P. B., & Worthen, D. L. (2011). Atmospheric Blocking and Atlantic Multidecadal Ocean Variability. *Science*, *334*(6056), 655–659,

https://doi.org/10.1126/science.1205683 https://www.science.org/doi/10.1126/science.1205683.

Halfar, J., Adey, W. H., Kronz, A., Hetzinger, S., Edinger, E., & Fitzhugh, W. W. (2013). Arctic sea-ice decline archived by multicentury annual-resolution record from crustose coralline algal proxy. *Proceedings of the National Academy of Sciences*, *110*(49), 19737–19741, https://doi.org/10.1073/pnas.1313775110 https://pnas.org/doi/full/10.1073/pnas.1313775110.

Halfar, J., et al. (2011). Coralline algal growth-increment widths archive North Atlantic climate variability. *Palaeogeography, Palaeoclimatology, Palaeoecology*, *302*(1-2), 71–80, https://doi.org/10.1016/j.palaeo.2010.04.009 https://linkinghub.elsevier.com/retrieve/pii/S003101821000218X.

Hanna, E., Cropper, T. E., Hall, R. J., & Cappelen, J. (2016). Greenland Blocking Index 1851–2015: a regional climate change signal. *International Journal of Climatology*, *36*(15), 4847–4861, https://doi.org/10.1002/joc.4673 https://rmets.onlinelibrary.wiley.com/doi/10.1002/joc.4673.

Hausfather, Z., Drake, H. F., Abbott, T., & Schmidt, G. A. (2020). Evaluating the Performance of Past Climate Model Projections. *Geophysical Research Letters*, *47*(1), e2019GL085378, https://doi.org/10.1029/2019GL085378 https://agupubs.onlinelibrary.wiley.com/doi/10.1029/2019GL085378.

Heinze, C., et al. (2021). The quiet crossing of ocean tipping points https://www.pnas.org/content/118/9/e2008478118https://www.pnas.org/content/118/9/e2008478118.abstract.

Hetzinger, S., et al. (2012). Marine proxy evidence linking decadal North Pacific and Atlantic climate. *Climate Dynamics*, *39*(6), 1447–1455, https://doi.org/10.1007/s00382-011-1229-4 https://link.springer.com/article/10.1007/s00382-011-1229-4.

Hetzinger, S., Pfeiffer, M., Dullo, W.-C., Garbe-Schönberg, D., & Halfar, J. (2010). Rapid 20th century warming in the Caribbean and impact of remote forcing on climate in the northern tropical Atlantic as recorded in a Guadeloupe coral. *Palaeogeography, Palaeoclimatology, Palaeoecology*, *296*(1-2), 111–124, https://doi.org/10.1016/j.palaeo.2010.06.019 https://linkinghub.elsevier.com/retrieve/pii/S0031018210003688.

Hiebenthal, C., Philipp, E., Eisenhauer, A., & Wahl, M. (2012). Interactive effects of temperature and salinity on shell formation and general condition

in Baltic Sea Mytilus edulis and Arctica islandica. *Aquatic Biology*, *14*(3), 289–298, https://doi.org/10.3354/ab00405.

Hilmer, M. & Jung, T. (2000). Evidence for a recent change in the link between the North Atlantic Oscillation and Arctic sea ice export. *Geophysical Research Letters*, *27*(7), 989–992, https://doi.org/10.1029/1999GL010944 https://agupubs.onlinelibrary.wiley.com/doi/10.1029/1999GL010944.

Höche, N., Walliser, E. O., de Winter, N. J., Witbaard, R., & Schöne, B. R. (2021). Temperature-induced microstructural changes in shells of laboratory-grown Arctica islandica (Bivalvia). *PLOS ONE*, *16*(2), e0247968, https://doi.org/10.1371/journal.pone.0247968 https://dx.plos.org/10.1371/journal.pone.0247968.

Höche, N., Walliser, E. O., & Schöne, B. R. (2022). Microstructural Mapping of Arctica islandica Shells Reveals Environmental and Physiological Controls on Biomineral Size. *Frontiers in Earth Science*, *9*, 1350, https://doi.org/10.3389/feart.2021.781305 https://www.frontiersin.org/articles/10.3389/feart.2021.781305/full.

Hodapp, D., et al. (2023). Climate change disrupts core habitats of marine species. *Global Change Biology*, *29*(12), 3304–3317, https://doi.org/10.1111/gcb.16612 https://onlinelibrary.wiley.com/doi/10.1111/gcb.16612.

Hofmann, J., et al. (2005). Catchment–coastal zone interaction based upon scenario and model analysis: Elbe and the German Bight case study. *Regional Environmental Change*, *5*(2-3), 54–81, https://doi.org/10.1007/s10113-004-0082-y http://link.springer.com/10.1007/s10113-004-0082-y.

Holland, H. A., Schöne, B. R., Lipowsky, C., & Esper, J. (2014). Decadal climate variability of the North Sea during the last millennium reconstructed from bivalve shells (Arctica islandica). *The Holocene*, *24*(7), 771–786, https://doi.org/10.1177/0959683614530438 http://journals.sagepub.com/doi/10.1177/0959683614530438.

Huang, B., et al. (2017). Extended Reconstructed Sea Surface Temperature, Version 5 (ERSSTv5): Upgrades, Validations, and Intercomparisons. *Journal of Climate*, *30*(20), 8179–8205, https://doi.org/10.1175/JCLI-D-16-0836.1 http://journals.ametsoc.org/doi/10.1175/JCLI-D-16-0836.1.

Huo, W., Drews, A., Martin, T., & Wahl, S. (2024). Impacts of North Atlantic Model Biases on Natural Decadal Climate Variability. *Journal of Geophysical*

Research: Atmospheres, *129*(4), https://doi.org/10.1029/2023JD039778 https://agupubs.onlinelibrary.wiley.com/doi/10.1029/2023JD039778.

Hurrell, J. W. (1995). Decadal Trends in the North Atlantic Oscillation: Regional Temperatures and Precipitation. *Science*, *269*(5224), 676–679, https://doi.org/10.1126/science.269.5224.676 https://www.science.org/doi/10.1126/science.269.5224.676.

Hurrell, J. W. & Deser, C. (2010). North Atlantic climate variability: The role of the North Atlantic Oscillation. *Journal of Marine Systems*, *79*(3-4), 231–244, https://doi.org/10.1016/j.jmarsys.2009.11.002 https://linkinghub.elsevier.com/retrieve/pii/S0924796309003224.

Ionita, M. (2014). The Impact of the East Atlantic/Western Russia Pattern on the Hydroclimatology of Europe from Mid-Winter to Late Spring. *Climate*, *2*(4), 296–309, https://doi.org/10.3390/cli2040296 https://www.mdpi.com/2225-1154/2/4/296.

Ionita, M., Boroneanț, C., & Chelcea, S. (2015). Seasonal modes of dryness and wetness variability over Europe and their connections with large scale atmospheric circulation and global sea surface temperature. *Climate Dynamics*, *45*(9-10), 2803–2829, https://doi.org/10.1007/s00382-015-2508-2 http://link.springer.com/10.1007/s00382-015-2508-2.

Ionita, M., Dima, M., Nagavciuc, V., Scholz, P., & Lohmann, G. (2021). Past megadroughts in central Europe were longer, more severe and less warm than modern droughts. *Communications Earth & Environment*, *2*(1), 61, https://doi.org/10.1038/s43247-021-00130-w https://www.nature.com/articles/s43247-021-00130-w.

Ionita, M., Lohmann, G., Rimbu, N., & Wiltshire, K. (2008). The influence of large-scale atmospheric circulation on the variability of salinity at Helgoland Roads station. *Tellus A: Dynamic Meteorology and Oceanography*, *60*(5), 1103, https://doi.org/10.1111/j.1600-0870.2008.00352.x https://www.tandfonline.com/doi/abs/10.1111/j.1600-0870.2008.00352.x.

Ionita, M., Nagavciuc, V., & Guan, B. (2020a). Rivers in the sky, flooding on the ground: the role of atmospheric rivers in inland flooding in central Europe. *Hydrology and Earth System Sciences*, *24*(11), 5125–5147, https://doi.org/10.5194/hess-24-5125-2020 https://hess.copernicus.org/articles/24/5125/2020/.

Ionita, M., Nagavciuc, V., Kumar, R., & Rakovec, O. (2020b). On the curious case of the recent decade, mid-spring precipitation deficit in central Europe. *npj Climate and Atmospheric Science*, *3*(1), 49, https://doi.org/10.1038/s41612-020-00153-8 https://www.nature.com/articles/s41612-020-00153-8.

Isachenko, A. I., Tsetlin, A. B., & Mokievskii, V. O. (2013). The structure and long-term dynamics of the communities of Arctica islandica (Bivalvia) in Rugozerskaya Guba of the White Sea. *Biology Bulletin*, *40*(8), 654–663, https://doi.org/10.1134/S1062359013080074 https://link.springer.com/article/10.1134/S1062359013080074.

Ivany, L. C., Wilkinson, B. H., Lohmann, K. C., Johnson, E. R., McElroy, B. J., & Cohen, G. J. (2004). Intra-Annual Isotopic Variation in Venericardia Bivalves: Implications for Early Eocene Temperature, Seasonality, and Salinity on the U.S. Gulf Coast. *Journal of Sedimentary Research*, *74*(1), 7–19, https://doi.org/10.1306/052803740007 https://pubs.geoscienceworld.org/jsedres/article/74/1/7-19/114172.

Jain, S., et al. (2023). Importance of internal variability for climate model assessment. *npj Climate and Atmospheric Science*, *6*(1), 68, https://doi.org/10.1038/s41612-023-00389-0 https://www.nature.com/articles/s41612-023-00389-0.

Johnstone, J. A. & Mantua, N. J. (2014). Atmospheric controls on northeast Pacific temperature variability and change, 1900–2012. *Proceedings of the National Academy of Sciences*, *111*(40), 14360–14365, https://doi.org/10.1073/pnas.1318371111 https://pnas.org/doi/full/10.1073/pnas.1318371111.

Jolliffe, I. (2005). Principal Component Analysis. In B. Everitt & D. Howell (Eds.), *Encyclopedia of Statistics in Behavioral Science*. Wiley https://onlinelibrary.wiley.com/doi/10.1002/0470013192.bsa501.

Jones, C. D. & Cox, P. M. (2001). Constraints on the temperature sensitivity of global soil respiration from the observed interannual variability in atmospheric CO 2. *Atmospheric Science Letters*, *2*(1-4), 166–172, https://doi.org/10.1006/asle.2001.0044 https://rmets.onlinelibrary.wiley.com/doi/10.1006/asle.2001.0044.

Jones, P. D., Jonsson, T., & Wheeler, D. (1997). Extension to the North Atlantic oscillation using early instrumental pressure observations from Gibraltar and south-west Iceland. *International*

Journal of Climatology, *17*(13), 1433–1450, https://doi.org/10.1002/(SICI)1097-0088(19971115)17:13<1433::AID-JOC203>3.3.CO;2-G http://doi.wiley.com/10.1002/{%}28SICI{%}291097-0088{%}2819971115{%}2917{%}3A13{%}3C1433{%}3A{%}3AAID-JOC203{%}3E3.3.CO{%}3B2-G.

Jouzel, J., et al. (2007). Orbital and Millennial Antarctic Climate Variability over the Past 800,000 Years. *Science*, *317*(5839), 793–796, https://doi.org/10.1126/science.1141038 https://www.science.org/doi/10.1126/science.1141038.

Karmouche, S., Galytska, E., Runge, J., Meehl, G. A., Phillips, A. S., Weigel, K., & Eyring, V. (2023). Regime-oriented causal model evaluation of Atlantic–Pacific teleconnections in CMIP6. *Earth System Dynamics*, *14*(2), 309–344, https://doi.org/10.5194/esd-14-309-2023 https://doi.org/10.5194/esd-14-309-2023https://esd.copernicus.org/articles/14/309/2023/.

Kautz, L. A., Martius, O., Pfahl, S., Pinto, J. G., Ramos, A. M., Sousa, P. M., & Woollings, T. (2022). Atmospheric blocking and weather extremes over the Euro-Atlantic sector - A review https://wcd.copernicus.org/articles/3/305/2022/.

Kim, J.-H., Schouten, S., Hopmans, E. C., Donner, B., & Sinninghe Damsté, J. S. (2008). Global sediment core-top calibration of the TEX86 paleothermometer in the ocean. *Geochimica et Cosmochimica Acta*, *72*(4), 1154–1173, https://doi.org/10.1016/j.gca.2007.12.010 https://linkinghub.elsevier.com/retrieve/pii/S0016703707007132.

Klippel, L., Krusic, P. J., Konter, O., St. George, S., Trouet, V., & Esper, J. (2019). A 1200+ year reconstruction of temperature extremes for the northeastern Mediterranean region. *International Journal of Climatology*, *39*(4), 2336–2350, https://doi.org/10.1002/joc.5955 https://rmets.onlinelibrary.wiley.com/doi/10.1002/joc.5955.

Knight, J. R., Allan, R. J., Folland, C. K., Vellinga, M., & Mann, M. E. (2005). A signature of persistent natural thermohaline circulation cycles in observed climate. *Geophysical Research Letters*, *32*(20), 1–4, https://doi.org/10.1029/2005GL024233 https://agupubs.onlinelibrary.wiley.com/doi/10.1029/2005GL024233.

Knudsen, M. F., Seidenkrantz, M.-S., Jacobsen, B. H., & Kuijpers, A. (2011). Tracking the Atlantic Multidecadal Oscillation through the last 8,000 years.

Nature Communications, *2*(1), 178, https://doi.org/10.1038/ncomms1186 https://www.nature.com/articles/ncomms1186.

Kobashi, T. & Grossman, E. L. (2003). The oxygen isotopic record of seasonality in Conus shells and its application to understanding late middle Eocene (38 Ma) climate. *Paleontological Research*, *7*(4), 343–355, https://doi.org/10.2517/prpsj.7.343 http://www.bioone.org/doi/abs/10.2517/prpsj.7.343.

Komagoe, T., Watanabe, T., Shirai, K., Yamazaki, A., & Uematu, M. (2018). Geochemical and Microstructural Signals in Giant Clam Tridacna maxima Recorded Typhoon Events at Okinotori Island, Japan. *Journal of Geophysical Research: Biogeosciences*, *123*(5), 1460–1474, https://doi.org/10.1029/2017JG004082 https://agupubs.onlinelibrary.wiley.com/doi/10.1029/2017JG004082.

Latif, M. & Barnett, T. P. (1994). Causes of Decadal Climate Variability over the North Pacific and North America. *Science*, *266*(5185), 634–637, https://doi.org/10.1126/science.266.5185.634 https://www.science.org/doi/10.1126/science.266.5185.634.

Lear, C. H., Elderfield, H., & Wilson, P. A. (2000). Cenozoic Deep-Sea Temperatures and Global Ice Volumes from Mg/Ca in Benthic Foraminiferal Calcite. *Science*, *287*(5451), 269–272, https://doi.org/10.1126/science.287.5451.269 https://www.science.org/doi/10.1126/science.287.5451.269.

Lejenäs, H. & Økland, H. (1983). Characteristics of northern hemisphere blocking as determined from a long time series of observational data. *Tellus A*, *35A*(5), 350–362, https://doi.org/10.1111/j.1600-0870.1983.tb00210.x http://tellusa.net/index.php/tellusa/article/view/11446.

Leutert, T. J., Auderset, A., Martínez-García, A., Modestou, S., & Meckler, A. N. (2020). Coupled Southern Ocean cooling and Antarctic ice sheet expansion during the middle Miocene. *Nature Geoscience*, *13*(9), 634–639, https://doi.org/10.1038/s41561-020-0623-0 https://www.nature.com/articles/s41561-020-0623-0.

Li, S., Liu, C., Huang, J., Liu, Y., Zheng, G., Xie, L., & Zhang, R. (2015). Interactive effects of seawater acidification and elevated temperature on biomineralization and amino acid metabolism in the mussel Mytilus edulis. *Journal of Experimental Biology*, *218*(22), 3623–3631, https://doi.org/

10.1242/jeb.126748 https://journals.biologists.com/jeb/article/doi/10.1242/jeb.126748/262031/Interactive-effects-of-seawater-acidification-and.

Linnaeus, C. (1758). *Systema Naturae per regna tria naturae, secundum classes, ordines, genera, species, cum characteribus, differentiis, synonymis, locis*. Editio decima, reformata [10th revised edition], vol. 1: 824 pp. Laurentius Salvius: Holmiae.

Linnaeus, C. (1767). *Systema naturae per regna tria naturae, secundum classes, ordines, genera, species, cum characteribus, differentiis, synonymis, locis*. Editio duodecima. 1. Regnum Animale. 1 & 2. Holmiae [Stockholm], Laurentii Salvii 1:532.

Lisiecki, L. E. & Raymo, M. E. (2005). A Pliocene-Pleistocene stack of 57 globally distributed benthic δ 18 O records. *Paleoceanography*, *20*(1), 1–17, https://doi.org/10.1029/2004PA001071 https://agupubs.onlinelibrary.wiley.com/doi/10.1029/2004PA001071.

Liu, Y.-W., Wanamaker Jr., A. D., Aciego, S. M., Searles, I., Hangstad, T. A., Chierici, M., & Carroll, M. L. (2023). Resistant calcification responses of Arctica islandica clams under ocean acidification conditions. *Journal of Experimental Marine Biology and Ecology*, *560*, 151855, https://doi.org/10.1016/j.jembe.2022.151855 https://linkinghub.elsevier.com/retrieve/pii/S0022098122001630.

Lohmann, G. & Schöne, B. R. (2013). Climate signatures on decadal to interdecadal time scales as obtained from mollusk shells (Arctica islandica) from Iceland. *Palaeogeography, Palaeoclimatology, Palaeoecology*, *373*, 152–162, https://doi.org/10.1016/j.palaeo.2012.08.006 https://linkinghub.elsevier.com/retrieve/pii/S0031018212004580.

Lohmann, G. & Wiltshire, K. H. (2012). Winter atmospheric circulation signature for the timing of the spring bloom of diatoms in the North Sea. *Marine Biology*, *159*(11), 2573–2581, https://doi.org/10.1007/s00227-012-1993-7 http://link.springer.com/10.1007/s00227-012-1993-7.

Lutz, R. A., Mann, R., Goodsell, J. G., & Castagna, M. (1982). Larval and Early Post-Larval Development of Arctica Islandica. *Journal of the Marine Biological Association of the United Kingdom*, *62*(4), 745–769, https://doi.org/10.1017/S0025315400070314 https://www.cambridge.org/core/product/identifier/S0025315400070314/type/journal{_}article.

Mangerud, J. & Svendsen, J. I. (2018). The Holocene Thermal Maximum around Svalbard, Arctic North Atlantic; molluscs show early and exceptional warmth. *Holocene*, *28*(1), 65–83, https://doi.org/10.1177/0959683617715701 http://journals.sagepub.com/doi/10.1177/0959683617715701.

Mann, M. E., Steinman, B. A., Brouillette, D. J., & Miller, S. K. (2021). Multidecadal climate oscillations during the past millennium driven by volcanic forcing. *Science*, *371*(6533), 1014–1019, https://doi.org/10.1126/science.abc5810 https://www.science.org/doi/10.1126/science.abc5810.

Mann, M. E., Steinman, B. A., & Miller, S. K. (2020). Absence of internal multidecadal and interdecadal oscillations in climate model simulations. *Nature Communications*, *11*(1), 49, https://doi.org/10.1038/s41467-019-13823-w https://www.nature.com/articles/s41467-019-13823-w.

Mann, M. E., et al. (2009). Global Signatures and Dynamical Origins of the Little Ice Age and Medieval Climate Anomaly. *Science*, *326*(5957), 1256–1260, https://doi.org/10.1126/science.1177303 https://www.science.org/doi/10.1126/science.1177303.

Mann, R. & Wolf, C. (1983). Swimming behaviour of larvae of the ocean quahog Arctica islandica in response to pressure and temperature. *Marine Ecology Progress Series*, *13*, 211–218, https://doi.org/10.3354/meps013211 http://www.int-res.com/articles/meps/13/m013p211.pdf.

Mantua, N. J., Hare, S. R., Zhang, Y., Wallace, J. M., & Francis, R. C. (1997). A Pacific Interdecadal Climate Oscillation with Impacts on Salmon Production*. *Bulletin of the American Meteorological Society*, *78*(6), 1069–1080, https://doi.org/https://doi.org/10.1175/1520-0477(1997)078<1069:APICOW>2.0.CO;2 https://journals.ametsoc.org/view/journals/bams/78/6/1520-0477{_}1997{_}078{_}1069{_}apicow{_}2{_}0{_}co{_}2.xml.

Marali, S. & Schöne, B. R. (2015). Oceanographic control on shell growth of Arctica islandica (Bivalvia) in surface waters of Northeast Iceland — Implications for paleoclimate reconstructions. *Palaeogeography, Palaeoclimatology, Palaeoecology*, *420*, 138–149, https://doi.org/10.1016/j.palaeo.2014.12.016 https://linkinghub.elsevier.com/retrieve/pii/S0031018214006117.

Marchitto, T. M., Jones, G. A., Goodfriend, G. A., & Weidman, C. R. (2000). Precise Temporal Correlation of Holocene Mollusk Shells Using Sclerochronology. *Quaternary Research*, *53*(2), 236–246, https://doi.org/10.1006/

qres.1999.2107 https://www.cambridge.org/core/product/identifier/S0033589400030702/type/journal{_}article.

Marin, F. (2012). The formation and mineralization of mollusk shell. *Frontiers in Bioscience*, *S4*(3), 321, https://doi.org/10.2741/s321 https://imrpress.com/journal/FBS/4/3/10.2741/S321.

Masson-Delmotte, V., et al. (2013). Information from paleoclimate archives. In T. Stocker, D. Qin, G. Plattner, M. Tignor, S. Allen, J. Boschung, A. Nauels, Y. Xia, V. Bex, & P. Midgley (Eds.), *Climate change 2013: the physical science basis. Contribution of working group I to the fifth assessment report of the intergovernmental panel on climate change* (pp. 383–464). Cambridge: Cambridge University Press.

Mette, M., Andersson, C., Schöne, B., Bonitz, F., Melvik, V., Trofimova, T., & Miles, M. (2023). Two centuries of southwest Iceland annually-resolved marine temperature reconstructed from Arctica islandica shells. *Estuarine, Coastal and Shelf Science*, *294*, 108525, https://doi.org/10.1016/j.ecss.2023.108525 https://linkinghub.elsevier.com/retrieve/pii/S0272771423003153.

Mette, M. J., Wanamaker, A. D., Carroll, M. L., Ambrose, W. G., & Retelle, M. J. (2016). Linking large-scale climate variability with Arctica islandica shell growth and geochemistry in northern Norway. *Limnology and Oceanography*, *61*(2), 748–764, https://doi.org/10.1002/lno.10252 https://aslopubs.onlinelibrary.wiley.com/doi/pdf/10.1002/lno.10252http://doi.wiley.com/10.1002/lno.10252.

Mette, M. J., Wanamaker, A. D., Retelle, M. J., Carroll, M. L., Andersson, C., & Ambrose, W. G. (2021). Persistent Multidecadal Variability Since the 15th Century in the Southern Barents Sea Derived From Annually Resolved Shell-Based Records. *Journal of Geophysical Research: Oceans*, *126*(6), 1–22, https://doi.org/10.1029/2020JC017074.

Milano, S., Nehrke, G., Wanamaker Jr., A. D., Ballesta-Artero, I., Brey, T., & Schöne, B. R. (2017). The effects of environment on Arctica islandica shell formation and architecture. *Biogeosciences*, *14*(6), 1577–1591, https://doi.org/10.5194/bg-14-1577-2017 https://bg.copernicus.org/articles/14/1577/2017/.

Miller, G. H. & Brigham-Grette, J. (1989). Amino acid geochronology: Resolution and precision in carbonate fossils. *Quaternary International*, *1*(C),

111–128, https://doi.org/10.1016/1040-6182(89)90011-6 https://linkinghub.elsevier.com/retrieve/pii/1040618289900116.

Mills, K., et al. (2013). Fisheries Management in a Changing Climate: Lessons From the 2012 Ocean Heat Wave in the Northwest Atlantic. *Oceanography*, *26*(2), https://doi.org/10.5670/oceanog.2013.27 https://tos.org/oceanography/article/fisheries-management-in-a-changing-climate-lessonsfrom-the-2012-ocean-heat-.

Minobe, S. (1997). A 50–70 year climatic oscillation over the North Pacific and North America. *Geophysical Research Letters*, *24*(6), 683–686, https://doi.org/10.1029/97GL00504 https://agupubs.onlinelibrary.wiley.com/doi/10.1029/97GL00504.

Moore, G. W. K., Halfar, J., Majeed, H., Adey, W., & Kronz, A. (2017). Amplification of the Atlantic Multidecadal Oscillation associated with the onset of the industrial-era warming. *Scientific Reports*, *7*(1), 40861, https://doi.org/10.1038/srep40861 https://www.nature.com/articles/srep40861.

Moore, G. W. K. & Renfrew, I. A. (2012). Cold European winters: interplay between the NAO and the East Atlantic mode. *Atmospheric Science Letters*, *13*(1), 1–8, https://doi.org/10.1002/asl.356 https://rmets.onlinelibrary.wiley.com/doi/10.1002/asl.356.

Morton, B. (2011). The biology and functional morphology of Arctica islandica (Bivalvia: Arcticidae) – A gerontophilic living fossil. *Marine Biology Research*, *7*(6), 540–553, https://doi.org/10.1080/17451000.2010.535833 https://www.tandfonline.com/doi/full/10.1080/17451000.2010.535833.

Nicol, D. (1951). Recent species of the veneroid pelecypod Arctica. *Journal of the Washington Academy of Sciences*, *41*(3), 102–106 http://www.jstor.org/stable/24533597.

North, G. R., Bell, T. L., Cahalan, R. F., & Moeng, F. J. (1982). Sampling Errors in the Estimation of Empirical Orthogonal Functions. *Monthly Weather Review*, *110*(7), 699–706, https://doi.org/10.1175/1520-0493(1982)110<0699:SEITEO>2.0.CO;2 http://journals.ametsoc.org/doi/10.1175/1520-0493(1982)110{%}3C0699:SEITEO{%}3E2.0.CO;2.

Oliver, E. C., et al. (2018). Longer and more frequent marine heatwaves over the past century. *Nature Communications*, *9*(1), 1–12, https://doi.org/10.1038/s41467-018-03732-9 https://www.nature.com/articles/s41467-018-03732-9.

Pearson, P. N., van Dongen, B. E., Nicholas, C. J., Pancost, R. D., Schouten, S., Singano, J. M., & Wade, B. S. (2007). Stable warm tropical climate through the Eocene Epoch. *Geology*, *35*(3), 211, https://doi.org/10.1130/G23175A.1 https://pubs.geoscienceworld.org/geology/article/35/3/211-214/129773.

Peharda, M., Vilibić, I., Black, B., Uvanović, H., Markulin, K., & Mihanović, H. (2019). A network of bivalve chronologies from semi-enclosed seas. *PLOS ONE*, *14*(7), e0220520, https://doi.org/10.1371/journal.pone.0220520 https://dx.plos.org/10.1371/journal.pone.0220520.

Perkins, S. E., Alexander, L. V., & Nairn, J. R. (2012). Increasing frequency, intensity and duration of observed global heatwaves and warm spells. *Geophysical Research Letters*, *39*(20), L20714, https://doi.org/10.1029/2012GL053361 https://agupubs.onlinelibrary.wiley.com/doi/10.1029/2012GL053361.

Piermattei, A., et al. (2017). Potential and limitation of combining terrestrial and marine growth records from Iceland. *Global and Planetary Change*, *155*, 213–224, https://doi.org/10.1016/j.gloplacha.2017.07.010 https://linkinghub.elsevier.com/retrieve/pii/S0921818117301510.

Poitevin, P., et al. (2019). Growth Response of Arctica Islandica to North Atlantic Oceanographic Conditions Since 1850. *Frontiers in Marine Science*, *6*(JUL), 483, https://doi.org/10.3389/fmars.2019.00483 https://www.frontiersin.org/article/10.3389/fmars.2019.00483/full.

Pozo-Vázquez, D., Esteban-Parra, M. J., Rodrigo, F. S., & Castro-Díez, Y. (2001). A study of NAO variability and its possible non-linear influences on European surface temperature. *Climate Dynamics*, *17*(9), 701–715, https://doi.org/10.1007/s003820000137 http://link.springer.com/10.1007/s003820000137.

Raffi, S. (1986). The significance of marine boreal molluscs in the Early Pleistocene faunas of the Mediterranean area. *Palaeogeography, Palaeoclimatology, Palaeoecology*, *52*(3-4), 267–289, https://doi.org/10.1016/0031-0182(86)90051-9 https://linkinghub.elsevier.com/retrieve/pii/0031018286900519.

Ragnarsson, S. Á., Thorarinsdóttir, G. G., & Gunnarsson, K. (2015). Short and long-term effects of hydraulic dredging on benthic communities and

ocean quahog (Arctica islandica) populations. *Marine Environmental Research*, *109*, 113–123, https://doi.org/10.1016/j.marenvres.2015.05.003 https://linkinghub.elsevier.com/retrieve/pii/S0141113615000707.

Rahmstorf, S., Box, J. E., Feulner, G., Mann, M. E., Robinson, A., Rutherford, S., & Schaffernicht, E. J. (2015). Exceptional twentieth-century slowdown in Atlantic Ocean overturning circulation. *Nature Climate Change*, *5*(5), 475–480, https://doi.org/10.1038/nclimate2554 https://www.nature.com/articles/nclimate2554.

Rayner, N. A., et al. (2003). Global analyses of sea surface temperature, sea ice, and night marine air temperature since the late nineteenth century. *Journal of Geophysical Research*, *108*(D14), 4407, https://doi.org/10.1029/2002JD002670 http://doi.wiley.com/10.1029/2002JD002670.

Reid, P. C., De Fatima Borges, M., & Svendsen, E. (2001). A regime shift in the north sea circa 1988 linked to changes in the north sea horse mackerel fishery. *Fisheries Research*, *50*(1-2), 163–171, https://doi.org/10.1016/S0165-7836(00)00249-6.

Reid, P. C. & Edwards, M. (2001). Long-term changes in the pelagos, benthos and fisheries of the North Sea. *Senckenbergiana maritima*, *31*(2), 107–115, https://doi.org/10.1007/BF03043021 http://link.springer.com/10.1007/BF03043021.

Rex, D. F. (1951). The Effect of Atlantic Blocking Action upon European Climate. *Tellus*, *3*(2), 100–112, https://doi.org/10.3402/tellusa.v3i2.8617.

Reynolds, D., et al. (2013). A multiproxy reconstruction of Hebridean (NW Scotland) spring sea surface temperatures between AD 1805 and 2010. *Palaeogeography, Palaeoclimatology, Palaeoecology*, *386*, 275–285, https://doi.org/10.1016/j.palaeo.2013.05.029 https://linkinghub.elsevier.com/retrieve/pii/S003101821300271X.

Reynolds, D. J., et al. (2018). Isolating and Reconstructing Key Components of North Atlantic Ocean Variability From a Sclerochronological Spatial Network. *Paleoceanography and Paleoclimatology*, *33*(10), 1086–1098, https://doi.org/10.1029/2018PA003366 https://agupubs.onlinelibrary.wiley.com/doi/10.1029/2018PA003366.

Reynolds, D. J., Hall, I. R., Slater, S. M., Scourse, J. D., Halloran, P. R., & Sayer, M. D. J. (2017). Reconstructing Past Seasonal to

Multicentennial-Scale Variability in the NE Atlantic Ocean Using the Long-Lived Marine Bivalve Mollusk Glycymeris glycymeris. *Paleoceanography*, *32*(11), 1153–1173, https://doi.org/10.1002/2017PA003154 https://agupubs.onlinelibrary.wiley.com/doi/10.1002/2017PA003154.

Reynolds, D. J., von Biela, V. R., Dunton, K. H., Douglas, D. C., & Black, B. A. (2022). Sclerochronological records of environmental variability and bivalve growth in the Pacific Arctic. *Progress in Oceanography*, *206*, 102864, https://doi.org/10.1016/j.pocean.2022.102864.

Rimbu, N. & Lohmann, G. (2011). Winter and summer blocking variability in the North Atlantic region - Evidence from long-term observational and proxy data from southwestern Greenland. *Climate of the Past*, *7*(2), 543–555, https://doi.org/10.5194/cp-7-543-2011.

Rimbu, N., Lohmann, G., Felis, T., & Pätzold, J. (2001). Arctic Oscillation signature in a Red Sea coral. *Geophysical Research Letters*, *28*(15), 2959–2962, https://doi.org/10.1029/2001GL013083 https://agupubs.onlinelibrary.wiley.com/doi/10.1029/2001GL013083.

Rimbu, N., Lohmann, G., Felis, T., & Pätzold, J. (2003). Shift in ENSO Teleconnections Recorded by a Northern Red Sea Coral. *Journal of Climate*, *16*(9), 1414–1422, https://doi.org/10.1175/1520-0442-16.9.1414 http://journals.ametsoc.org/doi/10.1175/1520-0442-16.9.1414.

Rimbu, N., Lohmann, G., & Ionita, M. (2014). Interannual to multidecadal Euro-Atlantic blocking variability during winter and its relationship with extreme low temperatures in Europe. *Journal of Geophysical Research: Atmospheres*, *119*(24), 13,621–13,636, https://doi.org/10.1002/2014JD021983 https://agupubs.onlinelibrary.wiley.com/doi/10.1002/2014JD021983.

Rodriguez-Ruano, V., Toth, L. T., Enochs, I. C., Randall, C. J., & Aronson, R. B. (2023). Upwelling, climate change, and the shifting geography of coral reef development. *Scientific Reports*, *13*(1), 1–15, https://doi.org/10.1038/s41598-023-28489-0 https://www.nature.com/articles/s41598-023-28489-0.

Ropes, J. (1984). Procedures for preparing acetate peels and evidence validating the annual periodicity of growth lines formed in the shells of ocean quahogs, Arctica islandica. *Marine Fisheries Review*, *46*(2), 27–35 http://spo.nmfs.noaa.gov/mfr462/mfr4623.pdf.

Ropes, J. W., Jones, D. S., Murawski, S. A., Serchuk, F. M., & Jearld, A. J. (1982). Documentation af annual growth lines in ocean quahogs; Arctica islandica. *Fishery Bulletin*, *82*(1), 1–19 https://digitalcommons.usf.edu/msc{_}facpub/2170.

Sabine, C. L., et al. (2004). The Oceanic Sink for Anthropogenic CO2. *Science*, *305*(5682), 367–371, https://doi.org/10.1126/science.1097403 https://www.science.org/doi/10.1126/science.1097403.

Saleuddin, A. S. M. & Wilbur, K. M. (1983). *The mollusca. Volume 4, Physiology. Part 1 / edited by A.S.M. Saleuddin, Karl M. Wilbur.* New York;: Academic Press.

Savitzky, A. & Golay, M. J. E. (1964). Smoothing and Differentiation of Data by Simplified Least Squares Procedures. *Analytical Chemistry*, *36*(8), 1627–1639, https://doi.org/10.1021/ac60214a047 https://pubs.acs.org/sharingguidelineshttps://pubs.acs.org/doi/abs/10.1021/ac60214a047.

Scherrer, S. C., Croci-Maspoli, M., Schwierz, C., & Appenzeller, C. (2006). Two-dimensional indices of atmospheric blocking and their statistical relationship with winter climate patterns in the Euro-Atlantic region. *International Journal of Climatology*, *26*(2), 233–249, https://doi.org/10.1002/joc.1250 https://onlinelibrary.wiley.com/doi/10.1002/joc.1250.

Schlesinger, M. E. & Ramankutty, N. (1994). An oscillation in the global climate system of period 65–70 years. *Nature*, *367*(6465), 723–726, https://doi.org/10.1038/367723a0 https://doi.org/10.1038/367723a0https://www.nature.com/articles/367723a0.

Schlüter, M. H., Merico, A., Wiltshire, K. H., Greve, W., & von Storch, H. (2008). A statistical analysis of climate variability and ecosystem response in the German Bight. *Ocean Dynamics*, *58*(3-4), 169–186, https://doi.org/10.1007/s10236-008-0146-5 http://link.springer.com/10.1007/s10236-008-0146-5.

Schober, P., Boer, C., & Schwarte, L. A. (2018). Correlation Coefficients: Appropriate Use and Interpretation. *Anesthesia & Analgesia*, *126*(5), 1763–1768, https://doi.org/10.1213/ANE.0000000000002864 https://journals.lww.com/00000539-201805000-00050.

Schöne, B. R. (2008). The curse of physiology—challenges and opportunities in the interpretation of geochemical data from mollusk shells. *Geo-*

Marine Letters, *28*(5-6), 269–285, https://doi.org/https://doi.org/10.1007/s00367-008-0114-6 http://link.springer.com/10.1007/s00367-008-0114-6.

Schöne, B. R. (2013). Arctica islandica (Bivalvia): A unique paleoenvironmental archive of the northern North Atlantic Ocean. *Global and Planetary Change*, *111*, 199–225, https://doi.org/10.1016/j.gloplacha.2013.09.013 https://linkinghub.elsevier.com/retrieve/pii/S0921818113002130.

Schöne, B. R., Dunca, E., Fiebig, J., & Pfeiffer, M. (2005a). Mutvei's solution: An ideal agent for resolving microgrowth structures of biogenic carbonates. *Palaeogeography, Palaeoclimatology, Palaeoecology*, *228*(1-2), 149–166, https://doi.org/10.1016/j.palaeo.2005.03.054 https://linkinghub.elsevier.com/retrieve/pii/S0031018205002804.

Schöne, B. R., et al. (2005b). Climate records from a bivalved Methuselah (Arctica islandica, Mollusca; Iceland). *Palaeogeography, Palaeoclimatology, Palaeoecology*, *228*(1-2), 130–148, https://doi.org/10.1016/j.palaeo.2005.03.049 https://www.sciencedirect.com/science/article/pii/S0031018205002695https://linkinghub.elsevier.com/retrieve/pii/S0031018205002695.

Schöne, B. R., et al. (2005c). Daily Growth Rates in Shells of Arctica islandica: Assessing Sub-seasonal Environmental Controls on a Long-lived Bivalve Mollusk. *PALAIOS*, *20*(1), 78–92, https://doi.org/10.2110/palo.2003.p03-101 https://pubs.geoscienceworld.org/palaios/article/20/1/78-92/100035.

Schöne, B. R., Kröncke, I., Houk, S. D., Freyre Castro, A. D., & Oschmann, W. (2003a). The Cornucopia of chilly winters: Ocean Quahog (Arctica islandica L., Mollusca) master chronology reveals bottom water nutrient enrichment during colder winters (North Sea). *Senckenbergiana Maritima*, *32*(1-2), 165–175, https://doi.org/10.1007/BF03043092 https://link.springer.com/article/10.1007/BF03043092http://link.springer.com/10.1007/BF03043092.

Schöne, B. R., et al. (2003b). North Atlantic Oscillation dynamics recorded in shells of a long-lived bivalve mollusk. *Geology*, *31*(12), 1037, https://doi.org/10.1130/G20013.1 https://pubs.geoscienceworld.org/geology/article/31/12/1037-1040/29166.

Schöne, B. R., Pfeiffer, M., Pohlmann, T., & Siegismund, F. (2005d). A seasonally resolved bottom-water temperature record for the period AD 1866–2002

based on shells of Arctica islandica (Mollusca, North Sea). *International Journal of Climatology*, *25*(7), 947–962, https://doi.org/10.1002/joc.1174 https://rmets.onlinelibrary.wiley.com/doi/10.1002/joc.1174.

Schrum, C. (1997). Thermohaline stratification and instabilities at tidal mixing fronts: Results of an eddy resolving model for the German Bight. *Continental Shelf Research*, *17*(6), 689–716, https://doi.org/10.1016/S0278-4343(96)00051-9.

Scourse, J., et al. (2006). First cross-matched floating chronology from the marine fossil record: data from growth lines of the long-lived bivalve mollusc Arctica islandica. *The Holocene*, *16*(7), 967–974, https://doi.org/10.1177/0959683606hl987rp http://journals.sagepub.com/doi/10.1177/0959683606hl987rp.

Slivinski, L. C., et al. (2019). Towards a more reliable historical reanalysis: Improvements for version 3 of the Twentieth Century Reanalysis system. *Quarterly Journal of the Royal Meteorological Society*, *145*(724), 2876–2908, https://doi.org/10.1002/qj.3598 https://doi.org/10.1002/qj.3598https://onlinelibrary.wiley.com/doi/10.1002/qj.3598.

Smale, D. A., et al. (2019). Marine heatwaves threaten global biodiversity and the provision of ecosystem services. *Nature Climate Change*, *9*(4), 306–312, https://doi.org/10.1038/s41558-019-0412-1 https://www.nature.com/articles/s41558-019-0412-1.

Soon, T. K. & Zheng, H. (2019). Climate Change and Bivalve Mass Mortality in Temperate Regions. In *Reviews of Environmental Contamination and Toxicology*, volume 251 (pp. 109–129). Springer New York LLC http://link.springer.com/10.1007/398{_}2019{_}31.

Stemmer, K., Nehrke, G., & Brey, T. (2013). Elevated CO2 Levels do not Affect the Shell Structure of the Bivalve Arctica islandica from the Western Baltic. *PLoS ONE*, *8*(7), e70106, https://doi.org/10.1371/journal.pone.0070106 https://dx.plos.org/10.1371/journal.pone.0070106.

Storlazzi, C. D., Cheriton, O. M., van Hooidonk, R., Zhao, Z., & Brainard, R. (2020). Internal tides can provide thermal refugia that will buffer some coral reefs from future global warming. *Scientific Reports*, *10*(1), 13435, https://doi.org/10.1038/s41598-020-70372-9 https://www.nature.com/articles/s41598-020-70372-9.

Stott, K., Austin, W., Sayer, M., Weidman, C., Cage, A., & Wilson, R. (2010). The potential of Arctica islandica growth records to reconstruct coastal climate in north west Scotland, UK. *Quaternary Science Reviews*, *29*(13-14), 1602–1613, https://doi.org/10.1016/j.quascirev.2009.06.016 https://linkinghub.elsevier.com/retrieve/pii/S0277379109002091.

Su, Z., Wang, J., Klein, P., Thompson, A. F., & Menemenlis, D. (2018). Ocean submesoscales as a key component of the global heat budget. *Nature Communications*, *9*(1), 775, https://doi.org/10.1038/s41467-018-02983-w https://www.nature.com/articles/s41467-018-02983-w.

Sully, S., Burkepile, D. E., Donovan, M. K., Hodgson, G., & van Woesik, R. (2019). A global analysis of coral bleaching over the past two decades. *Nature Communications*, *10*(1), 1–5, https://doi.org/10.1038/s41467-019-09238-2 https://www.nature.com/articles/s41467-019-09238-2.

Surge, D. M. & Schöne, B. R. (2013). Bivalve Sclerochronology. In *Encyclopedia of Scientific Dating Methods* (pp. 1–14). Dordrecht: Springer Netherlands http://link.springer.com/10.1007/978-94-007-6326-5{_}165-1.

Swanson, K. L., Sugihara, G., & Tsonis, A. A. (2009). Long-term natural variability and 20th century climate change. *Proceedings of the National Academy of Sciences*, *106*(38), 16120–16123, https://doi.org/10.1073/pnas.0908699106 https://pnas.org/doi/full/10.1073/pnas.0908699106.

Tardif, R., et al. (2019). Last Millennium Reanalysis with an expanded proxy database and seasonal proxy modeling. *Climate of the Past*, *15*(4), 1251–1273, https://doi.org/10.5194/cp-15-1251-2019 https://cp.copernicus.org/articles/15/1251/2019/.

Taylor, A. C. (1976). Burrowing behaviour and anaerobiosis in the bivalve Arctica islandica (L.). *Journal of the Marine Biological Association of the United Kingdom*, *56*(1), 95–109, https://doi.org/10.1017/S0025315400020464 https://www.cambridge.org/core/product/identifier/S0025315400020464/type/journal{_}article.

Thompson, I. & Jones, D. S. (1977). The ocean quahog, Arctica islandica, "tree" of the north Atlantic shelf. *Annual Meeting of the Geological Society of America Abstracts*, *9*(7), 1199.

Thompson, I., Jones, D. S., & Dreibelbis, D. (1980). Annual internal growth banding and life history of the ocean quahog Arctica islandica (Mollusca:

Bivalvia). *Marine Biology*, *57*(1), 25–34, https://doi.org/10.1007/BF00420964 https://link.springer.com/article/10.1007/BF00420964.

Thórarindsóttir, G. G., Gunnarsson, K., & Bogason, E. (2009). Mass mortality of ocean quahog, Arctica islandica, on hard substratum in Lonafjördur, northeastern Iceland after a storm. *Marine Biodiversity Records*, *2*, https://doi.org/10.1017/s1755267209000736.

Thórarinsdóttir, G. G. & Einarsson, S. T. (1996). Distribution, abundance, population structure and meat yield of the ocean quahog, Arctica islandica , in icelandic waters. *Journal of the Marine Biological Association of the United Kingdom*, *76*(4), 1107–1114, https://doi.org/10.1017/S0025315400040996 https://www.cambridge.org/core/product/identifier/S0025315400040996/type/journal{_}article.

Tierney, J. E., et al. (2015). Tropical sea surface temperatures for the past four centuries reconstructed from coral archives. *Paleoceanography*, *30*(3), 226–252, https://doi.org/10.1002/2014PA002717 https://agupubs.onlinelibrary.wiley.com/doi/10.1002/2014PA002717.

Torrence, C. & Compo, G. P. (1998). A Practical Guide to Wavelet Analysis. *Bulletin of the American Meteorological Society*, *79*(1), 61–78, https://doi.org/10.1175/1520-0477(1998)079<0061:APGTWA>2.0.CO;2 http://journals.ametsoc.org/doi/10.1175/1520-0477(1998)079{%}3C0061:APGTWA{%}3E2.0.CO;2.

Trofimova, T., et al. (2020). Fundamental questions and applications of sclerochronology: Community-defined research priorities. *Estuarine, Coastal and Shelf Science*, *245*, 106977, https://doi.org/10.1016/j.ecss.2020.106977 https://linkinghub.elsevier.com/retrieve/pii/S0272771420307083.

Trofimova, T., Andersson, C., Bonitz, F. G., Pedersen, L. E. R., & Schöne, B. R. (2021). Reconstructing early Holocene seasonal bottom-water temperatures in the northern North Sea using stable oxygen isotope records of Arctica islandica shells. *Palaeogeography, Palaeoclimatology, Palaeoecology*, *567*, 110242, https://doi.org/10.1016/j.palaeo.2021.110242 https://linkinghub.elsevier.com/retrieve/pii/S0031018221000274.

Trouet, V., Babst, F., & Meko, M. (2018). Recent enhanced high-summer North Atlantic Jet variability emerges from three-century context. *Nature Communications*, *9*(1), 180, https://doi.org/10.1038/s41467-017-02699-3 http://www.nature.com/articles/s41467-017-02699-3.

Turrell, W. R., Henderson, E. W., Slesser, G., Payne, R., & Adams, R. D. (1992). Seasonal changes in the circulation of the northern North Sea. *Continental Shelf Research*, *12*(2-3), 257–286, https://doi.org/10.1016/0278-4343(92)90032-F https://linkinghub.elsevier.com/retrieve/pii/027843439290032F.

Ünal-İmer, E., Shulmeister, J., Zhao, J.-X., Tonguç Uysal, I., Feng, Y.-X., Duc Nguyen, A., & Yüce, G. (2015). An 80 kyr-long continuous speleothem record from Dim Cave, SW Turkey with paleoclimatic implications for the Eastern Mediterranean. *Scientific Reports*, *5*(1), 13560, https://doi.org/10.1038/srep13560 https://www.nature.com/articles/srep13560.

Waelbroeck, C., et al. (2002). Sea-level and deep water temperature changes derived from benthic foraminifera isotopic records. *Quaternary Science Reviews*, *21*(1-3), 295–305, https://doi.org/10.1016/S0277-3791(01)00101-9 https://linkinghub.elsevier.com/retrieve/pii/S0277379101001019.

Wallace, J. M. & Gutzler, D. S. (1981). Teleconnections in the Geopotential Height Field during the Northern Hemisphere Winter. *Monthly Weather Review*, *109*(4), 784–812, https://doi.org/10.1175/1520-0493(1981)109<0784:TITGHF>2.0.CO;2 http://journals.ametsoc.org/doi/10.1175/1520-0493(1981)109{%}3C0784:TITGHF{%}3E2.0.CO;2.

Walsh, J. E. & Chapman, W. L. (2001). 20th-century sea-ice variations from observational data. *Annals of Glaciology*, *33*, 444–448, https://doi.org/10.3189/172756401781818671 https://www.cambridge.org/core/product/identifier/S0260305500264513/type/journal{_}article.

Walter, K. & Graf, H. F. (2002). On the changing nature of the regional connection between the North Atlantic Oscillation and sea surface temperature. *Journal of Geophysical Research Atmospheres*, *107*(17), ACL 7–1–ACL 7–13, https://doi.org/10.1029/2001JD000850 https://agupubs.onlinelibrary.wiley.com/doi/10.1029/2001JD000850.

Wanamaker, A. D., et al. (2019). Pacific climate influences on ocean conditions and extreme shell growth events in the Northwestern Atlantic (Gulf of Maine). *Climate Dynamics*, *52*(11), 6339–6356, https://doi.org/10.1007/s00382-018-4513-8 http://link.springer.com/10.1007/s00382-018-4513-8.

Wanamaker, A. D., et al. (2008). Coupled North Atlantic slope water forcing on Gulf of Maine temperatures over the past millennium. *Climate Dynamics*, *31*(2-3), 183–194, https://doi.org/10.1007/s00382-007-0344-8 http://link.springer.com/10.1007/s00382-007-0344-8.

Wang, B. & An, S. (2001). Why the properties of El Niño changed during the late 1970s. *Geophysical Research Letters*, *28*(19), 3709–3712, https://doi.org/10.1029/2001GL012862 https://agupubs.onlinelibrary.wiley.com/doi/10.1029/2001GL012862.

Wang, J., Yang, B., Ljungqvist, F. C., Luterbacher, J., Osborn, T. J., Briffa, K. R., & Zorita, E. (2017). Internal and external forcing of multidecadal Atlantic climate variability over the past 1,200 years. *Nature Geoscience*, *10*(7), 512–517, https://doi.org/10.1038/ngeo2962 http://www.nature.com/articles/ngeo2962https://www.nature.com/articles/ngeo2962.

Wang, Y., et al. (2008). Millennial- and orbital-scale changes in the East Asian monsoon over the past 224,000 years. *Nature*, *451*(7182), 1090–1093, https://doi.org/10.1038/nature06692 https://www.nature.com/articles/nature06692.

Wazneh, H., Gachon, P., Laprise, R., de Vernal, A., & Tremblay, B. (2021). Atmospheric blocking events in the North Atlantic: trends and links to climate anomalies and teleconnections. *Climate Dynamics*, *56*(7-8), 2199–2221, https://doi.org/10.1007/s00382-020-05583-x https://doi.org/10.1007/s00382-020-05583-x.

Wigley, T. M. L., Briffa, K. R., & Jones, P. D. (1984). On the Average Value of Correlated Time Series, with Applications in Dendroclimatology and Hydrometeorology. *Journal of Climate and Applied Meteorology*, *23*(2), 201–213, https://doi.org/10.1175/1520-0450(1984)023<0201:OTAVOC>2.0.CO;2 http://journals.ametsoc.org/doi/10.1175/1520-0450(1984)023{%}3C0201:OTAVOC{%}3E2.0.CO;2.

Wilks, D. S. (2019). Principal Component (EOF) Analysis. In *Statistical Methods in the Atmospheric Sciences* (pp. 617–668). Elsevier https://linkinghub.elsevier.com/retrieve/pii/B9780128158234000134.

Wiltshire, K. H., et al. (2010). Helgoland Roads, North Sea: 45 Years of Change. *Estuaries and Coasts*, *33*(2), 295–310, https://doi.org/10.1007/s12237-009-9228-y http://link.springer.com/10.1007/s12237-009-9228-y.

Wiltshire, K. H., et al. (2008). Resilience of North Sea phytoplankton spring bloom dynamics: An analysis of long-term data at Helgoland Roads. *Limnology and Oceanography*, *53*(4), 1294–1302, https://doi.org/10.4319/lo.2008.53.4.1294 http://doi.wiley.com/10.4319/lo.2008.53.4.1294.

Wiltshire, K. H. & Manly, B. F. J. (2004). The warming trend at Helgoland Roads, North Sea: phytoplankton response. *Helgoland Marine Research*, *58*(4), 269–273, https://doi.org/10.1007/s10152-004-0196-0 https://hmr.biomedcentral.com/articles/10.1007/s10152-004-0196-0.

Witbaard, R. (1994). Long-term trends on the effects of the southern North Sea beamtrawl fishery on the bivalve mollusc Arctica islandica L. (Mollusca, bivalvia). *ICES Journal of Marine Science*, *51*(1), 99–105, https://doi.org/10.1006/jmsc.1994.1009 https://dx.doi.org/10.1006/jmsc.1994.1009.

Witbaard, R. (1996). Growth variations inArctica islandica L. (Mollusca): a reflection of hydrography-related food supply. *ICES Journal of Marine Science*, *53*(6), 981–987, https://doi.org/10.1006/jmsc.1996.0122 https://academic.oup.com/icesjms/article-lookup/doi/10.1006/jmsc.1996.0122.

Witbaard, R. (1997). *Tree of the sea - The use of the internal growth lines in the shell of Arctica islandica (Bivalvia, Mollusca) for the retrospective assessment of marine environmental change*. PhD thesis, University of Groningen https://research.rug.nl/en/publications/tree-of-the-sea-the-use-of-the-internal-growth-lines-in-the-shell.

Witbaard, R. & Bergman, M. J. (2003). The distribution and population structure of the bivalve Arctica islandica L. in the North Sea: What possible factors are involved? *Journal of Sea Research*, *50*(1), 11–25, https://doi.org/10.1016/S1385-1101(03)00039-X https://linkinghub.elsevier.com/retrieve/pii/S138511010300039X.

Witbaard, R., Duineveld, G., & De Wilde, P. (1997). A Long-Term Growth Record Derived from Arctica Islandica (Mollusca, Bivalvia) from the Fladen Ground (Northern North Sea). *Journal of the Marine Biological Association of the United Kingdom*, *77*(3), 801–816, https://doi.org/10.1017/S0025315400036201 https://www.cambridge.org/core/product/identifier/S0025315400036201/type/journal{_}article.

Witbaard, R., Franken, R., & Visser, B. (1998). Growth of juvenileArctica islandica under experimental conditions. *Helgoländer Meeresuntersuchungen*, *51*(4), 417–431, https://doi.org/10.1007/BF02908724 https://link.springer.com/10.1007/BF02908724.

Witbaard, R., Jansma, E., & Sass Klaassen, U. (2003). Copepods link quahog growth to climate. *Journal of Sea Research*, *50*(1), 77–83, https://doi.org/

10.1016/S1385-1101(03)00040-6 https://linkinghub.elsevier.com/retrieve/pii/S1385110103000406.

Witbaard, R., Jenness, M. I., Van Der Borg, K., & Ganssen, G. (1994). Verification of annual growth increments in Arctica islandica L. from the North Sea by means of oxygen and carbon isotopes. *Netherlands Journal of Sea Research*, *33*(1), 91–101, https://doi.org/10.1016/0077-7579(94)90054-X https://linkinghub.elsevier.com/retrieve/pii/007775799490054X.

Yang, H., et al. (2020). Poleward Shift of the Major Ocean Gyres Detected in a Warming Climate. *Geophysical Research Letters*, *47*(5), e2019GL085868, https://doi.org/10.1029/2019GL085868 https://agupubs.onlinelibrary.wiley.com/doi/10.1029/2019GL085868.

Yeh, S., Yi, D., Sung, M., & Kim, Y. H. (2018). An Eastward Shift of the North Pacific Oscillation After the Mid-1990s and Its Relationship With ENSO. *Geophysical Research Letters*, *45*(13), 6654–6660, https://doi.org/10.1029/2018GL078671 https://agupubs.onlinelibrary.wiley.com/doi/10.1029/2018GL078671.

Zachos, J. C., Stott, L. D., & Lohmann, K. C. (1994). Evolution of Early Cenozoic marine temperatures. *Paleoceanography*, *9*(2), 353–387, https://doi.org/10.1029/93PA03266 https://agupubs.onlinelibrary.wiley.com/doi/10.1029/93PA03266.

Acknowledgements

Thomas Brey, thank you for being my doctoral father! I am deeply grateful for your encouragement and the invaluable feedback you provided during the review of my papers. I simply cannot overstate my appreciation for your prompt responses to my emails, which seems to be a rarity in academia. Thanks for sharing with me the data you had, only like this I could find the Helgoland chronology of *A. islandica* created by F. Bauer.

Gerrit Lohmann, thank you for our insightful discussions and feedback, and for pushing me to prepare better manuscripts. Many thanks for the COVID-19 pandemic contract extensions and signing all the necessary documents. I am happy to have taken part in your Paleoclimate Dynamics group.

I would like to express my gratitude towards my main supervisor, Monica Ionita, for conceiving the PALEX project in the first place and providing funding. Without PALEX, my research would not have been possible. I appreciate the level of freedom given to explore whichever idea I had, and our talks about life and academia. You were always swamped with work and duties, yet you still found time to read my paper drafts and answer my questions.

Norel Rimbu, thank you so much for your patience, expertise and help with the blocking index. Our conversations consistently inspired me, leaving me feeling more motivated!

I am very happy and delighted to have met Doris Abele! I cherish her enthusiasm for my topic and all the scientific and writing advice she gave me in the beginning of my PhD.

Thank you Claudia Hanfland and POLMAR for offering excellent courses and for your continued support of students!

Many thanks to all of my colleagues over the years: Daniel Balting, Lennert Stap, Evan Gowan, Lars Ackermann, Nadezhda Sokolova, Justus Contzen, Pengyang Song, for your companionship, advice and beers! Paul Gierz, you have genuinely helped me out figuring Python right in the beginning. Thank you, Jan Streffing, for improving the DeepL German translation of my abstract. **Special thanks** to Fernanda Matos, Smit Doshi, Zohreh Khozani, Viorica Nagavciuc for proof-reading and for being great people who really inspire me!

To my friends and family, no words can express my gratitude for your kind support and patience! The road was longer than ever expected!

Diana E. Caldarescu
June 2024